TOWARDS THE STRUCTURE AND FUNCTION OF CARBON-PHOSPHOROUS LYASE ENZYMES

by

Shu-Mei He

A thesis submitted to the Department of Chemistry

In conformity with the requirements for

The degree of Master of Science

Queen's University

Kingston, Ontario, Canada

(August, 2008)

Copyright ©Shu-Mei He, 2008

Abstract

Organophosphonates are characterized by a very stable carbon-phosphorus bond. *Eshcherichia coli* and many other strains of bacteria possess a multi-enzyme system called carbon-phosphorus (C-P) lyase that enables these organisms to cleave the C-P bond of organophosphonates when inorganic phosphate is scarce in the local environment. Genetic studies have demonstrated that C-P lyase is encoded by the fourteen-gene *phn* operon, *phnCDEFGHIJKLMNOP*. However, the mechanism for C-P bond cleavage is still unclear. We have expressed, purified, and characterized phnP from this operon. PhnP is a phosphodiesterase which will hydrolyze both bis-(*p*-nitrophenyl) phosphate and 2':3'-cyclic nucleotides as substrates. In collaboration with Dr. Zongchao Jia and Katarenya Podzelinska (Queen's Biochemistry), we have crystallized phnP and solved the crystal structure at a resolution of 1.3 Å. The structure displayed similarity to zinc-dependent metallo-β-lactamase family proteins. However, phnP displays unique structural features with two metal binding sites per monomer: the active site containing potentially two manganese ions, and a 'structural' site coordinating one zinc ion. Potential active site residues were identified and corresponding point mutations were generated by site-directed mutagenesis. Studies based on the importance of these residues and the knowledge from our high resolution structure will help elucidate the mechanism of phnP as well as its function in the C-P lyase pathway. Furthermore, we performed a broad range of ligand screening for phnH, another key member

from the C-P lyase pathway, by ITC experiments, co-crystallization and high throughput ligand screening. However, all the trials for the identification of the true physiological substrate for phnH proved unsuccessful. Although the mechanism of C-P bond cleavage by C-P lyase still remains unclear, we synthesized a fluorescently labelled organophosphonate (FPn) and utilized it for probing the *in vivo* degradation of the C-P bond by wild type *E. coli* and various mutants. Analysis by TLC and mass spectrometry demonstrated the production of the expected alkane product. With this promising fluorescent probe, potential intermediates and substrates can be identified for individual C-P lyase enzymes. Taken together, our studies on the C-P lyase pathway will contribute to elucidate the still unknown mechanism of the cleavage of the stable C-P bond.

Acknowledgements

First of all, I would like express my gratitude to my supervisor, Dr. David Zechel, for his guidance, supports and patience during my three years' Masters Program. I will never forget his sincerity, generosity and consideration for female students like me with kids and family. His wisdom, prudent attitude toward research, and passion for learning has encouraged me to overcome failures and frustrations, and to achieve many goals during my research. I can never express my gratitude to him enough. I would also like to express my thanks to the technical support of all the past and present members of our research group, Dr. Yan Luo, Dr. Anupam Bhattacharya, Meagan Perry and Ryan Latimer, as well as members of Pratt group, with whom I can share my happiness, sadness, ups and downs. Thank you Dr. Derek Pratt too, for your generous help and guidance in building up my chemistry knowledge. I would also like to thank Dr. Zongchao Jia, Kateryna Podzelinska, and Mr. Kim Munro from the Department of Biochemistry at Queen's University, as well as Dr. Diane Beauchemin, Dr. Yi-Min She, and especially Jessie Sui from the Depatment of Chemistry, for their cooperation, technical support and friendship.

I would like to acknowledge my husband, my son, my parents and my siblings. It is with their endless love and enduring support that I can finish my Master's study at Queen's. Thank you all for sharing every aspect of life with me, the encouragement, the understanding, the laughter, the tears and everything. Thank you, thank you, and thank you.

Statement of Originality

All work presented in this thesis was performed by the author under the supervision of Dr. David Zechel except for the following:

Kateryna Podzelinska from Department of Biochemistry, Queen's University, grew crystals of phnP with the native and selenium protein preparations provided by the author, and solved the X-ray crystal structure of phnP. Kateryna Podzelinska also performed the RNase assay (Figure 2-16) with wild type phnP and the virtually inactive D80A mutant provided by the author.

Dr. Bjarne Hove-Jensen from University of Cobenhagen, Denmark, performed the *in vivo* C-P lyase activity of wild type *E. coli* and *phn* knockout strains with the fluorescent compound FPn synthesized by the author (Figure 4-8).

Table of Contents

List of Figures

List of Tables

Abbreviation List

ADP	adenosine 5’-diphosphate
ADP-glucose	Adenosine-5′-diphospho-D-glucose
2-AEP	2-aminoethylphosphonate
AMP	adenosine 5’-monophosphate
3’-AMP	adenosine 3’-monophosphate
2’-AMP	adenosine 2’-monophosphate
ATP	adenosine 5’-triphosphate
bpNPP	bis(*p*-nitrophenyl) phosphate
bis-Tris	bis(2-hydroxyethyl)-imino-tris(hydroxymethyl)methane
BSA	bovine serum albumin
2’:3’-cAMP	adenosine 2’:3’-cyclic monophosphate
3’:5’-cAMP	adenosine 3’:5’-cyclic monophosphate
2’:3’-cCMP	cytidine 2’:3’-cyclic monophosphate
3’:5’-cCMP	cytidine 3’:5’-cyclic monophosphate
CDP-choline	cytidine 5′-diphospho choline
2’:3’-cGMP	guanosine 2’:3’-cyclic monophosphate
3’:5’-cGMP	guanosine 3’:5’-cyclic monophosphate
CIAP	calf intestinal alkaline phosphatase
DHB	2,5-dihydroxybenzoic acid
DTT	dithiothreitol
EDTA	ethylenediaminetetraaceticacid

FAD	flavin adenine dinucleotide
FMN	flavin mononucleotide
FPLC	fast protein liquid chromatography
FPn	fluorescent phosphonate
GDP-glucose	guanosine-5′-diphospho-D-glucose
GDP-mannose	guanosine-5′-diphospho-D-mannose
GTP	guanosine-5’-triphosphate
HEPES	4-(2-hydroxyethyl)-1-piperazineethanesulfonic Acid
HPLC	high performance liquid chromatography
HTS	high throughput screening
ICP-MS	inductively coupled plasma mass spectrometry
IMAC	immobilized metal affinity chromatography
IPTG	isopropyl β-D-1-thiogalactopyranoside
ITC	isothermal titration calorimetry
MALDI-MS	matrix-assisted laser desorption/ionization mass spectrometry
MePn	methylphosphonic acid
MES	2-(*N*-morpholino)ethanesulfonic acid
MOPS	3-(*N*-morpholino)propanesulfonic acid
MWCO	molecular weight cut off
NADH	nicotinamide adenine dinucleotide, reduced
NADPH	nicotinamide adenine dinucleotide 2′-phosphate, reduced

Ni-NTA resin	nickel-nitrilotriacetic acid resin
PCR	polymerase chain reaction
PDE	phosphodiesterase
PEG	polyethyleneglycol
PEP	phosphoenolpyruvate
Pi	orthophosphate
PLP	pyridoxyl-5-phosphate
pNPP	*p*-nitrophenyl phosphate
pppGPP	guanosine-3'-diphosphate 5'-triphosphate
ppGpp	guanosine-3',5'-bispyrophosphate
ppG2':3'p	guanosine-5'-diphosphate-2',3'-cyclic monophosphate
RFU	relative fluorescence units
SAM	*S*-adenosylmethionine
SDS-PAGE	sodium dodecyl sulfate polyacrylamide gel electrophoresis
TLC	thin layer chromatography
tpNPP	thymidine-5'-monophosphate-*p*-nitrophenylester
Tris	tris(hydroxymethyl)aminomethane
Tricine	*N*-(2-Hydroxy-1,1-bis(hydroxymethyl)ethyl)glycine
UDP-glucose	uridine 5′-diphospho-D-glucose
UDP-glucaronic acid	uridine 5′-diphospho-D-glucuronic acid
UDP-galactose	uridine 5′-diphospho-D-galactose

Chapter I
Introduction

1.1 Significance of phosphate and phosphonates in the environment

Phosphate is an essential macronutrient that is involved in numerous biological processes in all organisms, including the regulation of cellular signaling pathways, formation of membrane phospholipids, the structure of nucleic acids, and the storage of metabolic energy. Inorganic orthophosphate (P_i) **1 (Figure 1-1),** in which phosphorus is in its highest oxidation state (+5), is the most common form of phosphorus in nature and is readily used by microbial cells. However, other forms of phosphorous, such as organophosphonates, also form a significant fraction of the global phosphorus pool. Organophosphonates are characterized by the presence of a highly stable carbon-phosphorus (C-P) bond that resists chemical hydrolysis, thermal decomposition (1), and photolysis (2). Examples of these compounds include the naturally occurring phosphonopyruvate **2**, phosphonoacetate **3**, methyl phosphonate **5,** fosfomycin **6** (a commonly used antibiotic) (4), and 2-aminoethylphosphonate **4**, a common constituent of microbial phosphonolipids and the most abundant of the biogenic phosphonates. Synthetic and highly bioactive organophosphonates have also been developed for use as herbicides, such as glyphosate **7**, and chemical warfare nerve agents, such as VX **8** and sarin **9**. The chemically inert nature of the C-P bond has raised environmental concerns as toxic phosphonates accumulate in a number of ecosystems (5). Biodegradation of

organophosphonates may form one strategy to eliminate certain types of phosphonates from the environment.

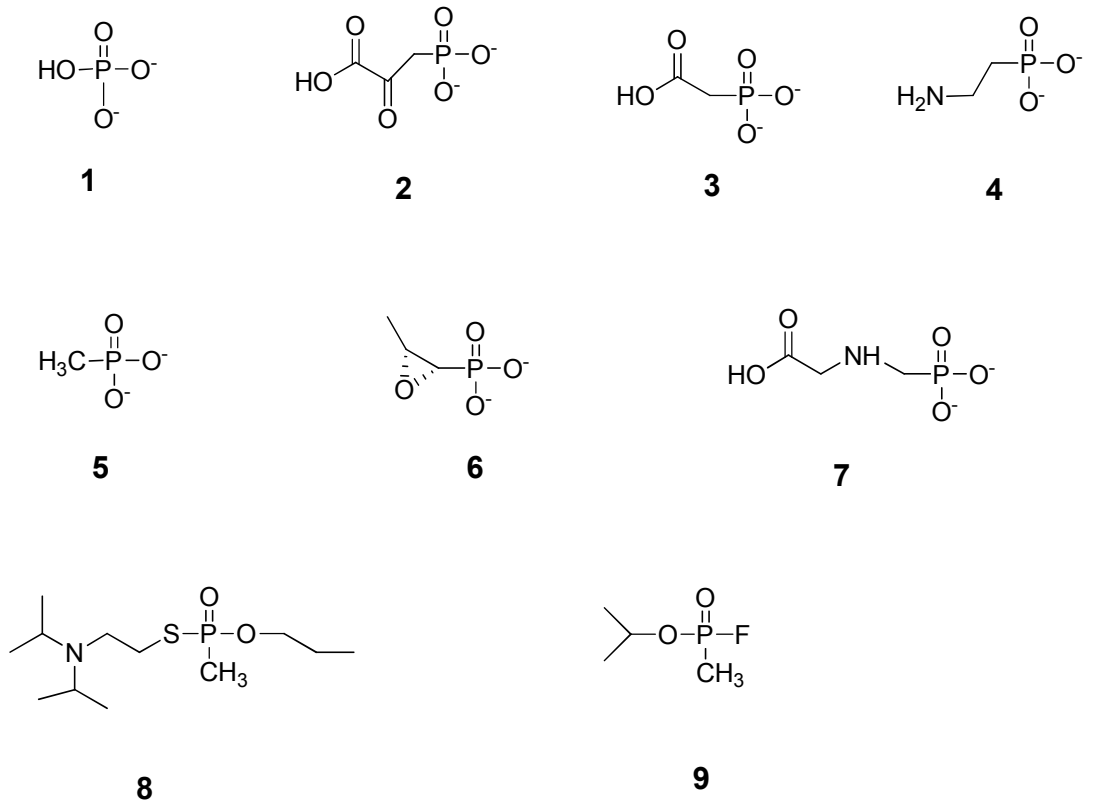

Figure 1-1: Structures of orthophosphate (**1**) and some examples of naturally occurring and synthetic organophosphonates: phosphonopyruvate (**2**), phosphonoacetate (**3**), 2-aminoethylphosphonic acid (**4**), methylphosphonate (**5**), fosfomycin (**6**), glyphosate (**7**), VX (**8**), Sarin (**9**).

1.2 Enzymatic pathways for degradation of phosphonates

The abundance of organophosphonates in the environment has enabled bacteria to evolve enzymatic means to hydrolytically cleave the C-P bond to

produce P_i and thereby gain an advantage in survival and growth (6). In *Pseudomonas stutzeri* and *Escherichia coli*, phosphonate utilization is mediated by a cluster of 14 genes, collectively called the *phn* operon (*phnCDEFGHIJKLM*), encoding a multi-enzyme system known as the carbon - phosphorus lyase pathway (33). The genome of *Trichodesmium erythraeum* IMS 101 reveals a similar gene cluster that consists of genes *phnC* to *phnM*, but lacks *phnF, phnN, phnO*, and *phnP*. This *phn* operon is also involved in the degradation of phosphonates in marine environments, where P_i is generally present in nanomolar concentrations, and organophosphonates are often more abundant (28). Recently, it was reported that a C-P lyase pathway is also present in *Acidithiobacillus ferrooxidans*, a bacterium that obtains its energy from the oxidation of other compounds (34). The *phn* operon is part of the *Pho* regulon, which consists of genes and operons whose transcription is induced under conditions of P_i starvation and mediates the adaptive response to P_i limitation (37).

There are currently five known enzyme activities capable of cleaving the C-P bond and two kinds of mechanisms of those activities have been proposed. Phosphonoacetaldehyde hydrolase (or 'phosphonatase') (7), phosphonoacetate hydrolase (8) and phosphonopyruvate hydrolase (8) act on substrates with carbonyl groups β to the phosphorus center. These enzymes all likely use a lysine residue to form a Schiff base (**2** in **Figure 1-2**) to activate their substrates. In the case of phosphonatase an aspartate residue attacks the Schiff base intermediate, which is subsequently hydrolyzed to form P_i and acetaldehyde (4 in

Figure 1-2) (7,10,11). The crystal structure of phosphonatase has been obtained and the enzyme was shown to be a member of the haloacid dehalogenase superfamily (11). Phosphonopyruvate (PEP) mutase is a magnesium dependent enzyme that catalyzes the interconversion of phosphoenopyruvate and phosphonopyruvate, a key step in the biosynthesis of most naturally occurring organophosphonates (4). The reactions catalyzed by these enzymes are illustrated in **Figure 1-3**.

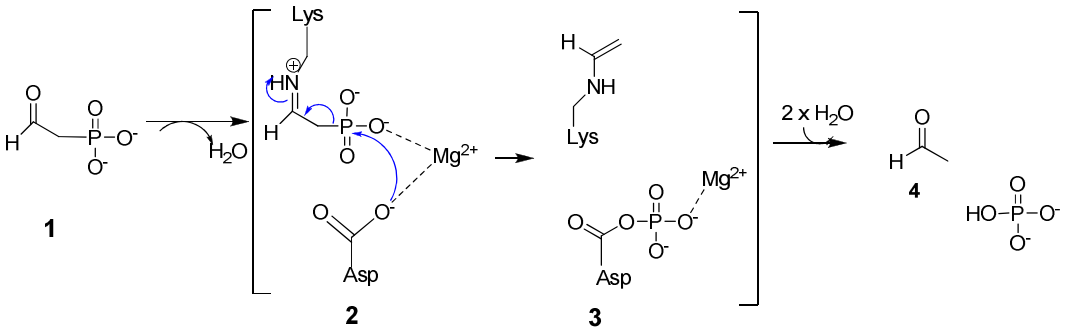

Figure 1-2. Proposed mechanism for cleavage of the C-P bond by phosphonoacetaldehyde hydrolase (phosphonatase) (7).

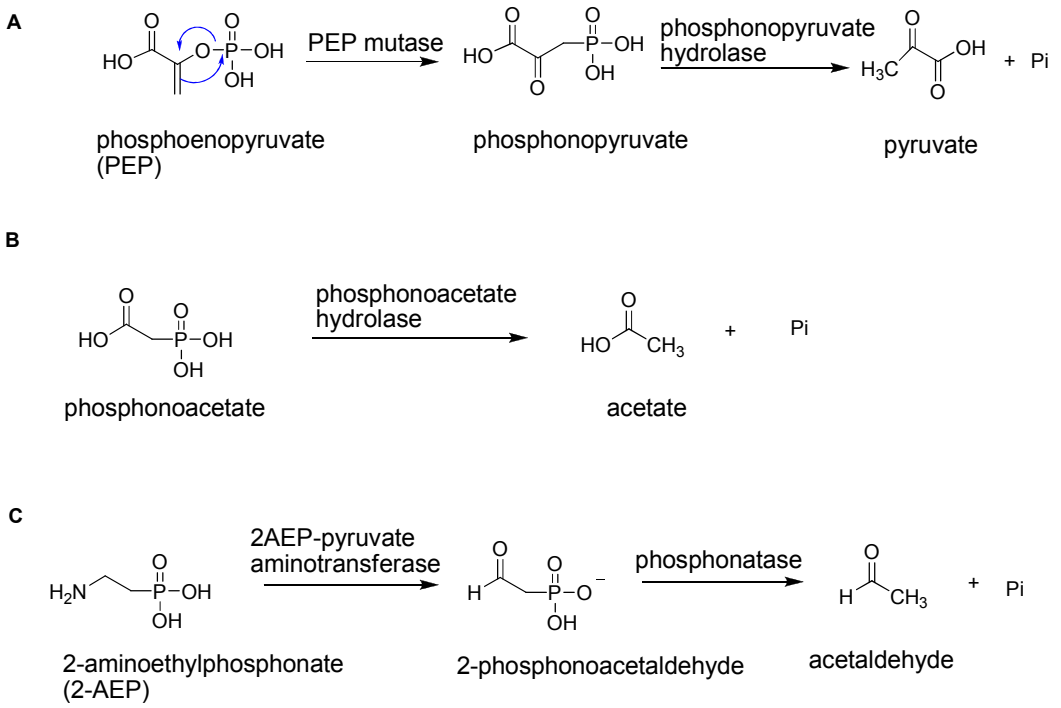

Figure 1-3. Enzymes that cleave carbon-phosphorus bonds. (A) phosphonopyruvate hydrolase; (B) phosphonoacetate hydrolase; (C) phosphonatase.

In contrast to these single enzyme activities, carbon-phosphorous lyase (C-P lyase), encoded by the *phn* operon described above, is a multi-enzyme system (14) that is capable of cleaving the C-P bond of a broad range of organophosphonates (**Figure 1-4A**) (14, 15), yielding the corresponding hydrocarbon and P_i (16). The formation of an alkane with trace amounts of alkenes from the degradation of organophosphonates is thought to proceed through a radical mechanism, in which the alkylphosphonate is either oxidized or reduced to form an alkylphosphonyl or alkylphosphoranyl radical, respectively (**Figure 1-4B**). The radical species subsequently undergoes C-P bond cleavage producing a phosphorus intermediate and an alkyl radical, which abstracts a

hydrogen (from an unknown donor) to form the alkane product (**Figure 1-4**). Similar alkane and alkene product mixtures are produced through the known radical based reaction for alkylphophonates with lead (IV) tetracetate (14). The formation of an alkyl radical intermediate by C-P lyase is also supported by the observation of 1-butene as a side product from the reaction with cyclopropylmethylphosphonate (**Figure 1-4A**). 1-Butene is known to be formed through the rearrangement of the cyclopropylmethylcarbinyl radical formed by this substrate. Currently, biochemical data such as the properties and the mechanism of the catalytic activity for the *in vitro* characterization of the C-P lyase pathway is very limited. The corresponding enzyme activity is lost upon the disruption of the cells, suggesting that the multi-enzyme system is membrane-associated (15, 17), although recent detection of C-P lyase activity in a cell-free system has been reported by Kononova *et al*. when ATP and NADH is added to the cell lysate (36).

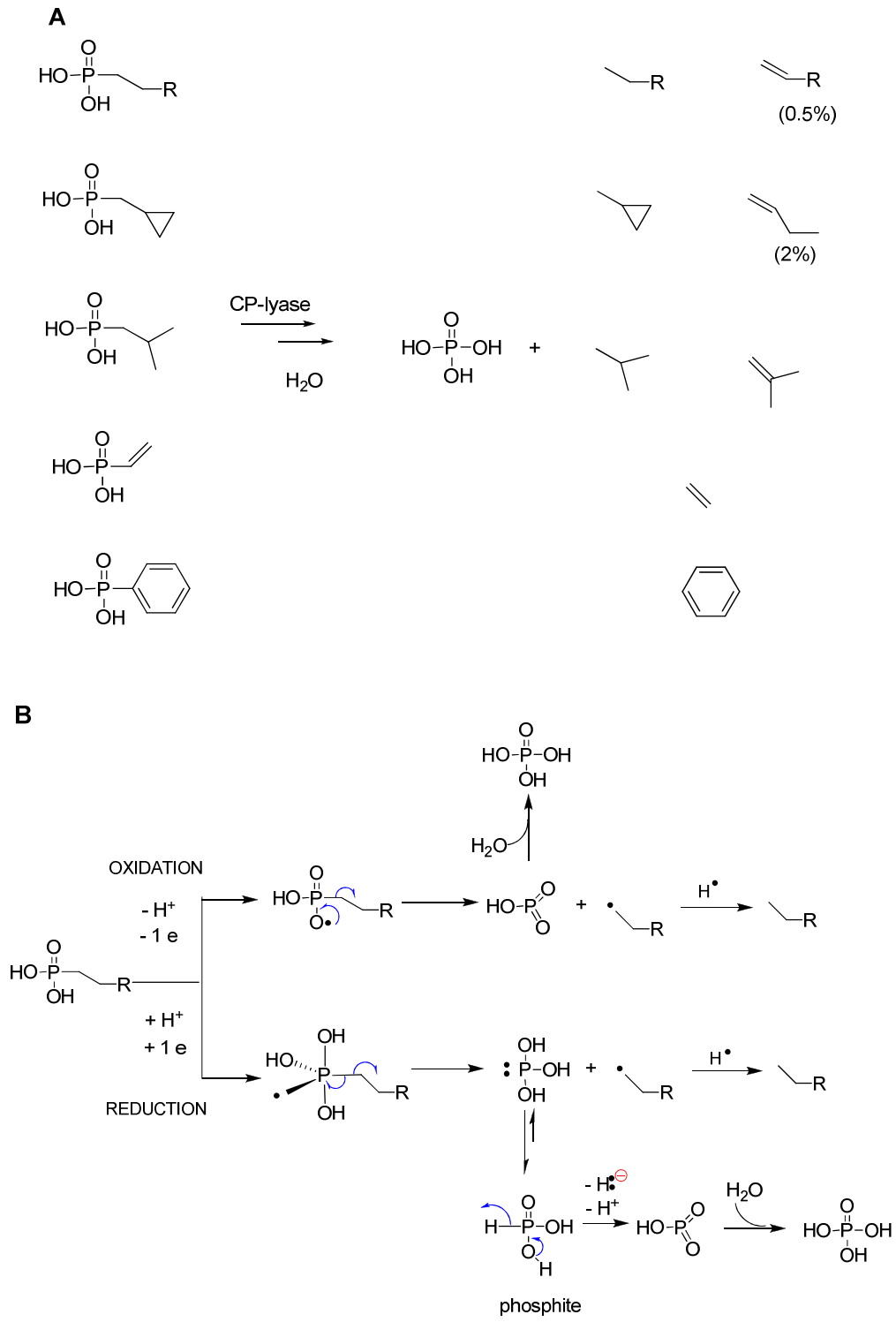

Figure 1-4: (**A**) Examples of known *in vivo* C-P bond cleavage reactions mediated by C-P lyase (14). (**B**) Possible radical mechanism for C-P bond cleavage by C-P lyase (14, 41).

1.3 *E. coli* C-P lyase pathway for degrading phosphonates

In *E. coli* the entire *phn* operon appears to be transcribed from a single promoter, located immediately upstream of the *phnC* gene (23) (**Figure 1-6A**). Sequence analysis has established that the gene products phnC, phnD, and phnE are components of an alkylphosphonate transport system, and gene knockout studies demonstrated that the minimum size of the *phn* operon required for the whole-cell C-P lyase is composed of *phnG, phnH, phnI, phnJ, phnK, phnL, phnM* genes (30) (**Figure 1-7**).

Despite extensive efforts to detect C-P lyase activity in *E. coli*, only phnD, phnF, phnH, phnN, phnO and phnP proteins from the *phn* operon have been characterized *in vitro*. PhnD has been identified as a periplasmic organophosphonate binding protein with a binding affinity of 5 nM for 2-AEP, and micromolar affinity for other phosphonates (38). Recently, phnF from *Mycobacterium smegmatis* has been reported as a transcriptional regulator of the *phn* operon (39), and its 3-dimensional structure has recently been reported (40). *E. coli* phnN has been characterized as an ATP dependent kinase, phosphorylating 5-phospho-α-D-ribofuranosyl-1,5-diphosphate to yield 5-phospho-α–D-ribofuranosyl pyrophosphate (PRPP), a precursor in the biosynthesis of NADH (as well as purine and pyrimidine nucleosides) (16, **Figure 1-5A**). It was demonstrated previously that α-D-ribofuranosyl ethylphosphonate was enriched in the culture medium when *E. coli* subsisted on ethylphosphonate as a sole phosphorus source (31). By contrast, a mutant strain of *E. coli* with an inoperative *phn* operon failed to produce this intermediate, indicating that the

biosythesis of this intermediate is mediated by C-P lyase enzymes. It was proposed that C-P bond cleavage may occur on this intermediate, which could then be phosphorylated by phnN to support NADH biosynthesis (16).

PhnO from *Salmonella enterica* is a homologue of phnO from *E. coli*. It has been characterized *in vitro* as an acetyl-CoA dependent N-acetyltransferase that is responsible for acetylating aminoalkylphosphonates (27, **Figure 1-5B**). The physiological role of phnO toward aminoalkylphosphonates was proposed to be for storage and protection in such a way that when large amounts of aminophosphonates are present in the environment exceeding the organism's requirements, these phosphonates could be stored in an acetylated form and later used after hydrolysis by a deacetylase (27).

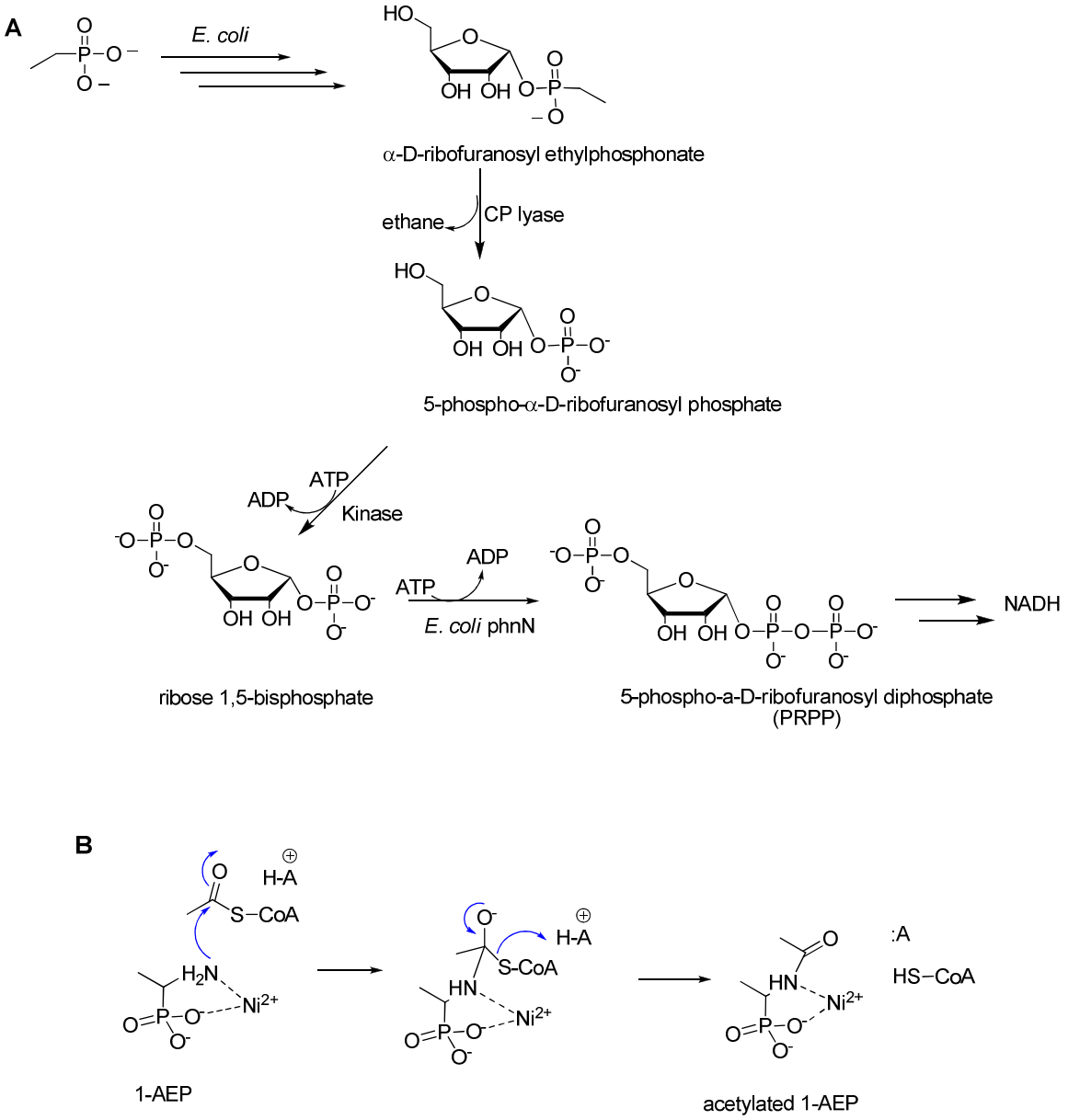

Figure 1-5. Proposed chemical mechanism for reactions catalyzed by phnN from *E. coli* (**A**) (16), and phnO from *Salmonella enterica* (**B**) (28).

The *E. coli phn* gene cluster *phnGHIJKLM* has been shown to be highly conserved (29) in bacteria, including the marine diazotroph *Trichodesmium erythraeum* IMS101 (28), *Thiobacillus denitrificans* (28), *Pseudomonas stutzeri*

(34), and chemolithoautotroph *Acidithiobacillus ferrooxidans* (35) (**Figure 1-6**), consistent with this subset of genes being essential for C-P bond cleavage (30).

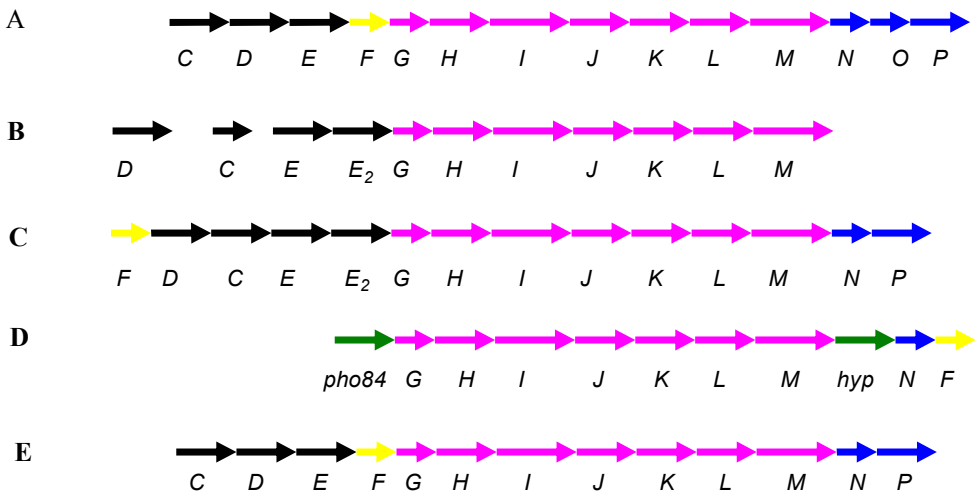

Figure 1-6. Comparison of *phn* operons from *E. coli* (**A**),*Trichodesmium* IMS 101(**B**), *Thiobacillus dentrificans* (**C**), *Acidithiobacillus ferrooxidans* (**D**) and *Pseudomonas stutzeri* (**E**). Genes encoding phosphonate transport (black), regulation (yellow), the C-P lyase subunits (magenta) and accessory proteins (blue) are shown. (28, 34, 35)

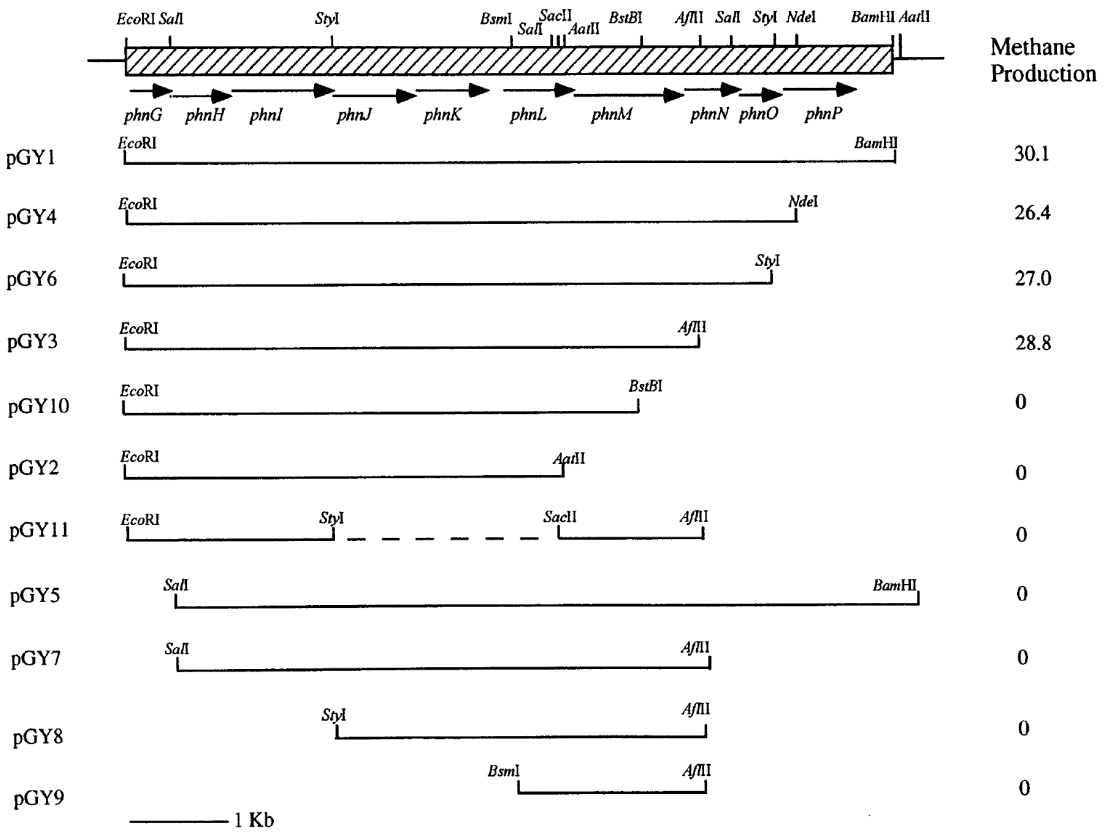

Figure 1-7. Schematic representation of various plasmid constructs of the *phn* operon used to determine the minimal set of genes necessary for C-P bond cleavage in *E. coli* using MePn as a phosphorous source. Figure adopted from (30).

Although the C-P lyase pathway has been extensively characterized at a genetic level, an *in vitro* reconstruction of C-P lyase activity has not yet been convincingly achieved (21, 23, 25, 26). In addition, the sequences of several of the *phnG-phnM* enzymes are quite unique, yielding no insight via homology into

their possible function. With the exception of phnH (32), none of the gene products of phnG-phnM from *E. coli* have been characterized *in vitro* at the protein level.

Motivated by the intriguing activity of C-P lyase, as well as by the growing accumulation of bioactive phosphonates in the environment, we carried out both *in vivo* and *in vitro* experiments in order to characterize the structures and mechanisms of the individual C-P lyase enzymes. In the following chapters, structural and kinetic characterization of phnP, the last gene product in the *E. coli phn* operon, will be discussed. In addition, our efforts to search for the physiological substrate or cofactors for phnH with ITC will be discussed. Lastly, a fluorescently labeled alkylphophonate was synthesized and shown to be a viable substrate for C-P lyase *in vivo*.

REFERENCES

1. Freedman LD, Doak GO: **The preparation and properties of phosphonic acids**. *Chem. Rev.* 1957, **57**:479-523.
2. Murai T, Tomizawa C: **Chemical transformation of S-benzyl O-ethyl phenylphosphonothiolate by ultraviolet light**. *J Environ Sci Health.* 1976*,* **11**:185-197.
3. Hilderbrand RL, Henderson TO: **Phosphonic acids in nature**. *Role Phosphonates Living Syst.* 1983*,* 5-29.
4. Seto H, Kuzuyama T: **Bioactive natural products with carbon-phosphorus bonds and their biosynthesis**. *Nat. Prod. Rep.* 1999, **16**:589-596.
5. Ternan NG, Grath JW, Mullan G, Quinn JP: **Organophosphonates: occurrence, synthesis and biodegradation by microorganisms**. *World J. Microbiol. Biotechnol.* 1998, **14**:635-647.
6. Kononova SV, Nesmeyanova MA: **Phosphonates and their degradation by microorganisms**. *Biochemistry (Moscow, Russ. Fed.)* 2002, **67**:184-195.
7 Morais MC, Zhang G, Zhang W, Olsen DB, Dunaway-Mariano D, Allen KN: **X-ray Crystallographic and Site-directed Mutagenesis Analysis of the Mechanism of Schiff-base Formation in Phosphonoacetaldehyde Hydrolase Catalysis**. *J. Biol. Chem.* 2004, **279**:9353-9361.
8. McGrath JW, Wisdom GB, McMullan G, Larkin MJ, Quinn JP: **The purification and properties of phosphonoacetate hydrolase. A novel carbon-phosphorus bond-cleavage enzyme from *Pseudomonas fluorescens* 23F**. *Eur. J. Biochem.* 1995, **234**:225-230.
9. Liu S, Lu Z, Han Y, Jia Y, Howard A, Dunaway-Mariano D, Herzberg O: **Conformational flexibility of PEP mutase**. *Biochemistry* 2004, **43**:4447-4453.
10. Galperin MY, Jedrzejas MJ: **Conserved core structure and active site residues in alkaline phosphatase superfamily enzymes**. *Proteins: Struct., Funct., Genet.* 2001, **45**:318-324.
11. Burroughs AM, Allen KN, Dunaway-Mariano D, Aravind L: **Evolutionary Genomics of the HAD Superfamily: Understanding the Structural Adaptations and Catalytic Diversity in a Superfamily of Phosphoesterases and Allied Enzymes**. *J. Mol. Biol.* 2006, **361**:1003-1034.
12. La Nauze JM, Rosenberg H, Shaw DC: **Enzymic cleavage of the carbon-phosphorus bond: purification and properties of phosphonatase**. *Biochim. Biophys. Acta, Enzymol.* 1970, **212**:332-350.
13. Lee SL, Hepburn TW, Swartz WH, Ammon HL, Mariano PS, Dunaway-Mariano D: **Stereochemical probe for the mechanism of phosphorus-carbon bond cleavage catalyzed by the *Bacillus cereus* phosphonoacetaldehyde hydrolase**. *J. Am. Chem. Soc.* 1992, **114**:7346-7354.

14. Frost JW, Loo S, Cordeiro ML, Li D: **Radical-based dephosphorylation and organophosphonate biodegradation**. *J. Am. Chem. Soc.* 1987, **109**:2166-2171.
15. Wackett LP, Shames SL, Venditti CP, Walsh CT: **Bacterial carbon-phosphorus lyase: products, rates, and regulation of phosphonic and phosphinic acid metabolism**. *J. Bacteriol.* 1987, **169**:710-717.
16. Hove-Jensen B, Rosenkrantz TJ, Haldimann A, Wanner BL: ***Escherichia coli* phnN, encoding ribose 1,5-bisphosphokinase activity (phosphoribosyl diphosphate forming): Dual role in phosphonate degradation and NAD biosynthesis pathways**. *J. Bacteriol.* 2003, **185**:2793-2801.
17. Cordeiro ML, Pompliano DL, Frost JW: **Degradation and detoxification of organophosphonates. Cleavage of the carbon-phosphorus bond**. *J. Am. Chem. Soc.* 1986, **108**:332-334.
18. Ahn Y, Ye Q, Cho H, Walsh CT, Floss HG: **Stereochemistry of carbon-phosphorus cleavage in ethylphosphonate catalyzed by C-P lyase from *Escherichia coli***. *J. Am. Chem. Soc.* 1992, **114**:7953-7954.
19. Shames SL, Wackett LP, LaBarge MS, Kuczkowski RL, Walsh CT: **Fragmentative and stereochemical isomerization probes for homolytic carbon to phosphorus bond scission catalyzed by bacterial carbon-phosphorus lyase**. *Bioorg. Chem.* 1987, **15**:366-373.
20. Chen CCH, Han Y, Niu W, Kulakova AN, Howard A, Quinn JP, Dunaway-Mariano D, Herzberg O: **Structure and Kinetics of Phosphonopyruvate Hydrolase from *Voriovorax* sp. Pal2: New Insight into the Divergence of Catalysis within the PEP Mutase/Isocitrate Lyase Superfamily**. *Biochemistry* 2006, **45**:11491-11504.
21. Metcalf WW, Steed PM, Wanner BL: **Identification of phosphate starvation-inducible genes in *Escherichia coli* K-12 by DNA sequence analysis of psi::lacZ(Mu d1) transcriptional fusions**. *J. Bacteriol.* 1990, **172**:3191-3200.
22. Metcalf WW, Wanner BL: **Involvement of the *Escherichia coli phn (psiD)* gene cluster in assimilation of phosphorus in the form of phosphonates, phosphite, inorganic phosphate esters, and inorganic phosphate**. *J. Bacteriol.* 1991, **173**:587-600.
23. Metcalf WW, Wanner BL: **Mutational analysis of an *Escherichia coli* fourteen-gene operon for phosphonate degradation, using TnphoA' elements**. *J. Bacteriol* 1993, **175**:3430-3442.
24. Wackett LP, Wanner BL, Venditti CP, Walsh CT: **Involvement of the phosphate regulon and the *psiD* locus in carbon-phosphorus lyase activity of *Escherichia coli* K-12**. *J. Bacteriol.* 1987, **169**:1753-1756.
25. Wanner BL, Boline JA: **Mapping and molecular cloning of the *phn (psiD*) locus for phosphonate utilization in *Escherichia coli***. *J. Bacteriol.* 1990, **172**:1186-1196.

26. Wanner BL, Metcalf WW: **Molecular genetic studies of a 10..9-kb operon in *Escherichia coli* for phosphonate uptake and biodegradation**. *FEMS Microbiol. Lett* 1992, **100**:133-139.
27. Errey JC, Blanchard JS: **Functional Annotation and Kinetic Characterization of PhnO from *Salmonella enterica***. *Biochemistry* 2006, **45**:3033-3039.
28. Dyhrman ST, Chappell PD, Haley ST, Moffett JW, Orchard ED, Waterbury JB, Webb EA: **Phosphonate utilization by the globally important marine diazotroph *Trichodesmium***. *Nature (London, U. K.)* 2006, **439**:68-71.
29. Huang J, Su Z, Xu Y: **The evolution of microbial phosphonate degradative pathways**. *J. Mol. Evol.* 2005, **61**:682-690.
30. Yakovleva GM, Kim SK, Wanner BL: **Phosphate-independent expression of the carbon-phosphorus lyase activity of *Escherichia coli***. *Appl. Microbiol. Biotechnol.* 1998, **49**:573-578.
31. Avila LZ, Draths KM, Frost JW: **Metabolites associated with organophosphonate carbon-phosphorus bond cleavage: chemical synthesis and microbial degradation of [^{32}P]-ethylphosphonic acid**. *Bioorg. Med. Chem. Lett.* 1991, **1**:51-54.
32. Adams MA, Luo Y, Hove-Jensen B, He S-M, van Staalduinen LM, Zechel DL, Jia Z: **Crystal structure of PhnH: an essential component of carbon-phosphorus lyase in *Escherichia coli***. *J. Bacteriol.* 2008, **190**:1072-1083.
33. White AK, Metcalf WW: **Two C-P lyase operons in *Pseudomonas stutzeri* and their roles in the oxidation of phosphonates, phosphite, and hypophosphite**. *J. Bacteriol.* 2004, **186**:4730-4739.
34. Vera M, Pagliai F, Guiliani N, Jerez CA: **The chemolithoautotroph Acidithiobacillus ferrooxidans can survive under phosphate-limiting conditions by expressing a C-P lyase operon that allows it to grow on phosphonates**. *Appl. Environ. Microbiol.* 2008, **74**:1829-1835.
35. Quinn JP, Kulakova AN, Cooley NA, McGrath JW: **New ways to break an old bond: the bacterial carbon-phosphorus hydrolases and their role in biogeochemical phosphorus cycling**. *Environ. Microbiol.* 2007, **9**:2392-2400.
36. Kononova SV, Trutko SM, Laurinavichus KS: **Detection of C-P-lyase activity in a cell-free extract of *Escherichia coli***. *Appl. Biochem. Microbiol.* 2007, **43**:394-398.
37. Monds RD, Newell PD, Schwartzman JA, O'Toole GA: **Conservation of the *Pho* regulon in *Pseudomonas fluorescens* Pf0-1**. *Appl. Environ. Microbiol.* 2006, **72**:1910-1924.
38. Rizk SS, Cuneo MJ, Hellinga HW: **Identification of cognate ligands for the *Escherichia coli* phnD protein product and engineering of a reagentless fluorescent biosensor for phosphonates**. *Protein Sci.* 2006, **15**:1745-1751.
39. Gebhard S, Cook GM: **Differential regulation of high-affinity phosphate transport systems of *Mycobacterium smegmatis*: identification of**

PhnF, a repressor of the *phnDCE* operon. *J. Bacteriol.* 2008, **190**:1335-1343.

40. Gorelik, M., Lunin, VV., Skarina, T. & Savchenko, A. **Structural characterization of GntR/HutC family signaling domain**. *Protein Sci*. 2006, **15**,1506-1511 .
41. Lim, M. & Cramer, C.J. ***Ab initio* calculations on PĐC bond cleavage in phosphoranyl radicals: implications for the biodegradation of organophosphonate derivatives**. *J. Phys. Org. Chem.* 1998, **11**, 149-154.

Chapter 2
Structure and functional characterization of phnP, a phosphodiesterase from the carbon-phosphorous lyase pathway

2.1 Introduction

In Gram negative bacteria such as *E. coli*, phosphonate utilization is mediated by a multi-enzyme complex called carbon-phosphorus lyase (C-P lyase). The C-P lyase pathway is encoded by the *phn* operon that is comprised of 14 genes (*phnCDEFGHIJKLMNOP)*, which allows the internalization and degradation of organophosphonates. Based on gene disruption studies of the *phn* operon in *E. coli, phnP*, the last gene in the operon, is postulated to have regulatory or accessory roles in metabolism (1, 44).

The primary amino acid sequence of phnP demonstrates homology to the metallo-β-lactamase super family of enzymes, which catalyze a wide variety of reactions using two active site metals. These enzymes are classified into 16 groups that act in several types of hydrolytic reactions, as well as in redox reactions (*2*). For instance, group I consists of the class B β-lactamases (EC 3.5.2.6) that hydrolyze the carbon-nitrogen bond of β-lactams (*3*). While most enzymes of this family require a binuclear zinc active site, some enzymes in this group appear to require only one zinc ion per active site for activity (*3*). Glyoxalase II (EC 3.1.2.6) falls in to group II, catalyzing the hydrolysis of the thioester of *S*-lactoylglutathione to produce *S*-glutathione and *D*-lactic acid.

Based on the X-ray crystal structures of several of the enzymes from this group (*4*), very flexible metal binding specificity was detected including iron, manganese and zinc. Group III contains redox active enzymes such as rubredoxin oxygen:oxidoreductase (ROO), which catalyzes the reduction of oxygen to water as the last step of three-component electron transfer chain for NAD^+ regeneration and oxygen utilization (6). The X-ray crystallographic structure of this redox protein from *Desulfovibrio gigas* reveals two domains: a β-lactamase domain with a di-iron site and a flavodoxin-like domain (*6*). Group IV consists of proteins processing the 3'-ends of pre tRNA. In this group fall the *E. coli* tRNase Z (ZipD), *Bacillus subtilis* tRNase Z and *Thermotoga maritima* tRNase Z. The tertiary structures of those enzymes exhibit a distinct protruding exosite that participates in binding tRNA substrates, as well as two catalytic zinc ions at the active site (*7-8*). The primary sequences of the hydrolytic enzymes in this family can be quite diverse and versatile; however, the short sequence motif HxHxDH is one of the few highly conserved patterns. Enzymes use this motif to bind the metal ions which are essential for activity. The metal coordination of those proteins have been extensively studied with mutagenesis and structural studies, which demonstrated that the enzymes contain a dinuclear zinc site with one zinc ion coordinated by three histidine residues and the second one is coordinated by an aspartate and two additional histidine residues. In addition, the two zinc ions are bridged by a second aspartate (*4,5,7,8,9*). The *E. coli* phnP protein belongs to the Group IV metallo-β-lactamase family. The X-ray crystallographic structure of phnP solved in collaboration with Dr. Zongchao Jia

and Kateryna Podzelinska (Queen's Biochemistry) reveals highly conserved active site residues; however, it also demonstrates distinct differences in that it has two metal binding sites per monomer: one zinc site for the structural role and a dinuclear manganese site for catalysis.

In this chapter, the crystal structure of *E. coli* phnP at a resolution of 1.4 Å will be described and a comparison with the structures of homologous enzymes from the same superfamily will also be analyzed. Its mechanistic function as a manganese dependent phosphodiesterase that can hydrolyze both bis-(*p*-nitrophenyl) phosphate and 2':3'-cyclic nucleotides will also be described with kinetic and mutagenesis studies. These analyses define *E. coli* phnP as a phosphodiesterase with a yet undefined role in the carbon-phosphorus pathway.

2.2 Experimental procedures and methods

2.2.1 Materials.

All chemicals were purchased from Sigma Aldrich (Oakville, Ontario and US). Luria Bertani (Miller) agar and Luria Bertani (Miller) broth, HEPES, sodium chloride and glucose were from Fisher Biosciences, Canada. Restriction enzymes and T4 DNA ligase were obtained from Fermentas or New England Biolabs. Oligonucleotides were synthesized by Sigma Genosys. DNA sequencing was performed by Robarts Research Institute (London, Ontario) and TCAG sequencing facility (The Hospital for Sick Children, Toronto, Ontario). Ampicillin was obtained from Roche Diagnostics Canada, IPTG was from Invitrogen, Pfu turbo DNA polymerase was from Invitrogen, and enterokinase was obtained from New England Biolabs. Protein standards for gel filtration column calibration, including apoferritin (440 kDa; 2.5 mg/ml), β-amylase (200 kDa; 4 mg/ml), alcohol dehydrogenase (150 kDa; 8 mg/ml), bovine serum albumin (66 kDa; 8 mg/ml), carbonic anhydrase (29 kDa; 3 mg/ml), and cytochrome c (13.6 kDa; 1,5 mg/ml) were purchased from Sigma-Aldrich (Oakville, Ontario). All protein molecular weight standards used in SDS-PAGE were purchased from BioRad. Ni-NTA resin was from Qiagen.

2.2.2 Over-expression and purification of His_6 tagged phnP

PhnP with a C-terminal His_6 tag was expressed by co-transformation of the plasmids pUHE23-2-phnP (obtained from Bjarne Hove-Jensen, University of Cobenhagen, Denmark) and pLacI (Novagen) into *Escherichia coli* BL21(DE3) heat shock competent cells (Novagen). pLacI is a chloramphenicol resistant plasmid that encodes the *lac* repressor protein. Co-transformation of pLacI was necessary as pUHE23-2-phnP lacks a *lac* repressor gene necessary to maintain strict regulation of transcription. Cells were grown in Luria-Bertani (Miller) medium with ampicillin (100 µg/mL) and chloramphenicol (30 µg/mL) in an air shaker (250 rpm, 30 ºC) until the A_{600} of the culture reached 0.6. At this point, the culture was induced with 0.5 mM IPTG. Approximately 7-10 hours at 15 °C, a second aliquot of ampicillin was added. After further incubation at 15 ºC for 20 hours, cells were harvested by centrifugation at 3000 × g at 4 ºC for 20 minutes. The cell pellet were then resuspended in 50 mM phosphate, 10 mM imidazole, 300 mM NaCl, pH 7.2 and lysed with an Emulsiflex-C5 homogenizer (Avestin, Canada). The lysed cells were then centrifuged at 40,000 × g at 4 ºC for 30 minutes. The supernatant was passed through Ni-NTA column and the His_6 tagged phnP was eluted with a gradient from 10 mM to 500 mM imidazole over 10 column volumes at a flow rate of 5 ml/min using an AKTA FPLC (GE Healthcare Life Sciences, USA). The eluted frations were analyzed by 15% SDS-PAGE gels followed by Coomassie Blue G-250 staining. Fractions containing >95% pure phnP as demonstrated by SDS-PAGE analysis were pooled, concentrated with Millipore Amicon Ultra centrifugal ultrafiltration devices (10,000

MWCO), and then further purified by gel filtration using a Sephacryl S-200 column (1.6 cm x 60 cm; GE Healthcare, USA) pre-equilibrated with 50 mM HEPES, pH 7.2, 150 mM NaCl at a flow rate of 0.5 ml/min. The pooled fractions from the gel filtration column were concentrated by ultrafiltration (10,000 MWCO, Amicon), followed sterile filtration (0.22 µm syringe filter). The concentration of purified protein was determined from the absorbance at 280 nm using the calculated extinction coefficient of ε_{280} = 33,835 M^{-1} cm^{-1}. The extinction coefficient was calculated from the amino acid sequence of phnP (34) using the web-based ProtParam tool (http://ca.expasy.org/tools/protparam.html). PhnP was also produced as a selenomethionine derivative in the methionine auxotroph strain DL41(DE3) grown in M9 SeMET High Yield media (Medicilon Inc., USA). The selenomethionine-labelled phnP was purified using the same procedure that was used for the native protein.

2.2.3 Cloning, expression and purification of tag free phnP

The pUHE23-2-phnP encodes phnP with a C-terminal His_6 tag, which cannot be removed by a protease. To obtain untagged phnP for ITC analysis, the following construct was used. The pUHE-23-2 phnP was used as a template for PCR. *Pfu* turbo DNA polymerase (Invitrogen) was used with oligonucleotides 5'-CGTTGGATCCGACGACGACGACAAAGCCATGGGTATGAGC CTGACCCTCACGC-3' and 5'-AATTAAGCTT**TTACTATCA**CGCCACCCCAA TCTCCATC-3' as forward and reverse primers, respectively, thereby introducing flanking *Bam*HI*, Nco*I*,* and *Hind*III restriction sites (underlined) and three stop codons (bold type). The PCR

product was digested with *Bam*HI and *Hind*III and ligated into the respective sites of the pQI-pD, yielding the pQI-pD-phnP plasmid. The pQI-pD-phnP plasmid encodes a His_6 tag at the N-terminus of the protein D, which is linked to phnP by an enterokinase peptide sequence. The His_6 tag can be removed from the final gene product by enterokinase cleavage between protein D and phnP (**Figure 1**). pQI-pD vector is a derivative of pQE-80L (a gift from Prof. Andreas Plückthun, Biochemistry Institute, University of Zürich) that is under control of a bacteriophage T5 promotor / *lac* operator element and specifies ampicillin resistance. The correct *phnP* nucleotide sequence was confirmed by sequencing both DNA strands with the same primers as used for PCR and the two following sequencing primers: 5'–CGTTATGAGGATGTGCTC-3' and 5'–GGTGATTCTGACCCATATC-3'.

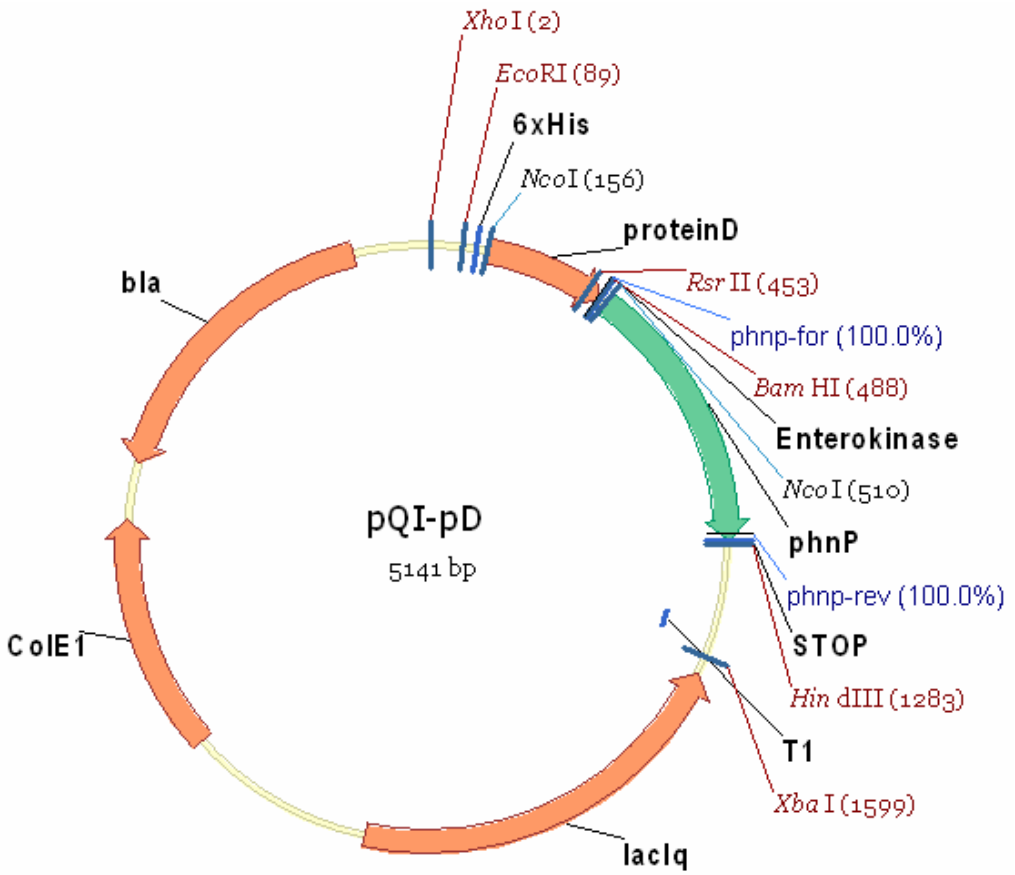

Figure 2-1. Scheme of the pQi-pD-phnP construct.

E. coli BL21 cells (Novagen) harboring pQI-pD-phnP were grown in Luria-bertani medium supplemented with 100 µg/ml ampicillin to an absorbance (A_{600}) 0.6 at 30 ºC followed by an induction with 0.5 mM IPTG at 15 ºC for 20 h. Purification of pD-phnP was carried out the same way as phnP with a C-terminal His tag. Cleavage of the His_6-tag was performed by adding 32 ng of enterokinase

and incubating at 25 ºC overnight. Ni-NTA agarose was used to remove the cleaved tag and uncleaved protein from the tag-free pQI-pD-phnP. Purification of pQI-pD-phnP from enterokinase and remaining contaminants was performed by gel filtration using a Sephacryl S-200 column (1.6 cm x 60 cm, GE Healthcare Life Sciences, USA) equilibrated with 50 mM Tris/HCl, 150 mM NaCl, pH 7.1 at a flow rate of 0.5 ml/min.

2.2.4 Substrate screening of phnP

General enzymatic screens for phosphatase, phosphodiesterase, esterase, protease, dehydrogenase, and oxidase activities of phnP were performed using native phnP by Dr. Alexander Yakunin and Prof. Aled Edwards at the Banting and Best Department of Medical Research, University of Toronto. Phosphodiesterase activity with 2':3'-cyclic nucleotide monophosphates was measured using a quantitative assay based on measurement of the alkaline phosphatase-sensitive nucleotide product as described by Yakunin *et al*. (10). The activity was assayed in an 80 µL reaction containing 50 mM Tricine (pH 8.5), 5 mM of metal (Mn^{2+}, Ni^{2+}, Co^{2+} or Mg^{2+}), 0.25 mM substrate, 2 µg of phnP incubated at 37 ºC for 20 minutes. The reaction was stopped by the addition of 80 µL of 2 x alkaline phosphatase buffer (0.2 M CHES buffer, 10 mM $MgCl_2$, pH 9.0) then incubated with 1 unit of alkaline phosphatase for 10 min. at 37 ºC. The reaction was terminated by the addition of Malachite Green reagent (11), and the production of free phosphate was measured at 630 nm.

2.2.5 Kinetic analysis of phnP

Standard conditions for phosphodiesterase activity with the substrate bis-(*p*-nitrophenyl) phosphate (bpNPP) were 50 mM Tris, pH 7.4, 150 mM NaCl, 1 mg/mL BSA, and 1 mM bpNPP. Release of *p*-nitrophenolate was continuously monitored for 1-2 minutes at 405 nm on a Cary 300 Bio UV-visible spectrophotometer (Varian) thermostated at 25 ^{o}C. The reaction rate was determined from initial rates using the molar extinction coefficient ε_{405} = 11,500 M^{-1} cm^{-1} (pH 7.4) for the product *p*-nitrophenolate (12). To determine the kinetic parameters k_{cat} and K_M, the initial velocities measured at various substrate concentrations were fitted to the Michaelis Menten equation (**Equation 1)** using GraFit 6.0 (Erithacus Software Limited, UK). Activity toward thymidine-5'-monophosphate-*p*-nitrophenylester was determined similarly. Kinetic analysis of the substrate 2':3'-cyclic nucleotide monophosphate was determined as described by Yakunin *et al*. (*10*). The reaction was assayed in 50 mM Tris, pH 7.4, 150 mM NaCl in a total volume of 200 µL. The reaction was initiated with 50 nM of enzyme and incubated at 25 ºC for 20 minutes, followed by quenching with 200 µL 2 x calf intestine alkaline phosphatase (CIAP) buffer (0.2 M Trizma,10 mM $MgCl_2$, pH 9.0). One unit of calf intestine alkaline phosphatase was added and incubated at 25 ºC for 10 minutes. Released phosphate was assayed with Malachite Green reagent (11). Background absorbance was subtracted from each reaction. The kinetic parameters K_M and k_{cat} were determined from the dependence of the initial reaction velocities on the substrate concentration by

Michaelis - Menten plot according to **Equation I** with GraFit 6 (Erithacus Software Limited, UK).

$$v = \frac{V_{\max}[S]}{K_m + [S]} \qquad \textbf{Eq. 1}$$

The allosteric characteristic of phnP was determined from the kinetic parameters k_{cat}, K_m and the Hill coefficient, n_H, calculated from the Hill equation (**Equation 2**) by nonlinear regression analysis implemented in Grafit 6. Each measurement was performed in triplicate for each concentration of the substrate.

$$v = \frac{V_{\max}[S]^n}{K^n + [S]^n} \qquad \textbf{Eq. 2}$$

The analysis of zinc inhibition toward the hydrolysis of bpNPP by phnP was carried out in reactions containing 50 mM Tris, 150 mM NaCl, pH 7.4, 1 mM bpNPP and various concentrations of zinc from 0-200 μM. The K_i value for zinc was determined using a “range finder” assay at fixed bpNPP concentration and various inhibitor concentrations and plotting the data in a Dixon plot (1/v vs 1/[I]), for which the intersection with the X-axis gives an approximate value of K_i. For phosphate and vanadate inhibition, assays were performed in 50 mM Tris, 150 mM NaCl, pH 7.4 using 1 mM bpNPP as substrate, 1 mM of Mn^{2+} and various

concentrations of inhibitor (phosphate, vanadate). The approximate K_i values for phosphate and vanadate were determined by using the "range finder" and plotting the data in a Dixon plot. A full K_i determination was then carried out at a series of five different substrate concentrations bracketing the K_M value (1/5 to 5 x K_M) with each of five inhibitor concentrations ranging from 1/5 to 5 times of the estimated K_i value. All the data were fit to **Equation 3** describing competitive inhibition, where [I] is the inhibitor concentration and [S] is the substrate (bpNPP) concentration and K_i is the inhibition constant.

$$v = \frac{V_{\max}[S]}{K_m\left[1 + \frac{[I]}{K_i}\right] + [S]} \qquad \text{Eq. 3}$$

2.2.6 Mutational Analysis

Site directed mutagenesis of phnP was carried out using either the QuikChange™ site-directed mutagenesis protocol (Stratagene) or by using 4-primer overlap extension PCR mutagenesis with *Pfu* turbo DNA polymerase (Stratagene). Overlap extension PCR mutagenesis involves designing two mutagenic primers containing the mutation that are partially or completely complementary to each other. Each mutagenic primer is used separately with a flanking primer (5' or 3' to the gene of interest). Two mutated gene fragments are generated after the first step of PCR, and the two fragments are put together in the second step of PCR, where they anneal in the complementary region and

generate the full length product containing the introduced mutation. All the mutagenic primers used are listed in **Table 2-1**. The wild type phnP gene in pUHE23-2-phnP was used as a template. The mutant sequences were verified by sequencing both DNA strands. Expression and purification of mutants were carried out at the same conditions as described above with wild type phnP. Kinetic analysis of mutant proteins were performed the same way as wild type phnP by fitting the data to Michaelis–Menten plot utilizing Grafit 6 (Erithacus Software Limited, UK).

Table 2-1 PhnP mutagenic primers

Mutant		Sequence (5'-3')	Mutagenic method
H78A	For	TTGCTGACGCATTATGCGATGGATCACGTCCAG	QuickChange™
	Rev	CTGGACGTGATCCATCGCATAATGCGTCAGCAA	
D80A	For	ACGCATTATCATATGGCTCACGTCCAGGGGCTG	QuickChange™
	Rev	CAGCCCCTGGACGTGAGCCATATGATAATGCGTC	
T75A	For	CCAGCAGTTTTTGCTGGCGCATTATCATATGGATC	QuickChange™
	Rev	GATCCATATGATAATGCGCCAGCAAAAACTGCTGG	
D164A	For	GTGGCGTGGCTGTCTGCCACCGCAGGTTTGCCG	QuickChange™
	Rev	CGGCAAACCTGCGGTGGCAGACAGCCACGCCAC	
H200A	For	GATGCACCGCGTAATGCCTGTGATTTAAATACC	QuickChange™
	Rev	GGTATTTAAATCACAGGCATTACGCGGTGCATC	
H222A	For	CGGGTGATTCTGACCGCGATCAGCCACCAGTTTG	QuickChange™
	Rev	CAAACTGGTGGCTGATCGCGGTCAGAATCACCCG	
D187A	For	CAGGTAATGGTGATGGCGTGCAGTCACCCGCCG	QuickChange™
	Rev	CGGCGGGTGACTGCACGCCATCACCATTACCTG	
C21S/C23S/C26S	For	CGGCATGGGGCTCCGAGTCTGCGGCCTCCGCCAGAGCGCG	QuickChange™
	Rev	CGCGCTCTGGCGGAGGCCGCAGACTCGGAGCCCCATGCCG	
D54A	For	CGCAATCACCCTGATCGCCGCCGGGCTGCACGATC	4-primer PCR
	Rev	GATCGTGCAGCCCGGCGGCGATCAGGGTGATTGCG	
C21S	For	GTTCCGGCATGGGGCTCCGAGTGTGCGGCCTGC	4-primer PCR
	Rev	GCAGGCCGCACACTCGGAGCCCCATGCCGGAAC	
phnP-flanking	For	CACACAGAATTCATTAAAGAGG	
phnP-flanking	Rev	GAGCCATGGTTATTAATGGTG	

Modified codons are underlined. For: forward primers; Rev: reverse primers.

2.2.7 Metal dependence of the *in vitro* processing reactions

To analyze which metal ions are required for the hydrolysis reaction, the apo-enzyme was obtained according to Vogel *et al*. (*12*). PhnP was first incubated with 10 mM EDTA for 1h at 4 ºC, followed by dialysis of the reaction mixture to remove the EDTA-metal complex and excess EDTA. Apo-enzyme was then incubated with different metals by addition of 0.2 mM Zn^{2+}, Mn^{2+}, Ni^{2+}, Co^{2+}, Ca^{2+}, Fe^{2+}, Fe^{3+} and Mg^{2+}. After 1 hour of incubation at 4 ºC, activity was assayed on both apo and metal saturated enzymes. To determine that phnP is a manganese dependent enzyme, the phnP sample initially saturated with 0.2 mM Zn^{2+} was incubated with 10 mM EDTA a second time to remove Zn^{2+} from the active site, then dialyzed to remove the EDTA-metal complex and excess EDTA, followed by incubation with 0.2 mM Mn^{2+}. The metal content of phnP was determined by ICP-MS (see below). The activity of metal reconstituted enzymes was done in 50 mM Tris, 150 mM NaCl, pH 7.1 with a Cary 300 Bio UV-visible spectrophotometer (Varian) by monitoring absorbance at 405 nm and using bpNPP as the substrate.

2.2.8 Metal Analysis by ICP-MS

The metal content of wild type phnP as purified and phnP mutants were analyzed using a Varian Inductively Coupled Plasma Mass Spectrometer (ICP-MS, Ultra Mass) by Prof. Diane Beauchemin in the Department of Chemistry at Queen's University. A scan of various divalent metals such as Zn^{2+}, Mn^{2+}, Cu^{2+}, Ni^{2+}, Co^{2+}, Ca^{2+}, and Mg^{2+} was performed first to determine which metal ions

were present in the wild type phnP preparation as isolated from *E. coli*. Samples for ICP-MS were treated in the following way: wild type phnP was dialyzed into 10 mM HEPES, pH 7.2 and diluted to a concentration of 10 μM before use. To determine the total zinc and manganese present in wild type phnP and mutants, proteins were treated the same way described as above. Standard curves of both manganese and zinc from 0 ppm to 1000 ppm were prepared. The total amount of manganese and zinc present in the protein was determined based on the standard curves. The metal content data are the average of three replicate trials.

2.2.9 pH profile

The pH dependence of k_{cat} and K_m values were determined using the 'substrate depletion' method at low substrate concentration (where [S] << K_M) according to **Equation 4** (*13*). Assays were monitored at 405 nm with a Cary UV 300 thermostated at 25 ºC using bpNPP as the substrate. Reactions were assayed using a final concentration of substrate at 150 μM, 1 mM Mn^{2+}, 50 mM buffers, and 1 mg/mL BSA in a total volume of 600 μL. The reaction was initiated with 0.5 μM of enzyme. Assays were carried out at pH ranges from 5.0 to 8.6. 50 mM MES buffer was used from pH 5 to 6.3, 50 mM Bis-Tris was used from pH 6.3 to 7.1, and 50 mM Tris was used from pH 7.1 to 8.6. Data was collected over 3-5 half lives and fit to a first order rate equation (**Equation 4**) using GraFit 6 (Erithacus Software Limited, UK). The observed rate constant (k_{obs}) determined from this curve, adjusted for the enzyme concentration, gives k_{cat}/K_M. The data

for k_{cat}/K_M dependence on pH were fit to a bell ionization curve (**Equation 5**) using GraFit 6.

$$A_{405}^{t} = A_{405}^{0}(1 - e^{(-k_{obs}t)}) + offset \qquad \textbf{Eq. 4}$$

$$k_{cat} / K_M = \frac{\text{limit x } 10^{(pH-pKa1)}}{10^{(2 \text{ x } pH - pKa1-pKa2)} + 10^{(pH - pKa1)} + 1} \qquad \textbf{Eq. 5}$$

2.2.10 Isothermal Titration Calorimetry (ITC)

Prior to the ITC analysis, purified phnP was dialyzed overnight into a buffer of 50 mM HEPES, 150 mM NaCl, pH 7.2 at 4 °C. The binding interaction between Mn^{2+} and phnP was measured using a VP-ITC microcalorimeter (MicroCal LLC, Northampton, MA) at 30 °C by Mr. Kim Munro (Protein Function and Discovery, Department of Biochemistry, Queen's University). A Mn^{2+} solution was prepared in the same buffer saved from the dialysis of phnP. All samples were passed through 0.22 µm filters and extensively degassed with stirring prior to use. Titrations were performed by injecting 10 µL aliquots of 14 mM $MnCl_2$ into the ITC sample cell (1.5 mL) containing phnP (0.78 mM) equilibrated at 30 ºC. The integrated heat of interaction values were fit using Origin 7.0 ITC data analysis software provided by MicroCal. The initial titration point was always discarded. The data were fit to a 2-site binding model using MicroCal software, which yielded the equilibrium association constant (K_a), the stoichiometry (n), and enthalpy (ΔH). The Gibbs free energy (ΔG) and entropy ($T\Delta S$) were calculated

using the equation ΔG = -RTlnK_a = ΔH - TΔS.

2.2.11 TLC analysis

The product of the hydrolysis of 2':3'-cyclic nucleotides were analyzed by TLC on cellulose plates (J.T. Baker Inc., Phillipsburg, Germany) in saturated ammonium sulfate, 3 M sodium acetate, isopropyl alcohol (80:6:2) as described previously (*14*). Reactions containing 100 µL 50 mM Tris, 150 mM NaCl, pH 7.2, 1 mM Mn^{2+}, and 20 mM 2',3'-cAMP were incubated for 1 hour at 37 ºC with 2 µM of wild type phnP or 5 µM of phnP mutant D80A . A control reaction without phnP was also carried out under the same conditions simultaneously. All the reactions were passed through an Amicon Ultra filtration filter (MWCO 10,000) to remove the enzyme. The flow-through was used to load the cellulose TLC plate. The reaction products and nucleotides standards were visualized under UV light (254 nm).

2.2.12 *In vitro* RNase processing assay (analysis performed by Kateryna Podzelinska, Queen's Biochemistry)

The RNase activity of phnP was assayed with the "RNaseAlert Lab Test Kit" from Ambion (catalogue # 1964). The substrate is a fluorescently labelled RNA oligonucleotide that fluorescences at λ = 520 nm when cleaved by RNase. RNase activity of phnP was carried out with wild type phnP and D80A and H200A variants in a mixture (50 µl) containing 20 mM HEPES (pH 7.5), 150 mM NaCl and 10 µM $MnCl_2$ at 37 ºC for an hour. A control reaction was performed

with 0.5 pg / well RNase A. PhnP wild type or mutant proteins were assayed at 10 ng / well. A negative control was performed the same way as the processing reactions except that no enzyme (wild type or mutants) or RNase A was added.

2.3 Results and discussion

2.3.1 Over-expression and purification of *E. coli* phnP

Expression of phnP as a C-terminal His_6 tagged fusion protein in *E. coli* yielded soluble recombinant protein in amounts of 150-180 mg/liter of culture. After the first purification step using a Ni-NTA column, the eluted fractions after FPLC contained highly pure protein as demonstrated by SDS-PAGE (**Figure 2-2A**), The relative mobility on SDS-PAGE corresponds well to the calculated molecular mass for the monomer of 28,670 Da. This was also confirmed by MALDI-MS (**Figure 2-2C**), where two major ions with *m/z* = 28,540 and *m/z* = 28,675 were observed. The first corresponds to phnP with the loss of the first methionine residue, possibly due to the post translational modification by *E. coli* methionine amino peptidase, and the second corresponds to a matrix molecule (2,5-dihydroxybenzoate, MW = 154) attached to phnP with the loss of the first methionine. The mass of phnP is within the error range of MALDI measurement; however, ESI-MS is more accurate to determine the mass. PhnP used for crystallization was further purified by size exclusion chromatography, after which it was > 95% pure as demonstrated by SDS-PAGE (**Figure 2-2B**). In solution phnP forms a dimer with a calculated mass of 48.2 kDa based on its relative elution volume from a calibrated size exclusion column.

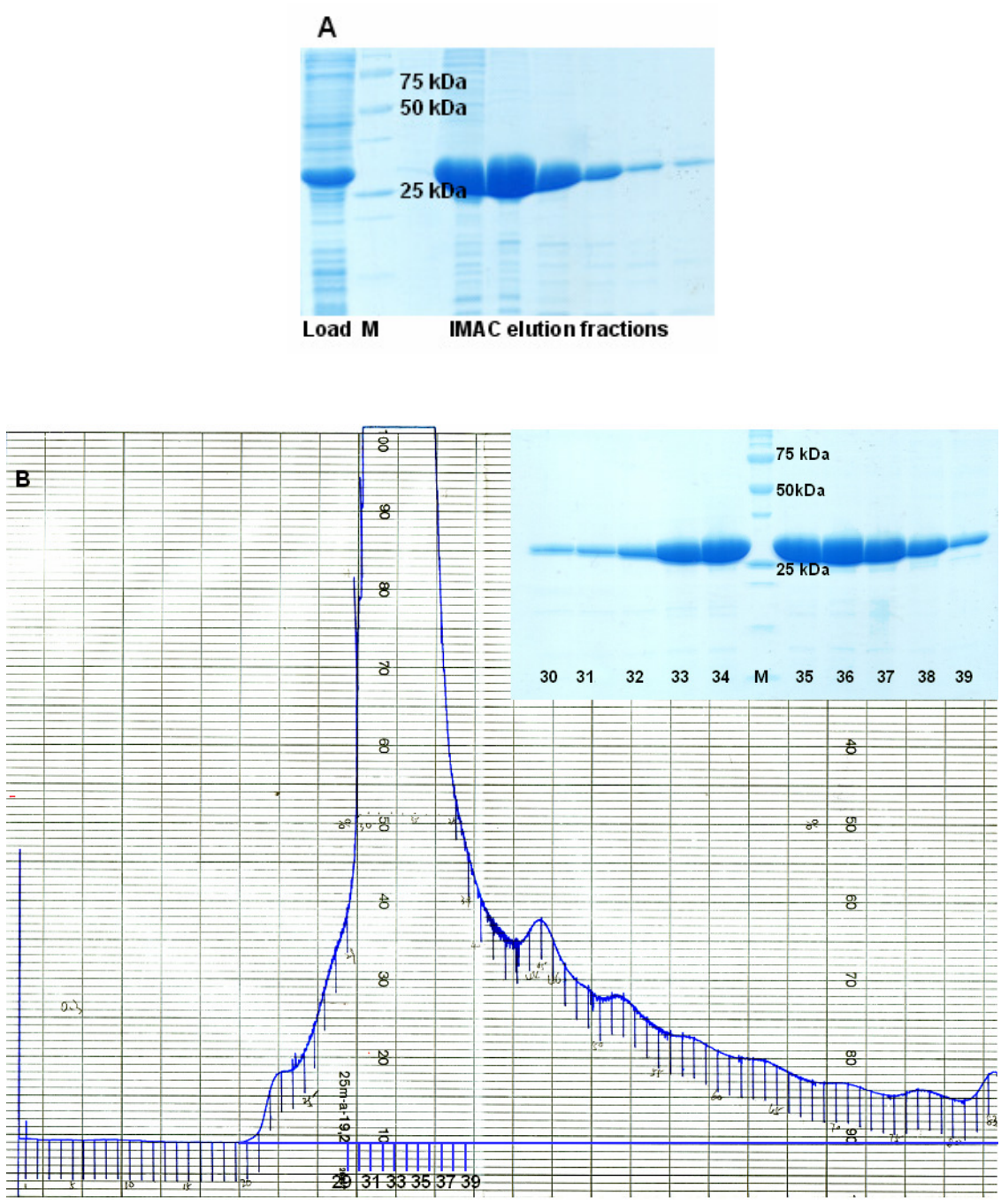

Figure 2-2. Purification of phnP**.** (A) Fractions from IMAC purification. L = load of crude lysate supernatant from *E. coli*; M = BioRad precision plus protein marker. (B) Size exclusion chromatogram of phnP. Insert is a 15% SDS-PAGE gel of the eluted fractions.

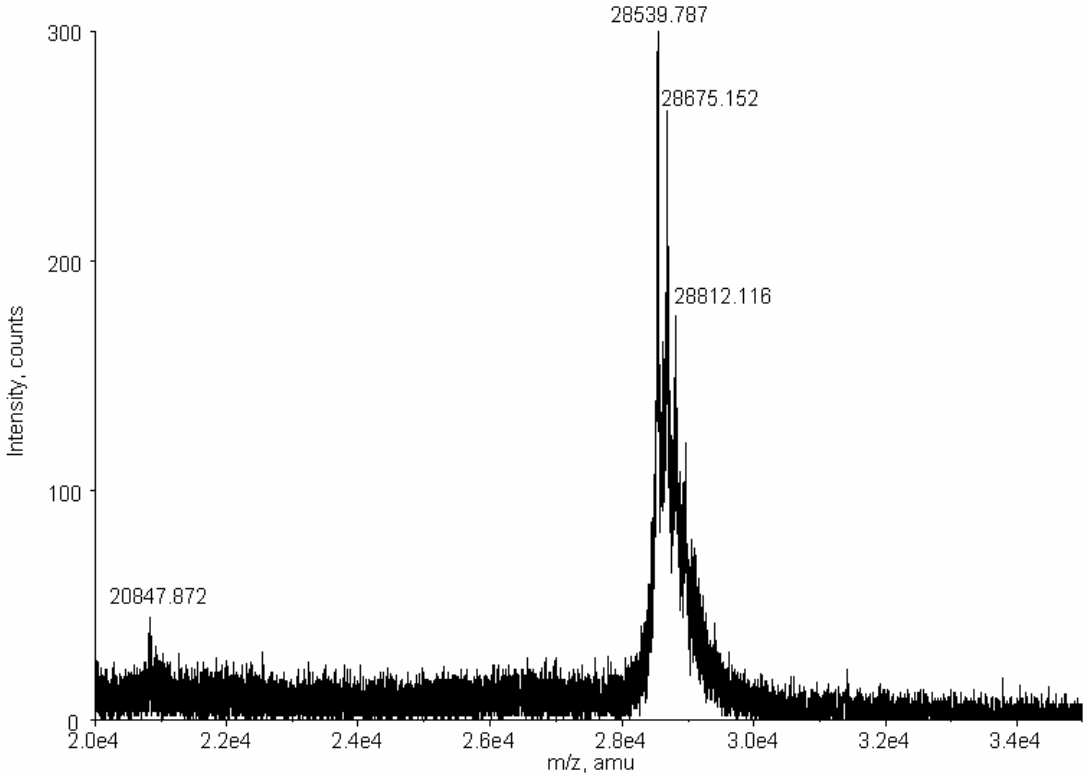

Figure 2-2C. MALDI-MS of phnP (theoretical MW = 28,670 Da).

2.3.2 PhnP has phosphodiesterase activity

A general enzymatic screen for phosphodiesterase activity identified phnP as a phosphodiesterase that can hydrolyze bpNPP into *p*-nitrophenol and *p*-nitrophenyl phosphate. Monoesterase activity toward *p*-nitrophenyl phosphate was not detected. The enzymatic activities of phnP toward tpNPP and *p*-nitrophenylphosphorylcholine were also tested. PhnP demonstrated very weak activity toward tpNPP with a k_{cat} of 0.08 ± 0.02 s^{-1}, and k_{cat}/K_M of 5.8 $s^{-1}M^{-1}$. This k_{cat}/K_M value is 74 times smaller than that for bpNPP (**Table 2-5**), indicating that phnP does not likely cleave the 3'-5' phosphodiester linkages of oligonucleotides.

PhnP did not exhibit hydrolytic activity toward *p*-nitrophenylphosphorylcholine, suggesting that phnP is not likely a phospholipase either. The structures of the substrates tested and the reaction products catalyzed by phnP are illustrated in **Figure 2-3**.

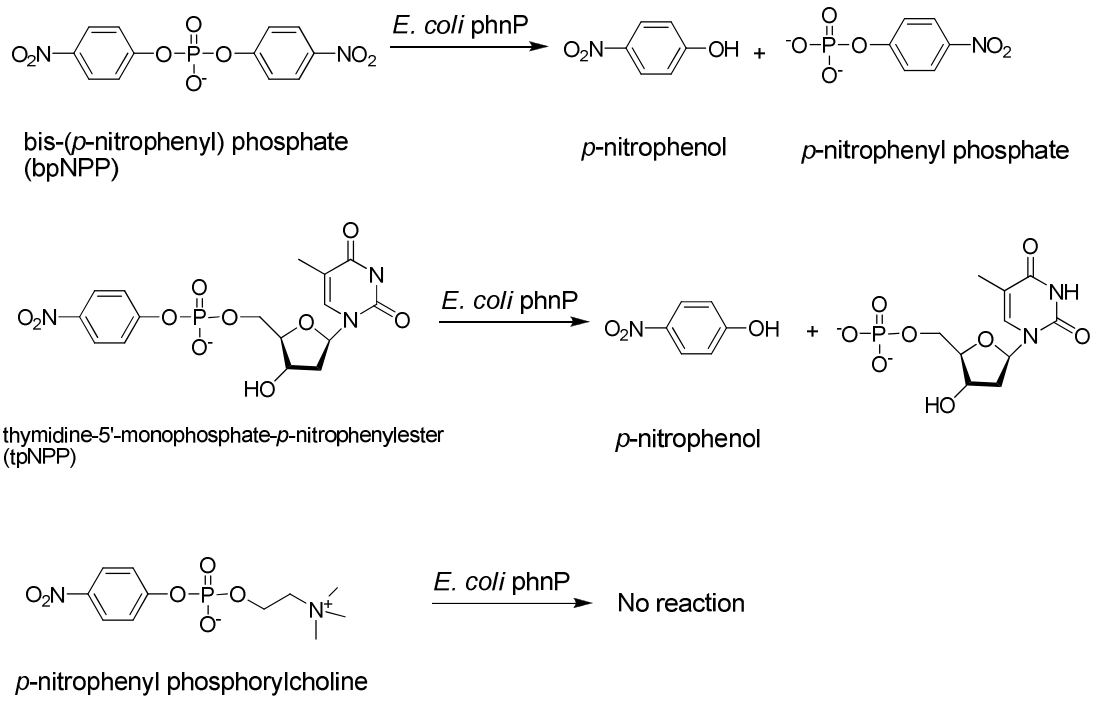

Figure 2-3. Hydrolytic reactions catalyzed by *E. coli* phnP.

In addition, phnP demonstrated allosteric phosphodiesterase activity towards bpNPP. The dependence of the velocity on the substrate concentration for bpNPP was measured with phnP and the data were fitted and analyzed

according to the Hill equation (**Equation 2**). The sigmoidal curve for bpNPP indicated modest positive cooperativity with a Hill coefficient n_H = 1.55 ± 0.04 (**Figure 2-4**), suggesting that the binding of a substrate molecule in one active site slightly increases the affinity for the second molecule in a second active site. Due to the low value of the Hill coefficient the initial rate data for phnP and its mutants were fit with the standard Michaelis-Menten equation, which results in only a modest change in k_{cat} and K_M values (**Table 2-2**). This behavior was not observed with 2':3'-cyclic nucleotides, in which the enzyme follows Michaelis-Menten kinetics (**Figure 2-8**).

Table 2-2 Kinetic parameters obtained with Michaelis-Menten plot and Hill equation

Method	K_M (mM)	k_{cat} (s^{-1})	k_{cat}/K_M ($s^{-1}M^{-1}$)	Chi square
MM plot	3.5 ± 0.6	1.06 ± 0.09	303	0.0016
Hill equation	2.7 ± 0.1	0.8 ± 0.01	296	$3.07X\ 10^{-5}$

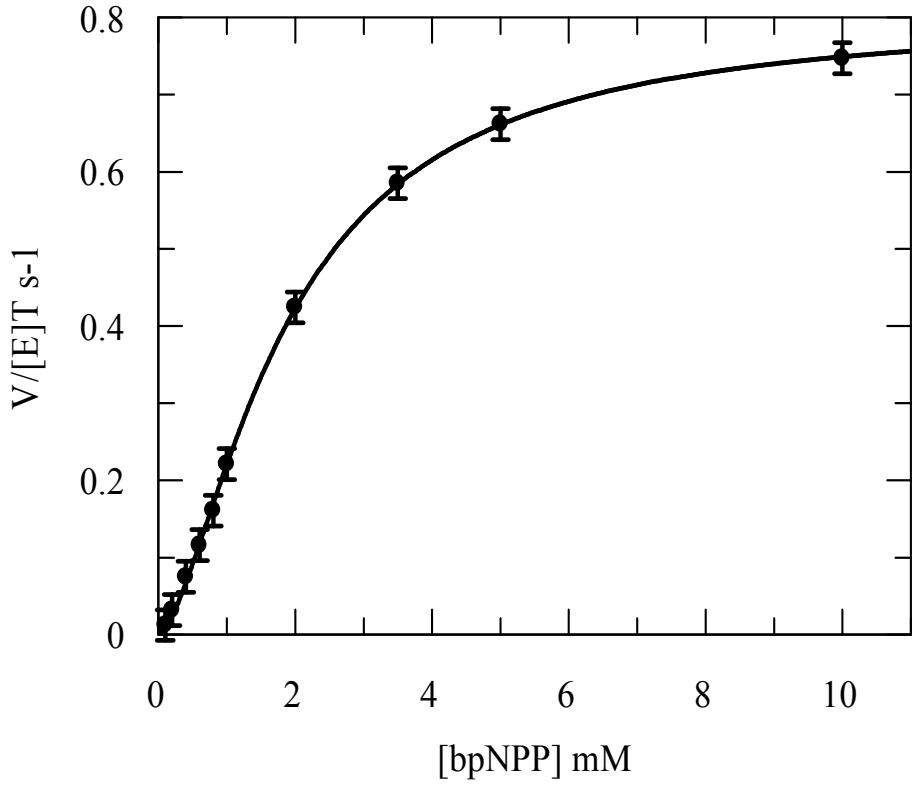

Figure 2-4. Cooperativity of *E. coli* phnP. Measurements were carried out in triplicate. The line represents the best fit of the data using the Hill equation. The fit yielded K_M = 2.7 ± 0.1 mM, k_{cat} = 0.8 ± 0.01 s^{-1}, and Hill coefficient n_H = 1.55 ± 0.04 for bpNPP.

2.3.3 Metal content determined by ICP-MS

The X-ray crystal structure of wild type phnP revealed two distinct metal binding sites per monomer. ICP-MS identified these as containing zinc and manganese. The metal content of phnP expressed in LB medium and purified after gel filtration was 0.13 manganese, and 1.26 zinc per protein (**Table 2-3**). The metal occupation of manganese less than one may be attributed to a loss of metal during purification or to a limited metal availability during over-expression in *E. coli*. However, even with this amount of manganese, phnP could hydrolyze bpNPP with a k_{cat}/K_M of 36.2 M^{-1} s^{-1}. With 1 mM additional Mn^{2+} present, the k_{cat}/K_M increased to 412 $M^{-1}s^{-1}$ (**Table 2-4**). Zinc binds more tightly than manganese, as evidenced by the analysis with ICP-MS. When phnP after gel filtration was incubated with 10 mM EDTA for one hour at 4°C, most of the manganese was lost (0.01 Mn^{2+} per protein was left), while most the zinc remained with it (0.78 Zn^{2+} per protein) (**Table 2-3**), indicating that the zinc is tightly bound.

Table 2-3. **Metal content determined by ICP-MS with phnP WT**

sample (10 μM)	[Mn] μM	[Zn] μM	Mn / Enz	Zn / Enz
phnP as purified	1.3 ± 0.1	13.8 ± 1.1	0.13	1.38
Apo-phnP treated with 10 mM EDTA	0.06 ± 0.01	7.8 ± 0.03	0.01	0.78

Data represents average of three replicates for each sample.
N.D.: not detected; value the same as the negative control (10 mM HEPES)

2.3.4 Metal dependence of phnP activity

The nature of the metal ions is very important for the activity of enzymes from the metallo-β-lactamase superfamily (2-5, 9, 12, and 15). To analyze which metal ions are required for the hydrolysis of bpNPP by phnP, reactions were carried out with EDTA treated enzyme (affording 0.78 Zn^{2+} and 0.01 Mn^{2+} per phnP monomer). Treatment of phnP with 10 mM EDTA resulted in essentially inactive enzyme (>600-fold rate decrease in activity in reaction with bpNPP) even with 0.78 Zn^{2+} present in the enzyme, suggesting that the phosphodiesterase activity of phnP is Mn^{2+} dependent, whereas zinc is bound in a non-catalytic site. When extra metals such as Ca^{2+}, Mg^{2+}, Fe^{2+}, Fe^{3+}, Co^{2+}, Zn^{2+}, Cu^{2+}, Ni^{2+}, or Mn^{2+} (0.2 mM each) were added to the reaction, Ca^{2+}, Mg^{2+}, Fe^{3+}, and Cu^{2+} did not recover significant hydrolytic activity, Fe^{2+}, Co^{2+}, Zn^{2+} showed very weak activity (~25 times less than Mn^{2+} and Ni^{2+}), Ni^{2+} and Mn^{2+} recovered the greatest activity toward bpNPP relative to the activity of phnP as purified. The loss of activity upon treatment with metal ion chelator and the manganese and nickel mediated restoration of activity suggest that manganese and nickel can bind in the phnP active site and support phosphodiesterase activity (**Figure 2-5**). Manganese, zinc, iron and nickel are known to support the hydrolytic reactions catalyzed by metalloenzymes such as glyoxalase(II) (which remarkably incorporates zinc, manganese or iron at the active site) and MJ0936, a phosphodiesterase from *Methanococcus jannaschii*(16) using bpNPP as a substrate. As for tRNase Z from *A. thaliana,* the chelator-treated enzyme remained capable of hydrolyzing bpNPP to the same extent as the “as isolated” enzyme, indicating the leftover

zinc ions (0.76 per dimer) are sufficient for bpNPP hydrolysis. Upon addition of other metals such as Mg^{2+}, Ca^{2+}, Mn^{2+}, Fe^{2+}, or Zn^{2+} to the bpNPP reaction, only Mn^{2+} and Zn^{2+} increased bpNPP cleavage 3-fold and 2-fold, respectively (*15*). To explore which divalent cations are more effective in activating bpNPP hydrolysis by phnP, k_{cat} and k_{cat}/K_M values were also determined for several metal cations at fixed, saturating metal concentrations. A 4-fold higher k_{cat} value and k_{cat}/K_m value were observed with Ni^{2+} compared with Mn^{2+} (**Table 2-4**). The specificity constant with zinc was considerably lower, with a k_{cat}/K_M value of 44 s^{-1} M^{-1} (**Table 2- 4**). In fact, excess zinc appears to inhibit the hydrolysis reaction with a K_i value of 235 μM, further supporting that phnP is not likely a zinc dependent, but rather a manganese and nickel dependent hydrolase.

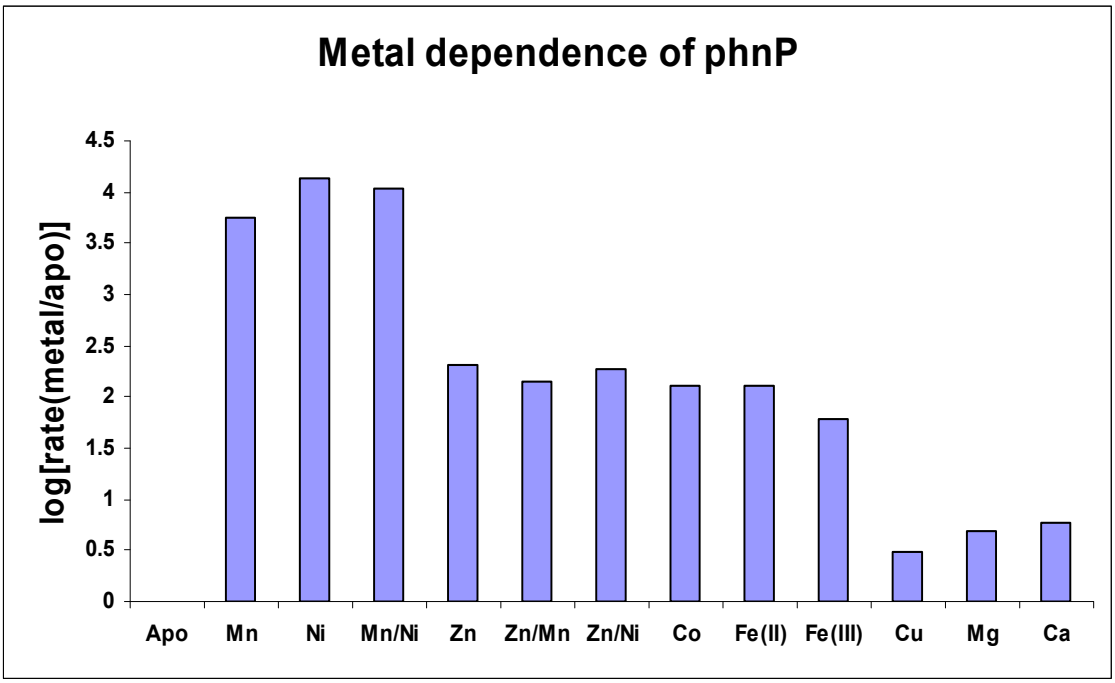

Figure 2-5. Metal dependence of phosphodiesterase activity of phnP with bpNPP as the substrate. The y-axis plots the log of the ratio of metal reconstituted enzyme relative to the metal stripped or apo enzyme.

Table 2-4 Kinetics of phnP with bpNPP and different metals

[Metal]	[phnP] μM	k_{cat} (s^{-1})	K_M (mM)	k_{cat}/K_M ($s^{-1}M^{-1}$)	K_M^{app} (μM)
Mn (1 mM)	0.5	1.19 ± 0.08	2.90 ± 0.50	412	130 ± 20
Ni (1 mM)	0.5	4.14 ± 0.20	2.30 ± 0.30	1770	94 ± 19
Zn (0.1 mM)	0.5	0.030 ± 0.001	0.68 ± 0.07	44	

The kinetic parameters were obtained with apo-phnP (phnP as purified was treated with 10 mM EDTA)

2.3.5 ITC analysis of phnP metal binding

ITC experiments were carried out to determine and compare the manganese-binding affinities and stoichiometry of the binding. ITC analysis of the His_6 tagged phnP was indicative of two sequential binding events, which agrees nicely with what was observed in the crystal structure of phnP (see below). The integrated binding heat was fitted to a two binding sites model, yielding a first dissociation constant (K_{D1}) of 37 μM and a second dissociation constant (K_{D2}) of 73 μM (**Figure 2-6A**). This corresponds well with the apparent K_M value of 48 ± 5 μM for Mn^{2+} observed through kinetic analysis. However, since phnP contains a His_6-tag, there is a possibility that when titrating Mn^{2+} to phnP solution, the His_6-tag might bind with Mn^{2+} as well. This would potentially interfere with the metal binding to the active site of phnP, which would lead to inaccuracy of the data obtained from the ITC titration. An ITC experiment with phnP after removal

of the His_6 tag by enterokinase was performed. However, it turned out to be unsuccessful (**Figure 2-6B**) possibly due to the low amount of protein (30 μM final concentration) and relatively low binding affinity of Mn^{2+} to the active site. Previous ITC analysis of Mn^{2+} binding to His_6 tagged phnH, another member from the C-P lyase pathway, demonstrated very weak affinity with a K_d value of ~0.64 mM (Figure **2-6C**). The dramatically different binding affinity of manganese towards two very different proteins, each bearing a His_6 tag, argues against the possibility that the two consecutive binding events of manganese on phnP were due to the His_6-tag alone, and more likely active site directed,

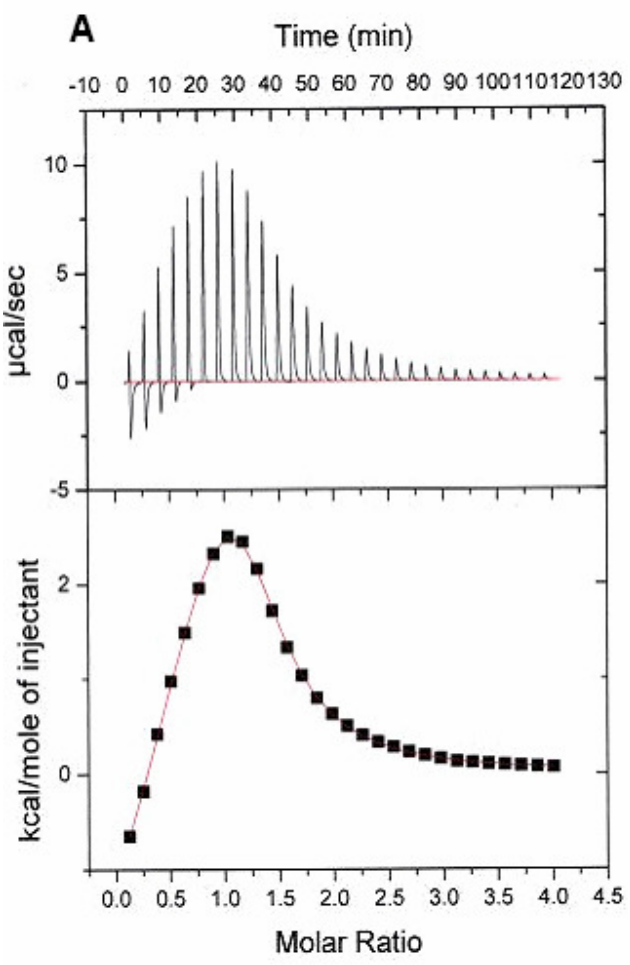

Figure 2-6A. ITC curves of manganese binding to phnP with a His_6 tag. Upper panels: raw data for sequential titrations of manganese solution into the protein solution. Lower panel: intergrated heats as a function of the Mn^{2+}/protein ratio.

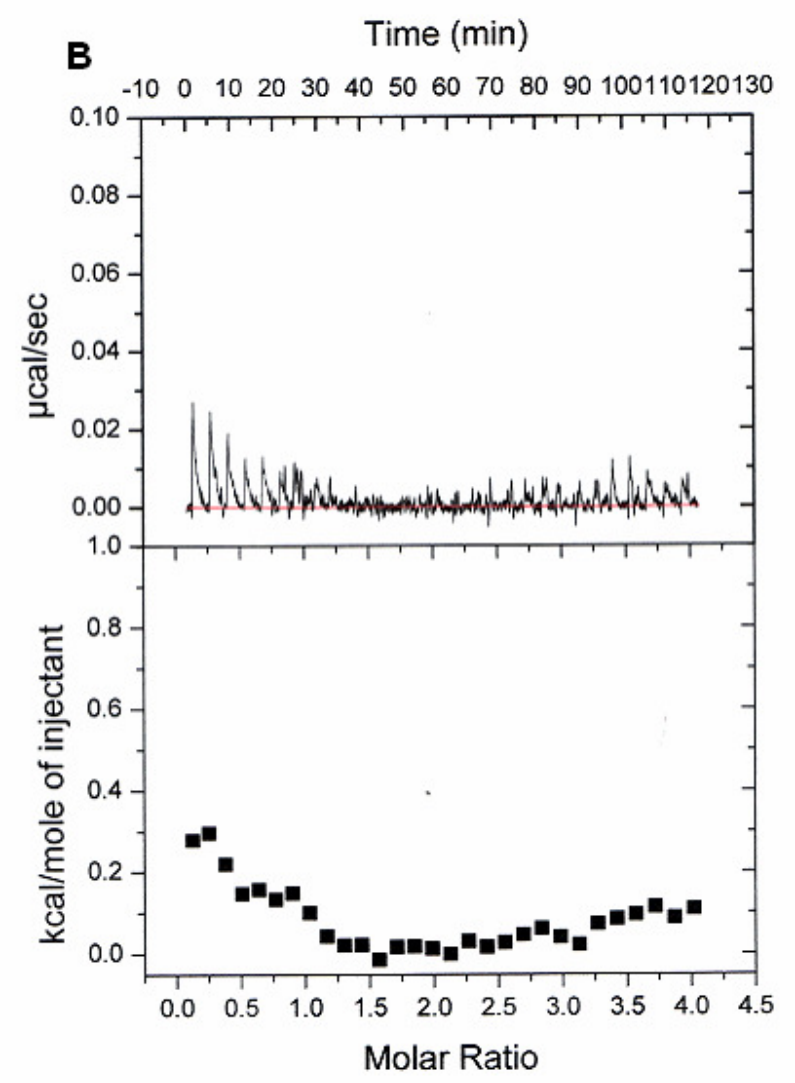

Figure 2-6B. ITC curves of manganese binding to phnP without a His_6 tag.

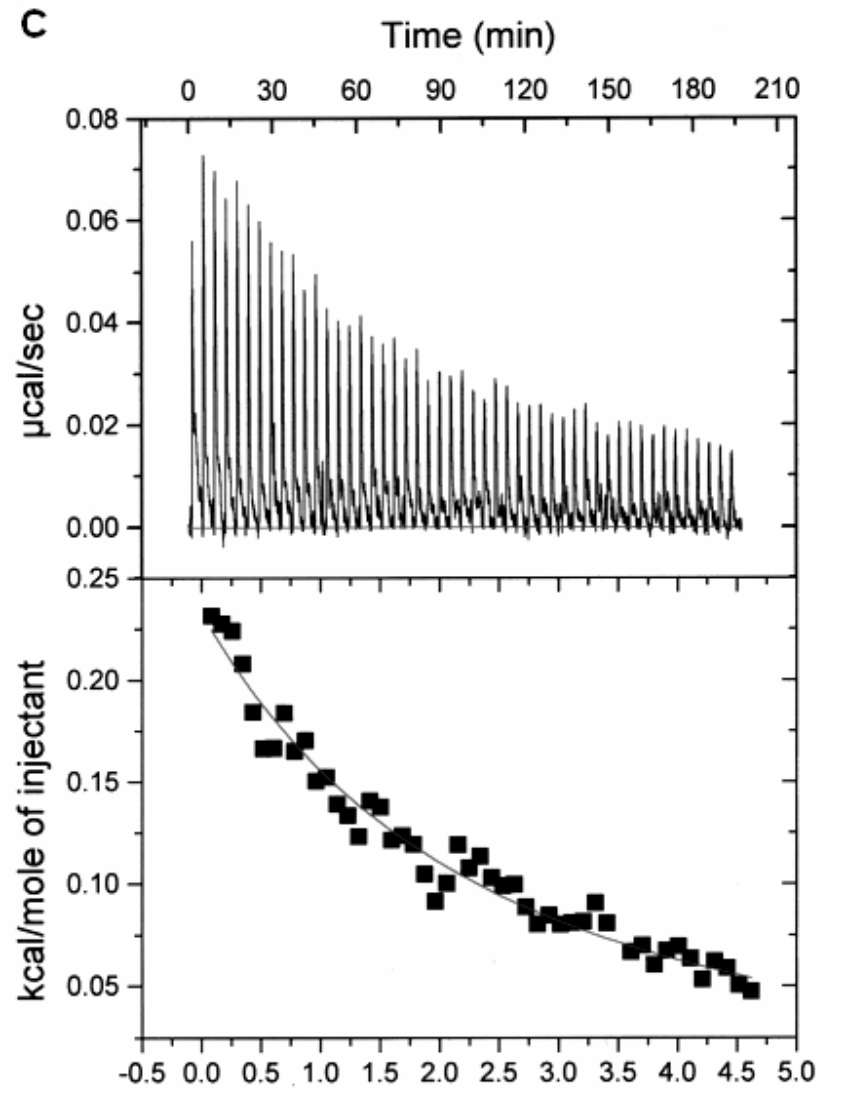

Figure 2-6C. ITC curves of manganese binding to phnH with a His_6 tag. Upper panels: raw data for sequential titrations of manganese solution into the protein solution. Lower panel: intergrated heats as a function of the Mn^{2+}/protein ratio.

2.3.6 Phosphodiesterase activity with physiological phosphodiesters

In order to identify a physiologically relevant substrate for PhnP the enzyme was screened against naturally occuring phosphodiester and phosphoanhydride substrates by Dr. Alexander Yakunin and Professor Aled Edwards at the Banting and Best Department of Medical Research (**Figure 2-7**). PhnP exhibitied high activity toward 2':3'-cyclic nucleotides, and very low or no activity against 3':5'-cyclic nucleotides. To explore which nucleotide is more specific to phnP, kinetic parameters such as k_{cat} and k_{cat} /K_M values for the hydrolysis of 2':3'-cyclic nucleotides were determined at various substrate concentrations and a saturating manganese concentration (1 mM). The k_{cat} constant is a first order rate constant and reflects the rate-determining step in the overall reaction and reveals the maximal turnover rate of substrate. The k_{cat}/K_M is the apparent second-order rate constant for the reaction between free enzyme and free substrate and includes the binding of substrate up to the first irreversible step. The k_{cat}/K_M parameter reveals the specificity of phnP and suggests which nucleotide is preferred as a substrate. PhnP demonstrated the highest specificity to 2':3'-cAMP with k_{cat}/K_M = 15.8 × 10^3 M^{-1} s^{-1} in the presence of 1 mM Mn^{2+}, whereas a similar k_{cat}/K_M value was observed for 2':3'-cGMP and 2':3'-cCMP with 3.91 × 10^3 M^{-1} s^{-1} and 4.22 × 10^3 M^{-1} s^{-1}, respectively (**Figure 2-8, Table 2-5**). The increase in k_{cat}/K_M values for 2':3'-cyclic nucleotides relative to bpNPP was almost entirely to a dramatic reduction in the K_M values, rather than an increase in k_{cat}. This suggests greater recognition of the substrate by phnP in the ground state configuration.

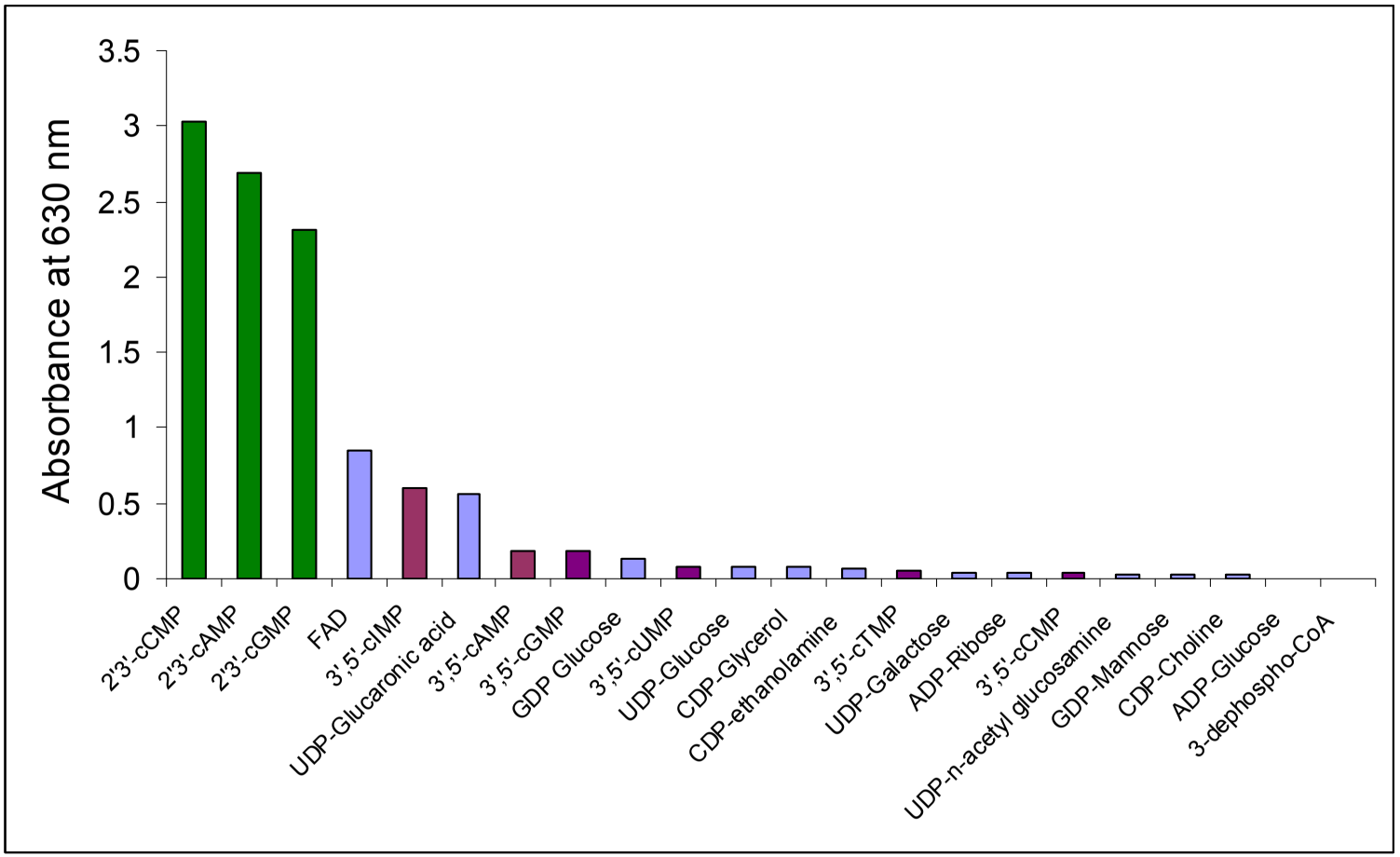

Figure 2-7. Secondary substrate screening of phnP with various biologically relevant phosphodiesters and phosphoanhydrides.

Moreover, with 1 mM Mn^{2+} present, phnP hydrolyzed 2':3'-cAMP regioselectively to 3'-AMP, as analyzed by cellulose TLC (**Figure 2-9**). Therefore, phnP is a regioselective 2':3'-cyclic nucleotide phosphodiesterase. The mechanism for the substrate specificity toward 2':3'-cyclic nucleotides and the regioselectivity for the 3'-product, but not the 2'-product, are still not clear. Compared with *E. coli* ZipD, one of the closest sequence homologues of phnP that does not hydrolyze either 2':3'-cyclic nucleotides or 3':5'-cyclic nucleotides (12), the catalytic activity of phnP toward 2':3'-cyclic nucleotides indicates that those nucleotides might be relevant to the physiological function of phnP, or they may have close structural similarities with the real physiological substrate that needs to be identified. A complex structure of phnP with 2':3'-cyclic nucleotides may provide direct information on the conformation of the substrate binding to the active site pocket to help explain the above observations. However, co-crystallization of phnP and the inactive D80A mutant with 2':3'-cyclic nucleotides have thus far been unsuccessful.

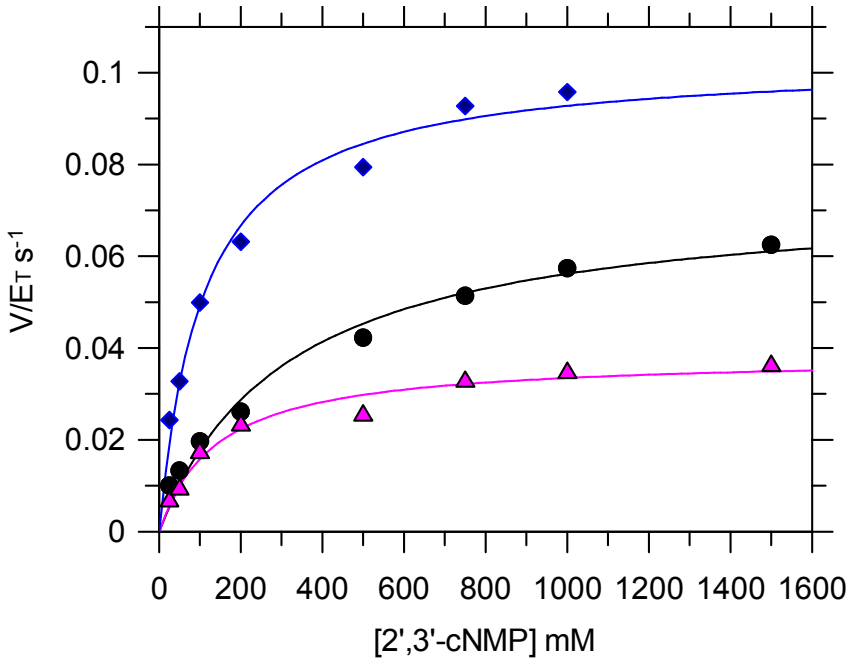

Figure 2-8. Phosphodiesterase activity of *E. coli* phnP toward 2',3'-cyclic nucleotides as a function of substrate concentration. ▲, 2',3'-cCMP; ●, 2',3'-cGMP; ♦, 2',3'-cAMP.

Table 2-5 Kinetic constants of wild type phnP with various substrates

sample	K_M (mM)	k_{cat} (s^{-1})	k_{cat} / K_M ($M^{-1} s^{-1}$)
2':3'-cAMP	0.11 ± 0.01	1.71 ± 0.06	15.8 x 10^3
2':3'-cGMP	0.31 ± 0.05	1.23 ± 0.07	3.91 x 10^3
2':3'-cCMP	0.14 ± 0.03	0.64 ± 0.03	4.22 x 10^3
bpNPP	3.5 ± 0.3	1.06 ± 0.09	303
tpNPP	14.6 ± 5.4	0.08 ± 0.02	5.8

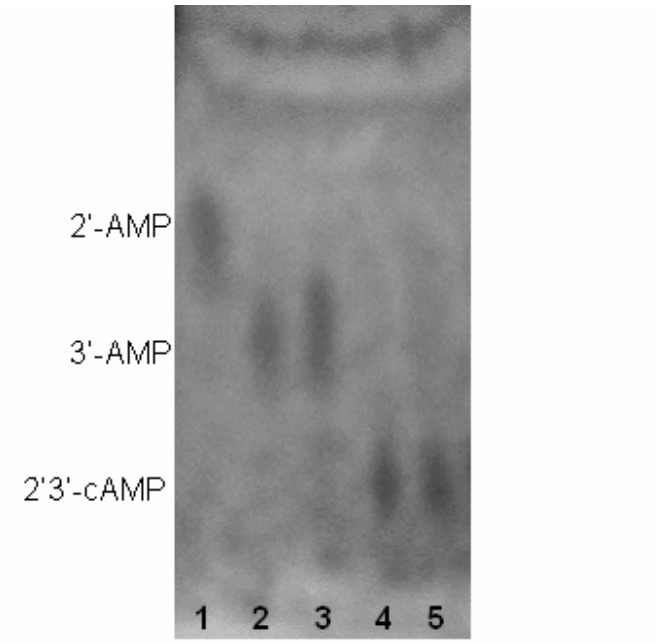

Figure 2-9. Cellulose TLC analysis of the reaction products: hydrolysis of 2':3'-cAMP. Lane 1: 2.5 mM 2' AMP standard. Lane 2: 2.5 mM 3' AMP standard. Lane 3: phnP (2 uM) with 20 mM 2':3'-cAMP and 1mM Mn^{2+}. Lane 4: Control reaction without phnP. Lane 5: 2.5 mM 2':3'- cAMP standard.

2.3.7 X-Ray Crystal structure of *E. coli* phnP

2.3.7.1 Overall structure

The structure of *E. coli* phnP was determined by X-ray diffraction to a resolution of 1.4 Å by Kateryna Podzelinska and Dr. Zongchao Jia (Department of Biochemistry, Queen's University). PhnP crystallized as a dimer, which is not likely due to the crystal environment, as phnP elutes from a size exclusion column as a dimer and displays modest cooperativity in its reaction with bpNPP. The tRNase Z sequence homologues of phnP are also active and have been crystallized as dimers (7,8). Each monomer of phnP exhibits the typical metallo-β–lactamase fold with a core of two seven-strand-β–sheets sandwiched on either side by α helices. The first four β strands are antiparallel followed by three parallel β strands (**Figure 2-10A**). A narrow cleft is formed jointly by the two monomers in which the active site and metal coordination residues are present (**Figure 2-10B and 2-10C**). Each monomer is bound to two catalytic manganese ions and one structural zinc ion (**Figure 2-10A**). At this structural resolution the difference between the manganese and zinc electron densities is observable (Kateryna Podzelinska, personal communication). Manganese I is coordinated by three histidines (His76, His78, and His143), and manganese II is coordinated by two histidines (H81, H222) and an aspartate (D80). In addition, an aspartate (D164) bridges the two manganese atoms (**Figure 2-11A**). This binuclear manganese active site constitutes one of the strikingly different features of phnP from other homologues, most of which have a binuclear zinc site, even though all of the above metal coordinating residues are strictly conserved.

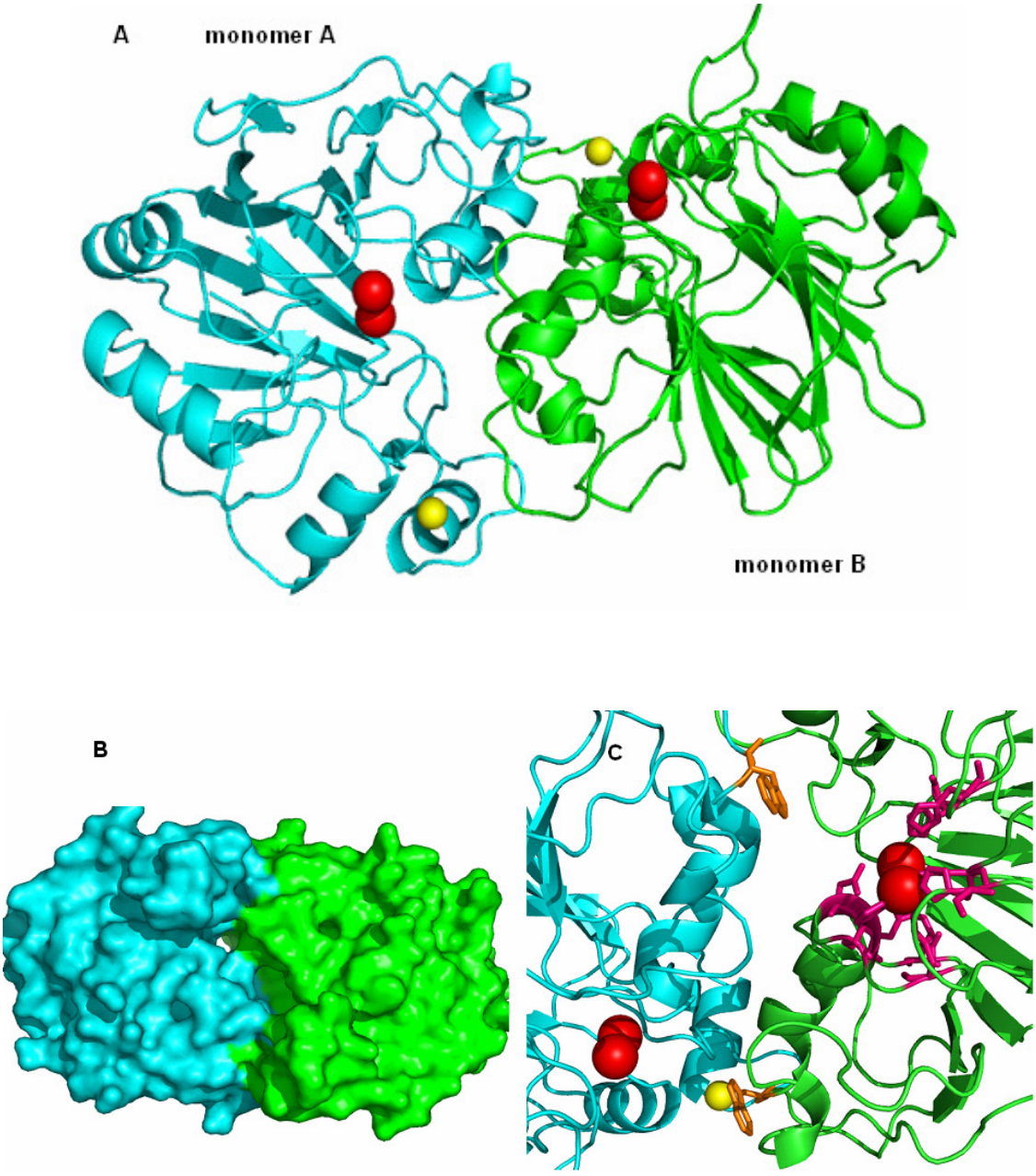

Figure 2-10. (A) Ribbon representation of phnP at 1.4 Å resolution. Subunit A is in blue, subunit B is in green, zinc ions are represented by yellow spheres, and manganese ions are in red. (B) Surface image of phnP showing the dimer interface where the active site lies. (C) Active site cleft of phnP dimer formed by monomer A and monomer B. Manganese binding residues are represented by pink sticks. W90 (orange sticks) is donated by one monomer to form the pocket of the active site in the other monomer. Images were generated using PyMol (Delano Scientific).

Another different feature demonstrated by the crystal structure is that *E. coli* phnP has an extra structural zinc site, which most likely is the high affinity zinc site identified by ICP-MS (**Figure 2-10A**). The zinc ion is coordinated by three cysteine residues (C21, C23 and C26) and one histidine (H225) (**Figure 2-10B**). This feature makes phnP distinct from other metallo-β–lactamase family enzymes. Interestingly, phnP shares the Zn^{2+} structural motif with pqqB from the pyrrolopyroquinoline biosynthetic pathway (38). The structure of pqqB has been determined (pdb code: 1XTO) and is the closest structural homologue to phnP (although not the closest sequence homologue). The three cysteine residues are strictly conserved in the phnP and pqqB families. Most of the enzymes in the metallo-β–lactamase family have a binuclear zinc active site, whereas phnP uses zinc as a structural metal. This structural role was confirmed with site-directed mutagenesis. After all three coordinating cysteines (C21, C23 and C26) were mutated to serines, the mutant protein could not be expressed in a soluble form as demonstrated by SDS-PAGE and Western blot (**Figure 2-12**). It is evident that without the zinc coordinating residues, the protein is not stable and tends to aggregate. This structure role was further confirmed by the metal dependence of wild type phnP. When the apo enzyme was reincubated with extra zinc ions (0.2 mM), very low activity was detected; however, when extra manganese (0.2 mM) was added to the apo enzyme, the activity was restored to the value obtained with the protein prior to treatment with the chelator (**Figure 2-13**). Therefore, zinc does not appear to play a catalytic role in phnP; instead, phnP is a manganese dependent phosphodiesterase and zinc stabilizes the enzyme structure.

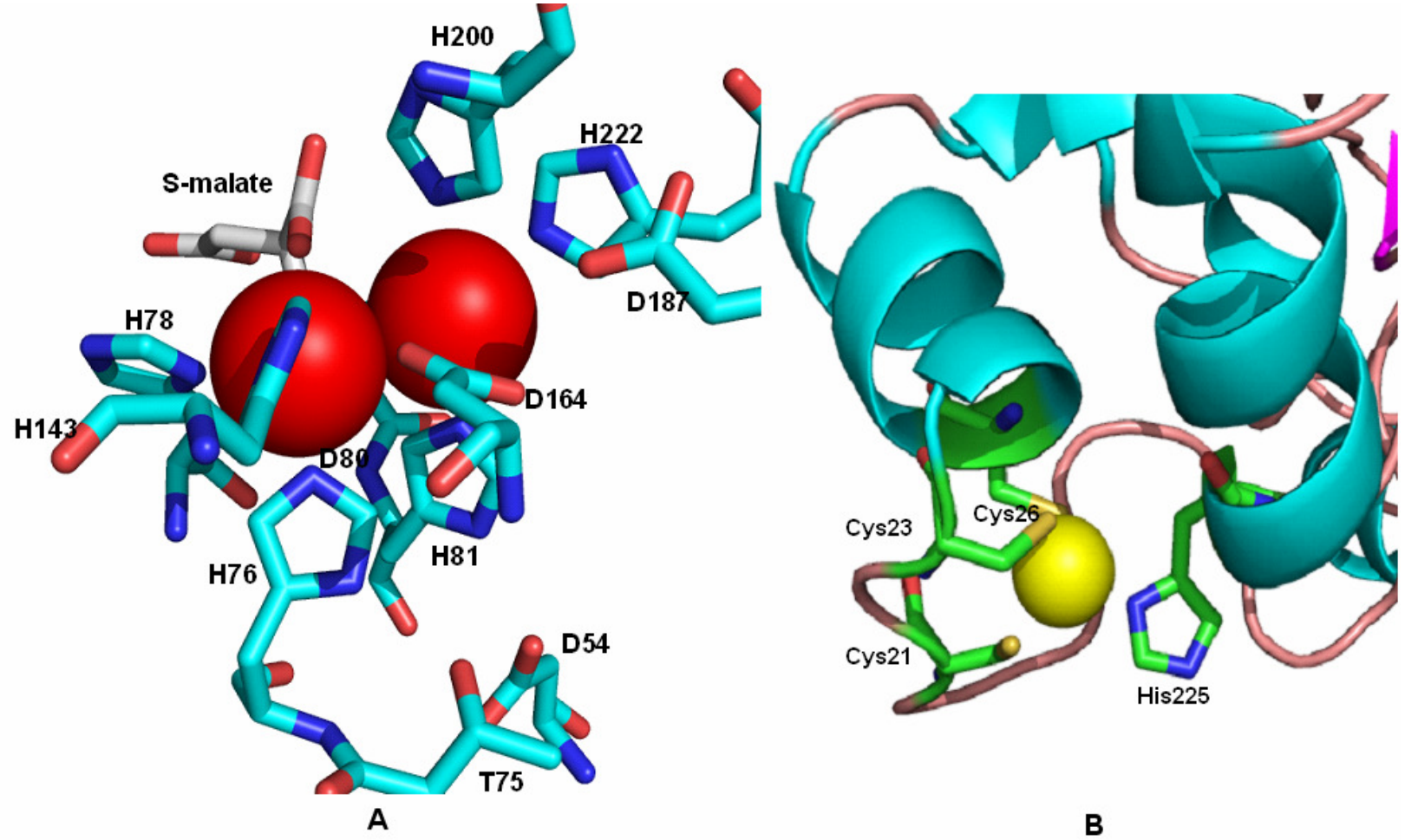

Figure 2-11. (A) Active site (Mn^{2+}) residues and (B) Structural zinc site residues of *E. coli* phnP. *S*-malate bound in the active site is shown in grey sticks.

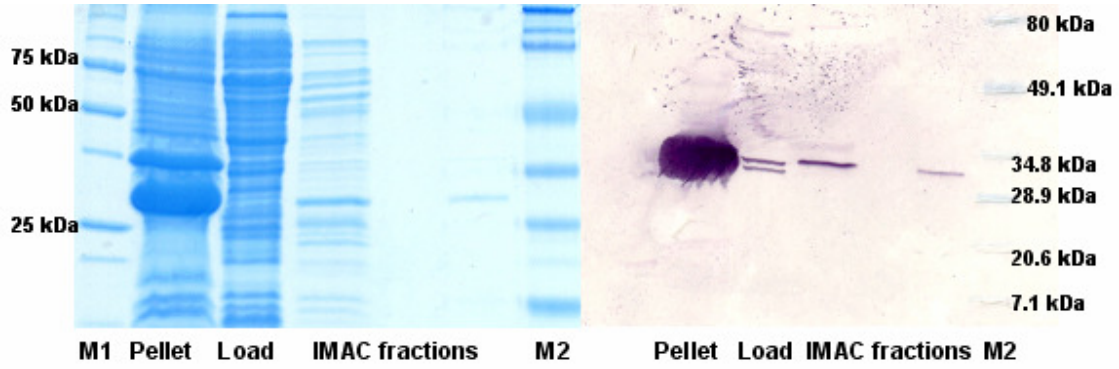

Figure 2-12. 15% SDS-PAGE (A) and Western blot (B) of phnP C21S/C23S/C26S triple mutant. M1: BioRad precision plus protein marker; M2: BioRad prestained protein marker (broad range). Pellet: cell pellet obtained after cell lysis and centrifugation; Load: supernatant obtained after cell lysis and centrifugation.

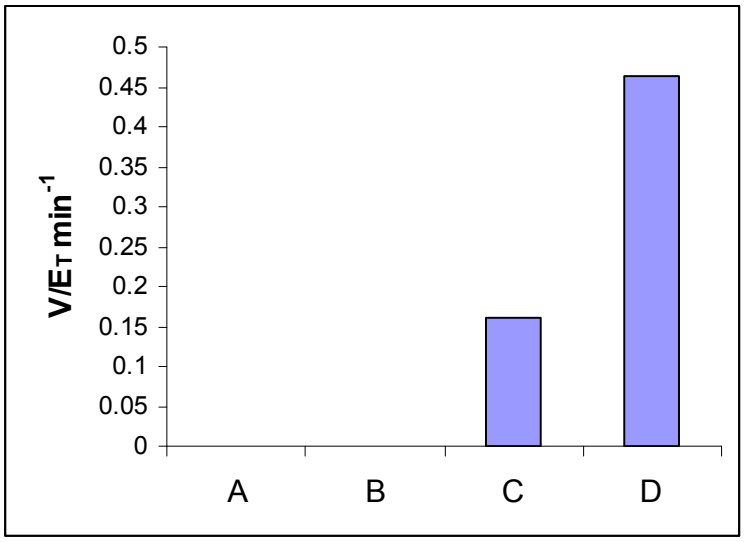

Figure 2-13. Dependence of PhnP activity on zinc and manganese (bpNPP as substrate). **A**: Apo-phnP (EDTA treated). .**B**: Apo-phnP incubated with 0.2 mM Zn^{2+}. **C**: PhnP in B incubated with EDTA, dialyzed, then reincubated with 0.2 mM Mn^{2+}. **D**: Apo-phnP incubated with 0.2 mM Mn^{2+}.

2.3.7.2 The active site of phnP

E. coli phnP belongs to the metallo-β-lactamase superfamily. The unifying character of this superfamily is the "β-lactamase" fold, which consists of a α–β/β–α structure. In addition to this structural fold, all metallo-β-lactamases contain five highly conserved motifs that participate in the binuclear metal coordination and the hydrolysis reactions (*17, 19, 20*). Motif I consists of an aspartate, and motif II, which is typical for this superfamily, consists of the highly conserved signature motif HXHXDH; these first two motifs are located at the end of two β-strands. Motif III (a histidine residue), motif IV (an aspartate residue), and motif V (a histidine residue) are also found at the end of β-sheets. Those five highly conserved motifs are also conserved with *E. coli* phnP (**Figure 2-14 A**). Motif I (D54) is located at the end of β3, motif II (H76, H78, D80 and H81) is located at the region connecting β4 and α2, motif III (H143) is located at the loop connecting β8 and β9, motif IV (D164) is located at the end of β10, and motif V (H222) is located at the end of β12 (**Figure 2-14B**). Structural and mutagenesis studies based on those metallo-β-lactamase enzymes revealed that all those motifs are essential for the metal supported hydrolysis activity, suggesting that those residues form a part of the active site (1,7,8,20). In fact, four of the residues, H76, H78, D80 and H81 are located close to each other and form half of the active site pocket. D54 interacts with the side chain of T75, which is either a threonine or a serine residue in the metallo-β-lactamase superfamily, and may

stabilize the active site pocket by forming a hydrogen bonding network (**Figure 2-11A**). Motif III, IV and V create another half of the active site pocket. At the active site of phnP, seven amino acid residues and one water molecule directly interact with two manganese ions (**Figure 2-11A**). Manganese 1 is coordinated by three histidines (H76, H78, and H143), manganese 2 is coordinated by two histidines (H81, H222) and an aspartate (D80). The two metals are separated by a distance of 3.54 Å and are bridged by a water molecule and single carboxy oxygen of D164. A molecule of *S*-malate fortuitously co-crystallized at the active site adds intriguing detail to the structure of phnP. The hydroxyl group of *S*-malate is sandwiched between two manganese ions, and forms a hydrogen bond with D80 with a distance of 2.6 Å. The carboxylate of *S*-malate interacts with H200 that is 2.8 Å away by forming an H-bond as well (**Figure 2-11A**). The active site residues of phnP superimpose very well with tRNase Z family members such as tRNase Z from *B. subtilis.* (See **Figure 2-15** and discussion below).

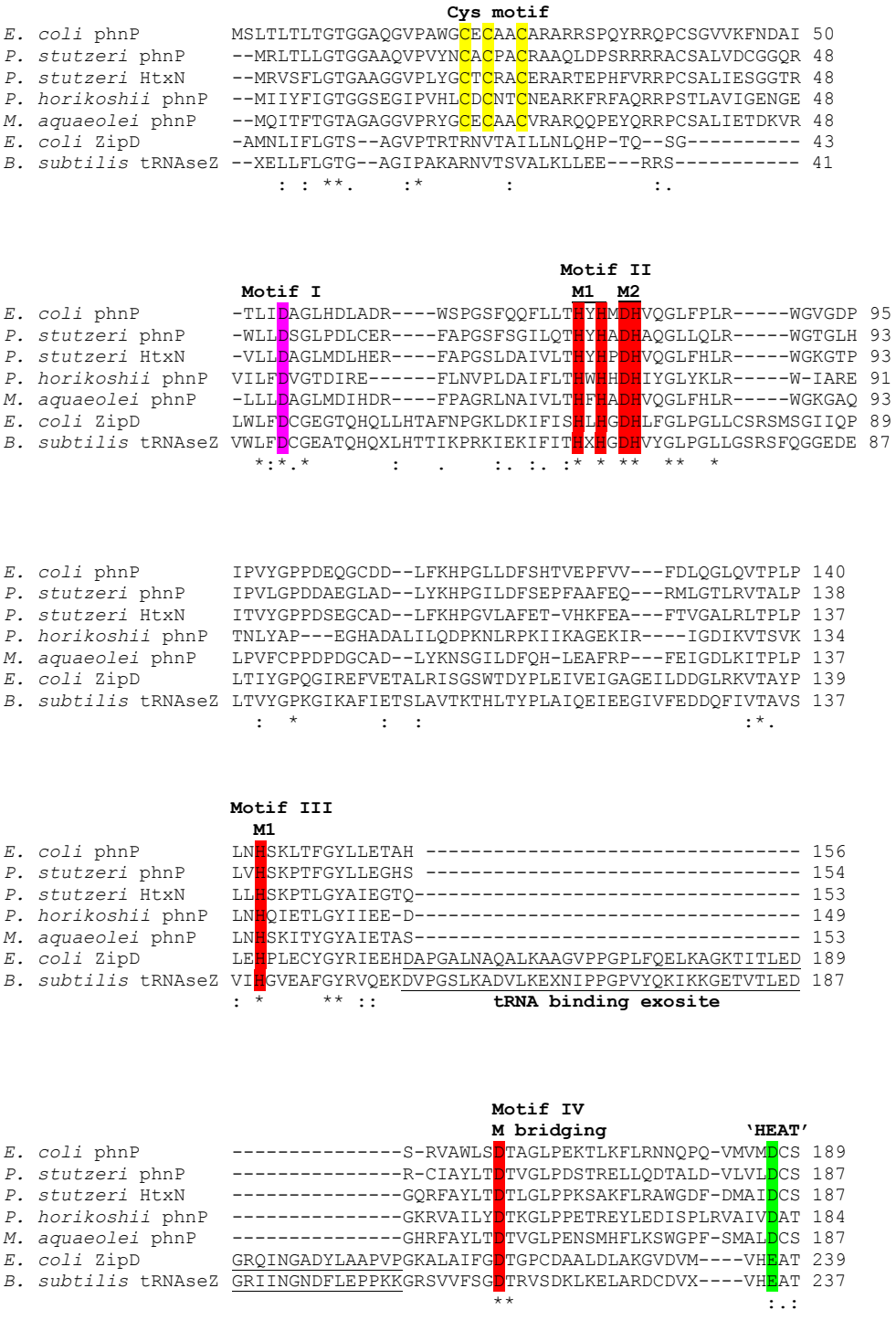
Cys motif
E. coli phnP MSLTLTLTGTGGAQGVPAWGCECAACARARRSPQYRRQPCSGVVKFNDAI 50
P. stutzeri phnP --MRLTLLGTGGAAQVPVYNCACPACRAAQLDPSRRRRACSALVDCGGQR 48
P. stutzeri HtxN --MRVSFLGTGAAGGVPLYGCTCRACERARTEPHFVRRPCSALIESGGTR 48
P. horikoshii phnP --MIIYFIGTGGSEGIPVHLCDCNTCNEARKFRFAQRRPSTLAVIGENGE 48
M. aquaeolei phnP --MQITFTGTAGAGGVPRYGCECAACVRARQQPEYQRRPCSALIETDKVR 48
E. coli ZipD -AMNLIFLGTS--AGVPTRTRNVTAILLNLQHP-TQ--SG---------- 43
B. subtilis tRNAseZ --XELLFLGTG--AGIPAKARNVTSVALKLLEE---RRS---------- 41
Motif II
Motif I M1 M2
E. coli phnP -TLIDAGLHDLADR----WSPGSFQQFLLTHYHMDHVQGLFPLR-----WGVGDP 95
P. stutzeri phnP -WLLDSGLPDLCER----FAPGSFSGILQTHYHADHAQGLLQLR-----WGTGLH 93
P. stutzeri HtxN -VLLDAGLMDLHER----FAPGSLDAIVLTHYHPDHVQGLFHLR-----WGKGTP 93
P. horikoshii phnP VILFDVGTDIRE------FLNVPLDAIFLTHWHHDHIYGLYKLR-----W-IARE 91
M. aquaeolei phnP -LLLDAGLMDIHDR----FPAGRLNAIVLTHFHADHVQGLFHLR-----WGKGAQ 93
E. coli ZipD LWLFDCGEGTQHQLLHTAFNPGKLDKIFISHLHGDHLFGLPGLLCSRSMSGIIQP 89
B. subtilis tRNAseZ VWLFDCGEATQHQXLHTTIKPRKIEKIFITHXHGDHVYGLPGLLGSRSFQGGEDE 87
IPVYGPPDEQGCDD--LFKHPGLLDFSHTVEPFVV---FDLQGLQVTPLP 140
IPVLGPDDAEGLAD--LYKHPGILDFSEPFAAFEQ---RMLGTLRVTALP 138
ITVYGPPDSEGCAD--LFKHPGVLAFET-VHKFEA---FTVGALRLTPLP 137
TNLYAP---EGHADALILQDPKNLRPKIIKAGEKIR----IGDIKVTSVK 134
LPVFCPPDPDGCAD--LYKNSGILDFQH-LEAFRP---FEIGDLKITPLP 137
LTIYGPQGIREFVETALRISGSWTDYPLEIVEIGAGEILDDGLRKVTAYP 139
LTVYGPKGIKAFIETSLAVTKTHLTYPLAIQEIEEGIVFEDDQFIVTAVS 137
Motif III
M1
LNHSKLTFGYLLETAH ---------- 156
LVHSKPTFGYLLEGHS ---------- 154
LLHSKPTLGYAIEGTQ---------- 153
LNHQIETLGYIIEE-D---------- 149
LNHSKITYGYAIETAS---------- 153
LEHPLECYGYRIEEHDAPGALNAQALKAAGVPPGPLFQELKAGKTITLED 189
VIHGVEAFGYRVQEKDVPGSLKADVLKEXNIPPGPVYQKIKKGETVTLED 187
tRNA binding exosite
Motif IV
M bridging
'HEAT'
----------S-RVAWLSDTAGLPEKTLKFLRNNQPQ-VMVMDCS 189
----------R-CIAYLTDTVGLPDSTRELLQDTALD-VLVLDCS 187
----------GQRFAYLTDTLGLPPKSAKFLRAWGDF-DMAIDCS 187
----------GKRVAILYDTKGLPPETREYLEDISPLRVAIVDAT 184
----------GHRFAYLTDTVGLPENSMHFLKSWGPF-SMALDCS 187
GRQINGADYLAAPVPGKALAIFGDTGPCDAALDLAKGVDVM----VHEAT 239
GRIINGNDFLEPPKKGRSVVFSGDTRVSDKLKELARDCDVX----VHEAT 237

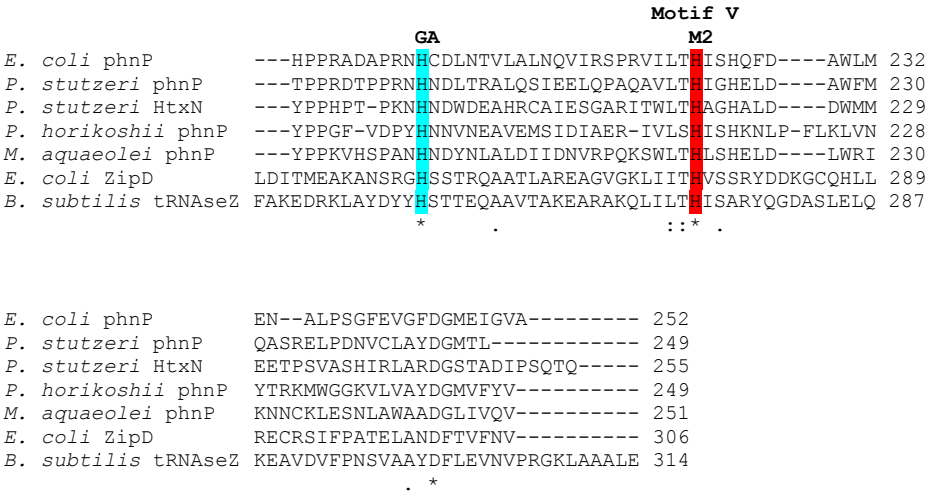

Figure 2-14A: Multiple sequence alignment of phnP homologues (first 5 entries) and tRNase Z family enzymes with known structures (last 2 entries). Amino acid sequences are for *E. coli* K-12 phnP (gi: 536936), *Pseudomonas stutzeri* phnP (gi: 40804950), *Pseudomonas stutzeri* HtxN (gi: 40787179), *Pyrococcus horikoshii* OT3 phnP (gi: 14591382), *Marinobacter aquaeolei* VT8 phnP (gi: 120555210), *E. coli* ZipD (gi: 90109091, PDB 2cbn), *B. subtilis* tRNaseZ (gi: 60594108, PDB 1y44). The Cys motif for phnP homologues is highlighted in yellow. Residues involved in binding the two active site metals (M1 and M2, numbering based on reference (7) are highlighted in red. The putative general acid catalyst is highlighted in turquoise and the conserved Glu / Asp of the 'HEAT' motif is shown in green. The exosite of the tRNAase Z enzymes involved in binding tRNA is underlined. Completely highly conserved and moderately conserved residues are indicated by asterisks, colons and periods respectively. The sequence alignment was performed using ClustalW (46) then edited by eye.

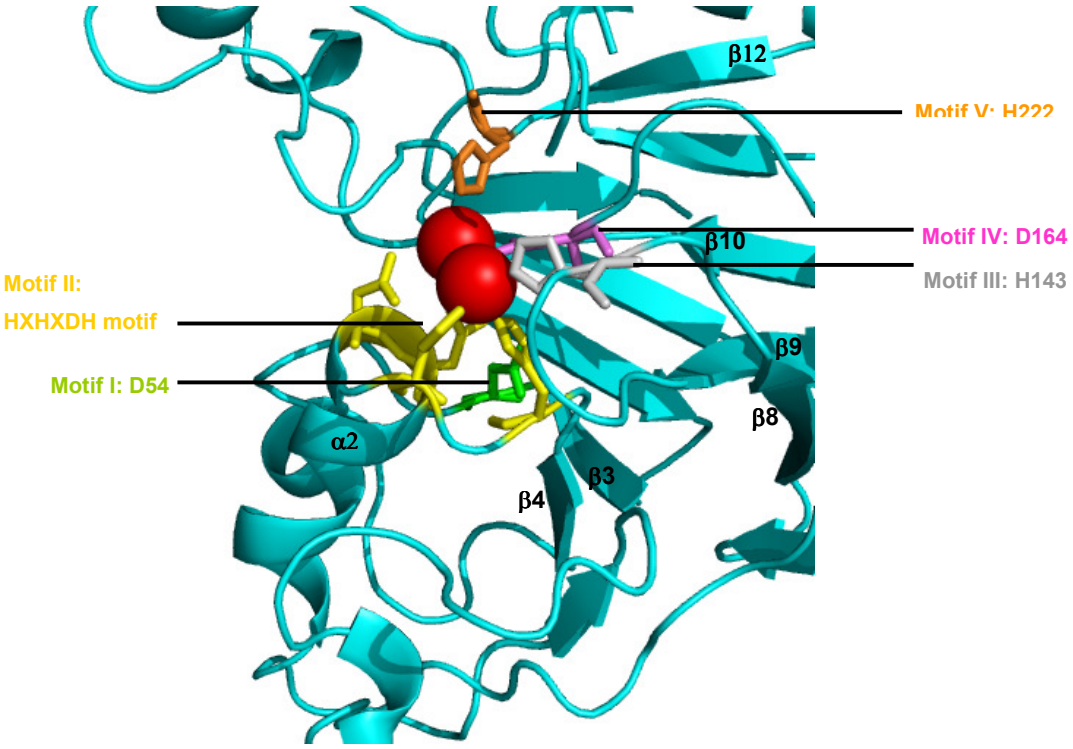

Figure 2-14B. Ribbon representation of one subunit of phnP demonstrates the positions of all the five conserved motifs at the active site. Motif I-V residues are colored as green, gold, grey, pink, and orange sticks respectively. Manganese ions are represented in red spheres.

2.3.7.3 Comparison of phnP structure with homologues of known structures

Based on sequence homology, phnP was grouped with tRNase Z enzymes of the metallo-β-lactamase superfamily (17). At the level of protein sequence, *E. coli* phnP is 25% identical to tRNase Z from *B. subtilis* and 22% identical to tRNase Z from *E. coli* (**Figure 2-14A**). In addition, a structural similarity search using DaliLite (35) with known three-dimensional protein structures in the Protein Data Bank (PDB) also revealed that the overall architecture of phnP shares a common fold with those of the metallo-β-lactamases, such as tRNase Z from *E. coli* (PDB code 2cbn), *B. subtilis* (PDB code 1y44), and *T. maritima* (PDB code 1ww1) (**Figure 2-15A**). All of these enzymes are homodimers, and each monomer contains fully occupied metal sites except 1y44 (tRNase Z from *B. subtilis*). The characteristic metal coordinating motif HXHXDH is highly conserved and is located at the end of two β-strands.

The conservation of the structural fold and the metal coordinating framework at the active site suggest a similar catalytic mechanism for hydrolytic reactions (*19*). Enzymes from this superfamily hydrolyze a wide variety of substrates. For example, class B β-lactamases hydrolyze lactams; glyoxalase II catalyzes the hydrolysis of a thioester, *S*-D-lactoylglutathione; cAMP phosphodiesterases hydrolyzes phosphate diesters, and arylsulfatase hydrolyzes suflate esters (19). PhnP and tRNase Z are both phosphodiesterases, using binuclear active site to stabilize negative charge development on the phosphate

during hydrolysis, while simultaneously lowering the *p*Ka of the attacking water molecule.

In addition to the above similarities, there are three distinctive differences between *E. coli* phnP and tRNase Z enzymes. First of all, phnP has two metal sites, with two catalytic manganese ions at the active site, and one zinc ion at a distance of 19.97 Å from the active site, which is a key for structure stabilization (**Figure 2-10A, 15A**). Most of the enzymes in the same metallo-β-lactamase family only have one binuclear metal site for activity, whereas phnP has an extra metal site for a structure role as demonstrated by mutagenesis. Secondly, within the metallo-β-lactamase superfamily, catalytic activity requires one or two metal ions. *E. coli* ZipD requires two zinc ions for full phosphodiesterase activity (12), glyoxalase II binds zinc, iron, and manganese (4), while the rubredoxin:oxygen oxidoreductase contains a di-iron center (5). PhnP incorporates two manganese ions at the active site, adding another unique feature to the metallo-β-lactamase fold that is capable of binding different divalent metals. Lastly, crystal structures of tRNase Z from *B.subtilis* and ZipD from *E. coli* exhibit a protruding arm (exosite, **Figure 2-15A**) that is essential for substrate recognition (7, 8). Mutagenesis studies indicated that ZipD lost binding to and subsequent processing of the tRNA substrate upon removal of the exosite while the hydrolysis toward bpNPP was not affected (36). *E. coli* phnP does not have an exosite, neither does it show any activity towards single stranded RNA as demonstrated by RNase analysis with phnP carried out by Kateryna Podzelinska (Queen's Biochemistry). The low RNase activity exhibited by phnP was believed

to be caused by RNase contamination from purification of phnP as similar low activity was demonstrated with the inactive D80A mutant and H200A mutant (**Figure 2-16**), further suggesting that phnP is not an RNase even though it shares strikingly identical and highly conserved residues at the active site with tRNase enzymes (**Figure 2-15B**).

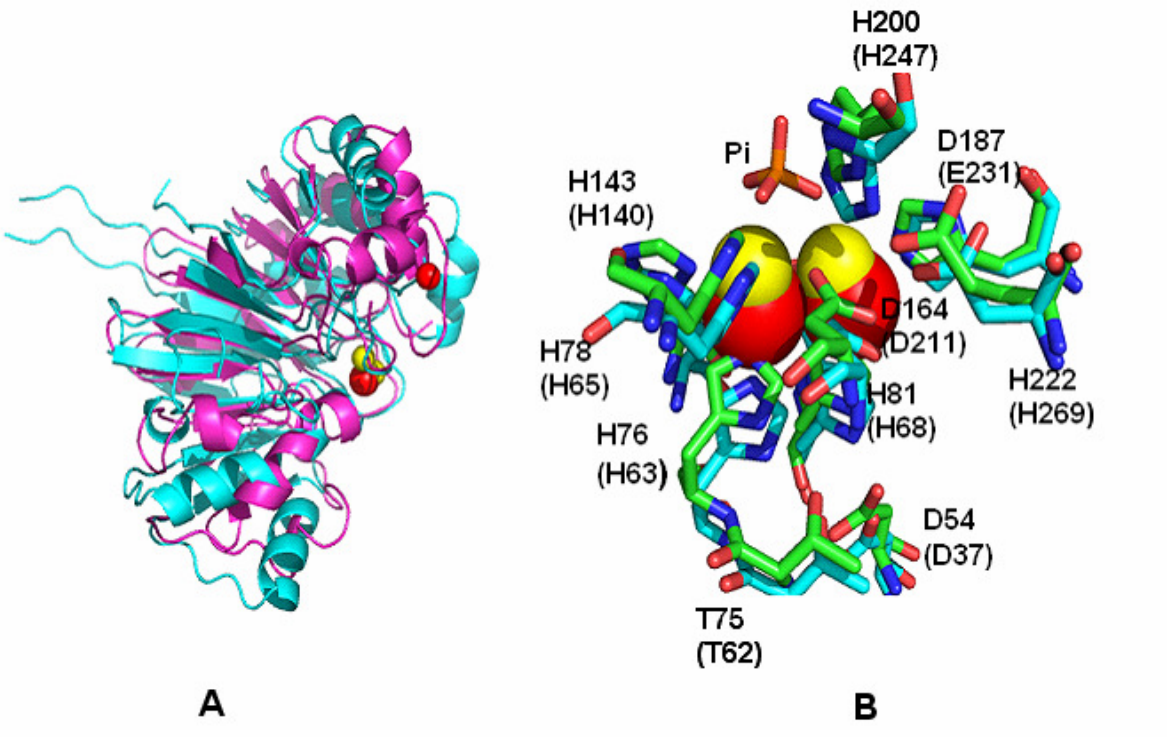

Figure 2-15. (A) PhnP (in pink) overlayed with tRNase Z (in cyan) (PDB code: 1y44). Two metal sites of phnP with the catalytic manganese and structural zinc are colored red, while two catalytic zinc ions of tRNase Z are in yellow. (B). PhnP active site residues (in cyan) overlayed with active site residues from 1y44 (in green). Two catalytic manganese ions from phnP are in red, and two catalytic zinc ions from 1y44 are in yellow. The phosphate ion complex with 1y44 is in red sticks. PhnP active site residues are labeled above 1y44 active site residues (in parentheses).

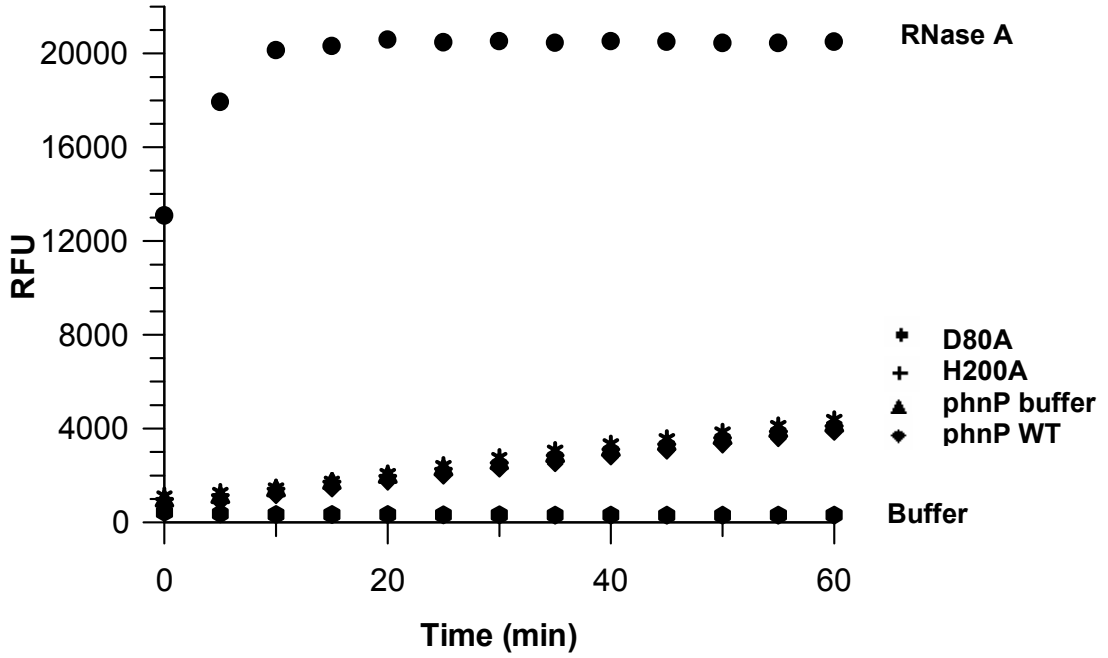

Figure 2-16. *In vitro* RNase assay for phnP.

2.3.8 Mutagenesis studies

2.3.8.1 Purification of phnP mutants

All phnP mutants were expressed at a similar level as wild-type phnP in a soluble form except the C21S/C23S/C26S triple mutant. After the first purification step using a Ni-NTA column the eluted fractions of each mutant were greater than 95% pure as shown by SDS-PAGE analysis (**Figure 2-17A** as an example). Although the C21S/C23S/C26S mutant was not soluble (**Figure 2-12**), the point

mutant C21S was partially soluble as evidenced by SDS-PAGE and western blot (**Figure 2-17B**).

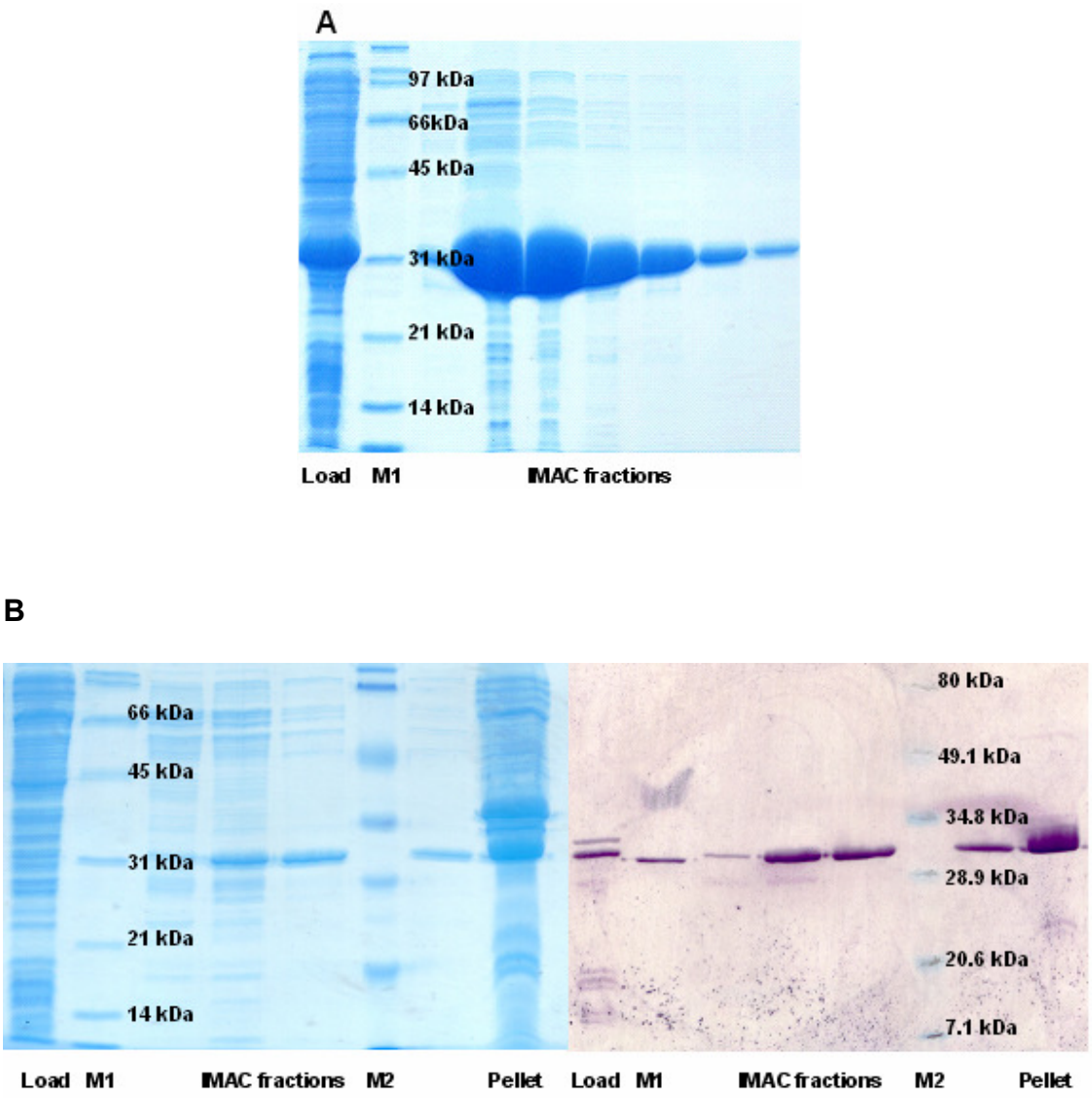

Figure 2-17. (A) Purification of phnP D164A by Ni-NTA chromatography shown by 15% SDS-PAGE. **(**B) Purification of phnP C21S. C21S mutant was partially soluble as demonstrated by 15% SDS-PAGE and Western blot. M1: BioRad broad range protein marker. M2: BioRad prestained protein marker (broad range).

2.3.8.2 ICP-MS on mutants

The metal content of phnP mutants were determined by ICP-MS. Not surprisingly, only trace amounts of manganese were detected with all the active site mutants such as D54A, H78A and H200A, however, the amount of zinc incorporated in the enzyme did not change significantly (**Table 2-6**). This indicates that without active site coordinating ligands such as histidines and aspartates, no manganese could be incorporated into the enzyme even with the same kind of expression LB medium and purified under the same conditions.

Table 2-6. **Metal content determined by ICP-MS with phnP WT and mutants**

sample (10 μM)	[Mn] μM	[Zn] μM	Mn / Enz	Zn / Enz
phnP as purified	1.3 ± 0.1	13.8 ± 1.1	0.13	1.38
Apo-phnP (treated with 10 mM EDTA)	0.06 ± 0.01	7.8 ± 0.03	0.01	0.78
D54A	N.D.	8.9 ± 0.3	N.D.	0.9
H78A	N.D.	19.2 ± 0.6	N.D.	1.92
D80A	N.D.	10.5 ± 0.2	N.D.	1.05
H200A	N.D.	11.2 ± 0.1	N.D.	1.12

Data represents average of three replicates for each sample.
N.D.: not detected, negligible as negative control (10 mM HEPES)

2.3.8.3 Kinetic analysis of phnP mutants

Based on the sequence homology, phnP belongs to the metallo-β-lactamase superfamily, which contains five highly conserved typical motifs for metal coordination and hydrolysis reactions. Thus we selected highly conserved residues from those five motifs, including D54 from motif I, D80 and H78 from motif II, D164 from motif IV, H222 from motif V (**Figure 2-14A**). T75 was selected due to the fact that it is previously discussed as involved in a hydrogen bonding network with D54 to stabilize one of the metal ligands, His 81 (*8*). In addition, to prove that the zinc ion coordinated by C21, C23, C26, and H225 plays a role in stabilizing the enzyme, the three cysteines were selected at first to be substituted by three serines to maintain the polarity environment but to change the affinity of the residues towards zinc (serine has a hydroxyl group and is not expected to bind the zinc ion as strongly). Those substitutions resulted in totally insoluble phnP as evidenced by SDS-PAGE and western blot (**Figure 2-12**). Therefore, we changed strategy to mutate just one of the three cysteines, C21. Although most of the protein still was not soluble (**Figure 2-17**) some soluble mutant protein was obtained for kinetic analysis.

All the variants demonstrated very low or no activity toward bpNPP hydrolysis without extra metal (1 mM Mn^{2+}) added to the reaction mixture even with much higher concentrations of enzyme than wild type (10 times higher in cases of D80A, D164A, D54A and H78A). However, with Mn^{2+} present, the activity of the mutants could be restored to different levels. The apparent K_M of all the mutants toward Mn^{2+} was determined at a fixed concentration of bpNPP (1

mM) and by varying the concentration of Mn^{2+}. All the mutants demonstrated reduced affinity towards Mn^{2+} as evidenced by increased apparent K_M values compared to wild type phnP (**Table 2-8, Figure 2-18B**). Further kinetics studies to determine the K_M and k_{cat} values of the bpNPP hydrolysis reaction with 1 mM Mn^{2+} present were carried out as well. All the kinetic results are presented in **Figure 2-18 and Tables 2-6 and 2-7.**

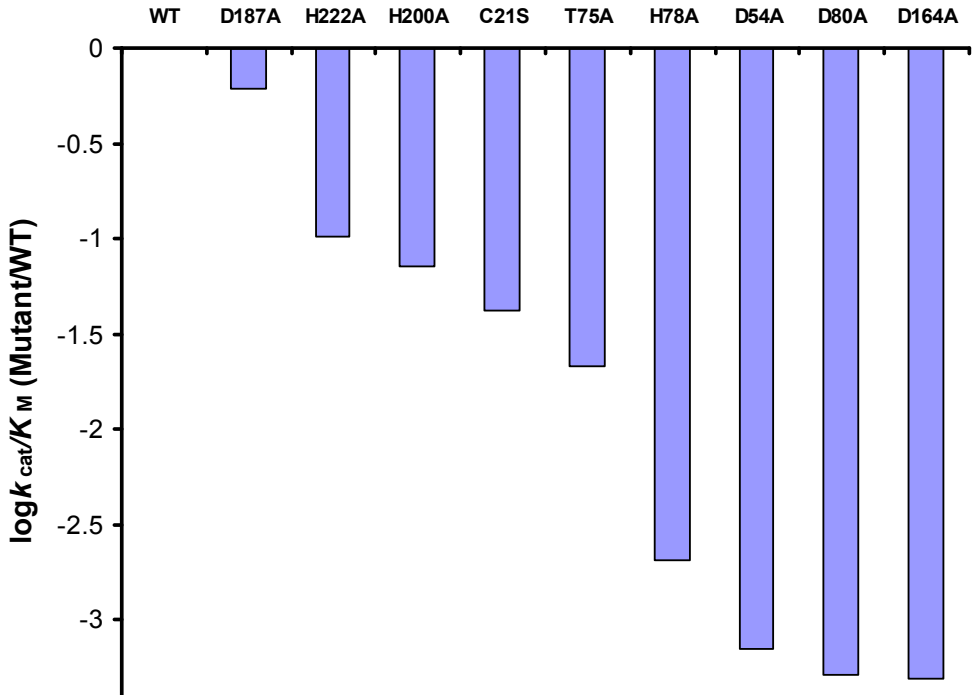

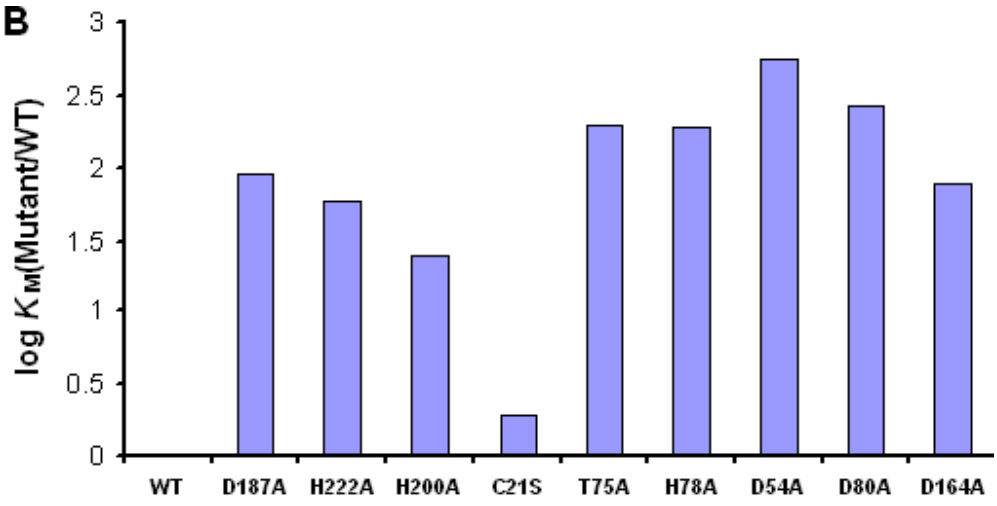

Figure 2-18. Bar graphs illustrating the effects of substitutions in conserved regions at the active site and zinc structural site on k_{cat}/K_M (A) and on K_M values toward Mn^{2+} (B). The k_{cat}/K_M to wild type (taken from column 5 in Table 2-5), and K_M toward Mn^{2+} (taken from column 4 in **Table 2-7**) are presented on a log scale.

Table 2-7 Kinetic constants of PhnP mutants toward bpNPP

sample	rel k_{cat} (%)	k_{cat} (min^{-1})	K_M (mM)	k_{cat}/K_M ($M^{-1}s^{-1}$)
wild type	100	64 ± 2	3.5 ± 0.3	305
D54A	0.07	0.042 ± 0.002	2.4 ± 0.3	0.30
H200A	51.6	33 ± 4	18 ± 3	30.4
H78A	0.31	0.20 ± 0.02	3.8 ± 0.8	0.88
D164A	0.07	0.047 ± 0.003	3.7 ± 0.5	0.21
H222A	12.3	7.9 ± 0.4	3.0 ± 0.6	44
C21S	5.78	3.7 ± 0.3	3.5 ± 0.6	18.0
D80A	0.08	0.05±0.002	3.7 ± 0.4	0.22
T75A	23.4	15 ± 4	28 ± 10	9.1
D187A	83	53 ± 4	3.4± 0.6	264

The kinetic parameters for wild type phnP was obtained with phnP as purified

Table 2-8 Kinetic Constants of phnP mutants toward Mn^{2+}

sample	K_M^{app} (mM)	*[Enz]* µM (used in assay)	relative K_M
WT as purified	0.048± 0.005	1	1
H78A	9.1 ± 0.6	5	190
D54A	27 ± 8	4.5	563
H200A	1.16 ± 0.06	2	24
D164A	3.7 ± 0.5	4.7	78
H222A	2.9 ± 0.4	5	60
C21S	0.09 ± 0.008	5.1	1.9
D80A	13 ± 2	10	265
T75A	9.3±0.8	5.5	194
D187A	4.4 ± 0.8	1.2	92

Aspartate 54 has been previously shown to be essential for catalysis and has been mutated to alanine in phnP homologues (*8, 23*). Mutation of D54 in phnP reduces the k_{cat} / K_M more than 1,000-fold (**Table 2-7 and Figure 2-18A**). Thus, D54 appears to play a key role in maintaining the catalytic site in an active conformation by forming hydrogen bond along with T75, to stabilize one of the metal coordination ligands, H81 (*8*) (**Figure 2-11A**). However, this aspartate residue does not bind to one of the metals directly, but it is located in the second shell around the metals along with T75 (*18*). Substitution of the highly conserved T75 with alanine did not impair the activity to the same extent as D54, but the substitution reduced the catalytic efficiency (k_{cat}/K_M value) by 33-fold compared to

the wild type (**Table 2-7 and Figure 2-18)**. In addition, substitution of T75 with alanine increased the K_M^{app} value toward Mn^{2+} by 194- fold (**Table 2-8**), further suggesting that T75 indirectly interacts with the metal by stabilizing one of the metal ligands, His81.

H78 and D80 are key residues in the signature motif HXHXDH and have been previously shown to be essential metal ligands in coordinating two metal ions at the active site (*23*). Substitutions of those two residues with alanines caused a large reduction in phnP activity: with 1 mM Mn^{2+} present the activity was reduced by 344-fold for H78A and 1400-fold for D80A, respectively (**Table 2-7 and Figure 2-18A**), indicating that these two residues play a key role in coordinating the two metal ions. Compared to wild type phnP, the K_M values for bpNPP of those two mutants did not change at all, however, k_{cat} changed dramatically (**Table 2-7**), suggesting that these residues are not involved in substrate positioning or binding, but for metal coordination. Moreover, substitution of H78 and D80 with alanine increased the K_M^{app} value toward Mn^{2+} by 90-fold and 270-fold, respectively (**Table 2-8**), confirming their essential roles in coordinating with the two metal ions. D80 is unique in that it may play an additional role in positioning or ionizing the nucleophilic water molecule (see section **2.3.7.2** for interaction of this residue with a bound molecule of S-malate). Such a role has also been proposed for *B.subtilis* tRNase Z, in which D67 (D80 in *E. coli* phnP) acts as a general base to generate a hydroxide ion as a nucleophile to attack the phosphate group (8).

D164 substitution with alanine dramatically impaired the enzyme catalytic activity by 1,400 fold (k_{cat} /K_M value) compared with wild type phnP, consistent with the fact that D164 bridges two metal ions (*2, 7, 8*). Additionally, kinetic studies with the D164A mutant revealed that the substitution didn't change the K_M value for bpNPP compared with the wild type (**Table 2-7**), but increased the K_M^{app} value toward Mn^{2+} by 80 fold (**Table 2-8**), indicating that this aspartate residue is fully involved in coordination with two metal ions and not likely in substrate binding.

H200 in the HST loop of phnP (**Figure 2-14**) has previously been suggested to be important for catalysis as a general acid (*9, 24, 25*). However, substitution of H200 with alanine reduced k_{cat} by only 2 fold compared to wild type phnP (**Table 2-7, Figure 2-18A**), whereas the K_M value increased dramatically to 18 mM, indicating a minor role for this residue in transition state stabilization as a general acid. This is in direct contrast to what was observed with other tRNase Z enzymes such as ZipD, where the substitution of this residue with alanine did not change the K_M value, but the k_{cat} values decreased by 1200 times (*9*). 'Rescue' of activity in mutants of the Zn^{2+} dependent *T. maritima* tRNase Z by Mn^{2+} was used as the primary argument that the Motif II aspartate (D80 in phnP) and histidine of the HST loop (H200 in phnP) provide general base and general acid catalysis, respectively (*25*). Additionally, Karkashon *et al.* (21) proposed that the highly conserved glutamate residue E231 in *B. subtilis,* which resides in the HEAT motif of the metallo-β-lactamase super family (**Figure 2-14A**) has the right charge and position to maintain the general

acid H247 of this enzyme (H200 in *E. coli* phnP) in the required protonated state (**Figure 2-19)**. The human CPSF-73 enzyme responsible for the cleavage step in mRNA maturation (29,30) is proposed to work by the same mechanism using the homologous residues E204 and H396 (29). The Glu residue that contacts the proposed general acid (21) tRNase Z enzymes and human CPSF-73 is slightly different in the phnP structure; instead, phnP has an Asp residue in this role (D187) that is virtually superimposable on those tRNase Z enzymes (**Figure 2-19**). The only difference between the aspartate and glutamate residue is that a glutamate has one more methylene carbon on the side chain. Nevertheless, substitution of D187 residue with alanine yielded a mutant that is almost as active as the wild type, indicating that its interaction with H200 does not play a major role in substrate recognition or transistion state stabilization (**Table 2-7** and **Figure 2-18A**). This mutation also reaffirms the minor role H200 plays in transition state stabilization.

Homologous structures, conserved sequences as well as kinetic analysis with homologous enzymes suggest that H200 in phnP may contribute directly to catalysis as a general acid, and its ionization state maintained by hydrogen bonding to an ionized D187 residue. However, the mutagenesis data for phnP above indicate a different role for H200. This is most likely in ground state binding of the substrate. This may take the form of a positively charged H200 hydrogen bonded or ion-paired with the negatively charged oxygen of the substrate phosphate diester. Although such an interaction would also be expected to stabilize the transistion state for phosphodiester hydrolysis, the

mutatgenesis data above indicate this is not the case for phnP, at least with the activated substrate bpNPP.

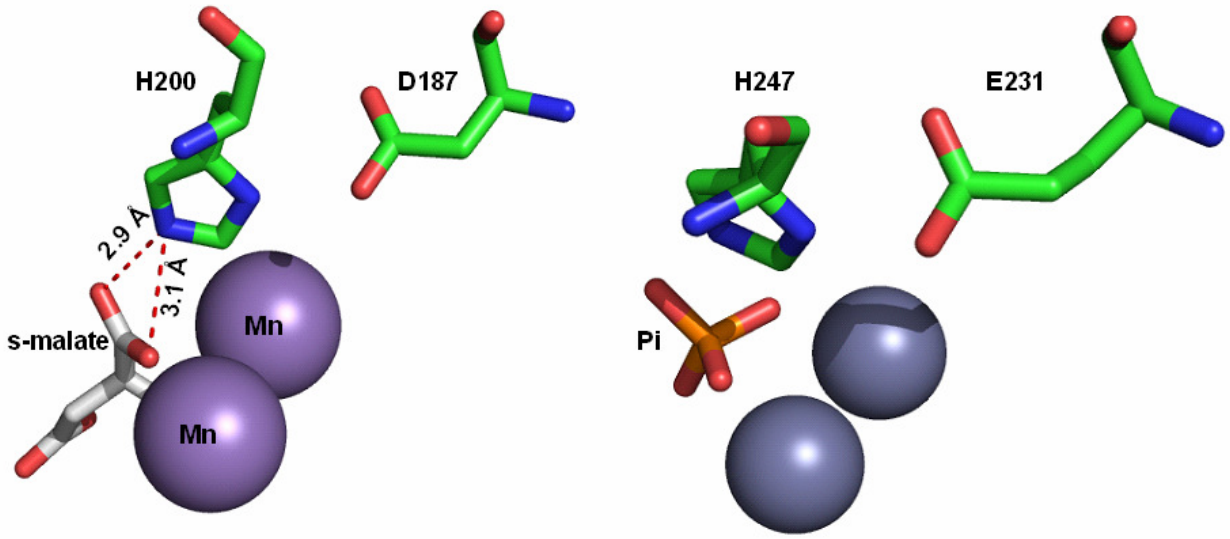

Figure 2-19. The D187-H200 interaction in phnP. (A) D187 and H200 are shown with sphere corresponding to one manganese ion. (B) Structurally similar placement of E231 and H247 in *B. subtilis* tRNase Z (PDB code 1y44), shown along with spheres corresponding to two zinc ions at the active site.

Histidine 222 contributes to coordinating one of the manganese ions, MnII. With 1 mM Mn^{2+} present, the substitution of H222 with alanine reduces the catalytic efficiency (k_{cat}/K_M value) 10-fold compared with the wild type phnP, whereas the K_M did not change significantly (**Table 2-7, Figure 2-18A**). An analogous but more dramatic effect has been reported by Vogel *et al.* in that the mutation of H270 (H222 in phnP) to alanine dramatically lowered the k_{cat} by ~ 3000-fold, while the K_M value increased by 5-fold, indicating that this residue is

primarily involved in transition state stabilization by acting as a metal ligand (9). Although an increase of the K_M value was not observed with the H222A mutant of phnP, the 10-fold reduction in k_{cat}/K_M and the 60-fold decrease of the K_M^{app} value toward Mn^{2+} (**Table 2-8**) suggest a similar role for this residue in coordinating one of the metal ions. The less impairment of this substitution might indicate that this histidine residue motif is less rigid than other motif residues.

Based on the kinetic investigations with all the alanine mutants, the residues involved in the binuclear metal binding at the active site (H78A, D80A, D164A, D54A, and H222A) all demonstrated reduced k_{cat} values 1-3 orders of magnitude of the wild type, but had relatively very minor effects on the K_M values. The Michaelis constant (K_M) is related to a dissociation constant that reflects the binding affinity of the substrate to the free enzyme. Small effects on K_M values of the alanine mutants and large decrease of k_{cat} values suggest that these residues are involved with metal ion binding and catalysis, but not directly involved with substrate recognition and binding.

2.3.9 pH dependence of phnP

To determine the ionizations important for catalysis and substrate binding, the dependence of k_{cat}/K_M upon pH was measured at low substrate concentration ([S] << K_M) by the substrate depletion method using bpNPP as the substrate. The k_{cat} and k_{cat}/K_M values were obtained at various pH values and saturating concentration of Mn^{2+}. Due to the precipitation of Mn^{2+} at basic pH values, data could not be collected at pH values higher than 8.5. A bell-shaped profile with an

optimum pH at approximately 7.1 for k_{cat}/K_M was observed (**Figure 2-20**). The plot also revealed one ionization state that must be deprotonated for catalysis with a pK_a value of 6.49 ± 0.03, as well as another ionization that must be protonated for catalysis with a pK_a value of 7.65 ± 0.03. The pH profile of wild type phnP may arise from a number of scenarios: ionization of residues involved in general acid and general base catalysis; ionization of metal ligands; and ionization of the metal bound water. Based on our mutagenesis, kinetic and structural investigations on phnP, an ionized D80 could simultaneously coordinate Mn I as well as act as a general base to deprotonate water, thereby giving rise to the ionization with a pK_a of 6.49, as has been suggested by others (*8*). Simultaneously, H200 in a protonated state, corresponding to the ionization state with a pK_a of 7.65, can donate a proton to be transferred to the final step to cleave the phosphodiester bond to form the product. However, mutation of H200 suggests only a minor effect on transition state stabilization, which is not consistent with this role. The pH dependence of the H200A mutant would help to clarify the origin of this alkaline pK_a.

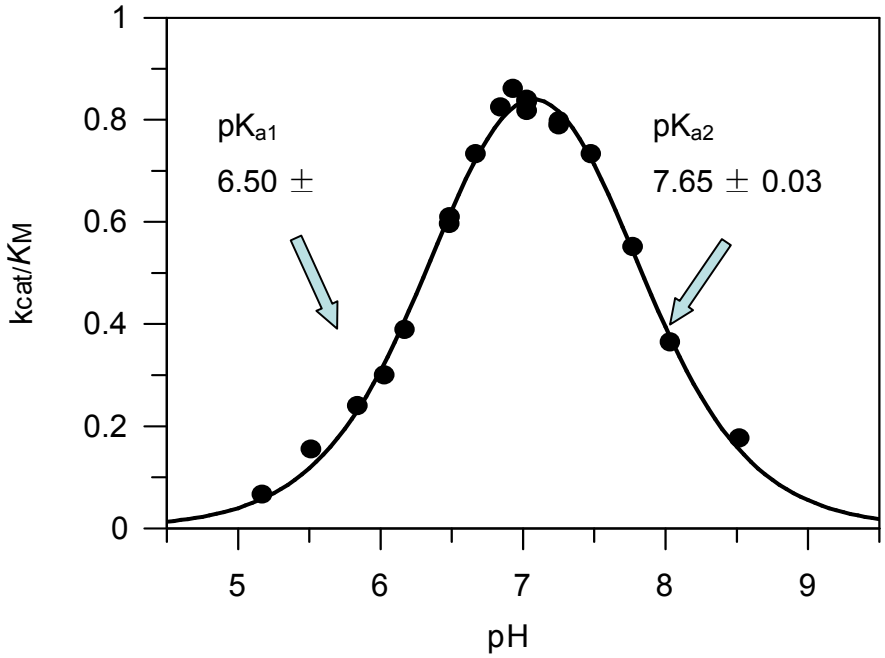

Figure 2-20. k_{cat}/K_M for the pH dependence of hydrolysis of bpNPP (with 1mM Mn^{2+} present) by *E. coli* phnP.

2.3.10 Inhibition studies with phosphate and vanadate

Enzymes from the metallo-β-lactamase superfamily share the common characteristic that two metal ions are utilized for catalyzing hydrolysis. In addition, several histidines and aspartates at the active site are positioned to interact with the metals or the substrate. It is believed that at the transition state of the hydrolysis of a phosphodiester, a pentacoordinate, trigonal bipyramidal, or phosphorane, geometry is formed around the central phosphorus atom. Vanadate (VO_4^{3-}) under alkaline conditions or in enzyme active sites can form

VO_5^{4-}, a close structural and charge mimic of the phosphorane, and thus can act as an analog of the transition state expected for phosphoryl transfer (31). Accordingly, vanadate is typically an inhibitor of many phosphoryl transfer enzymes (32, 33). Since we are not fully clear about the full catalytic mechanism for phnP, including substrate specificity and regioselectivity of phnP toward 2':3'-cyclic nucleotides, structures of transition state analogs could help clarify the roles of active site residues and reveal conformational changes during the catalysis. Attempts to co-crystallize phnP with vanadate and nucleosides have so far not succeeded. On the other hand, the inhibition dissociation constant (K_i) for vanadate could be determined by kinetic studies using bpNPP as the substrate in the presence of 1 mM Mn^{2+} (**Figure 2-21**). Vanadate demonstrated competitive inhibition during the catalysis of bpNPP with a K_i value of 67 μM, suggesting that pentavalent vanadate (VO_5^{4-}) is a reasonable approximation of the phnP transition state. P_i also exhibited competitive inhibition activity toward bpNPP hydrolysis by phnP with a K_i value of 208 μM (**Figure 2-22**). P_i is not a product from the hydrolysis of bpNPP, because phnP does not have phosphomonoesterase activity toward *p*-nitrophenyl phosphate. Nevertheless, it behaves as a competitive inhibitor but with a lower affinity (3 times lower based on the K_i values) than vanadate. The higher *K*i value relative to vanadate is consistent with the tetrahedral geometry of P_i, which resembles the ground state configuration of a substrate for phnP.

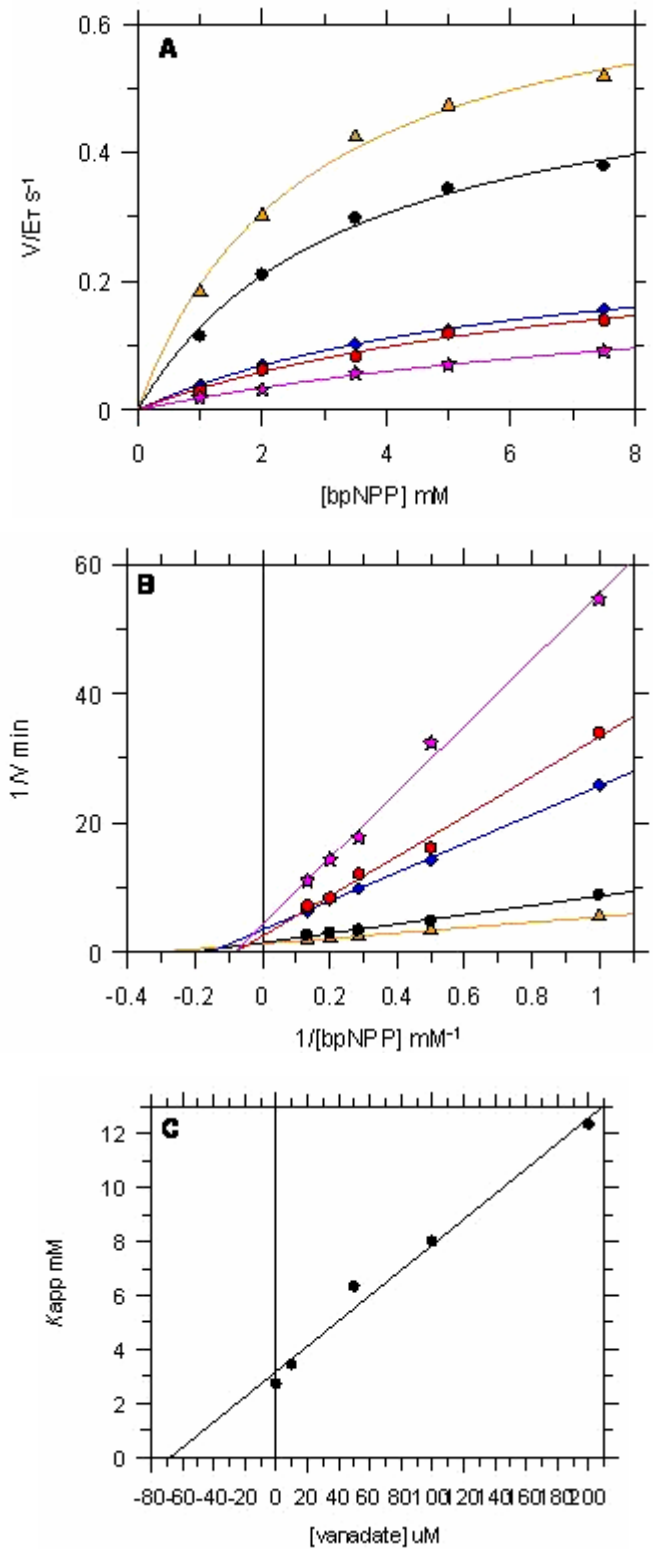

Figure 2-21. Michaelis-Menten plot (A), Lineweaver-Burk plot (B), and K_{app} vs [I] plot (C) of vanadate inhibition of hydrolysis of bpNPP by phnP. The vanadate concentrations were as follows: ▲, 0 μM; ●,10 μM; ◆, 50 μM; ● , 100 μM; ★, 200 μM.

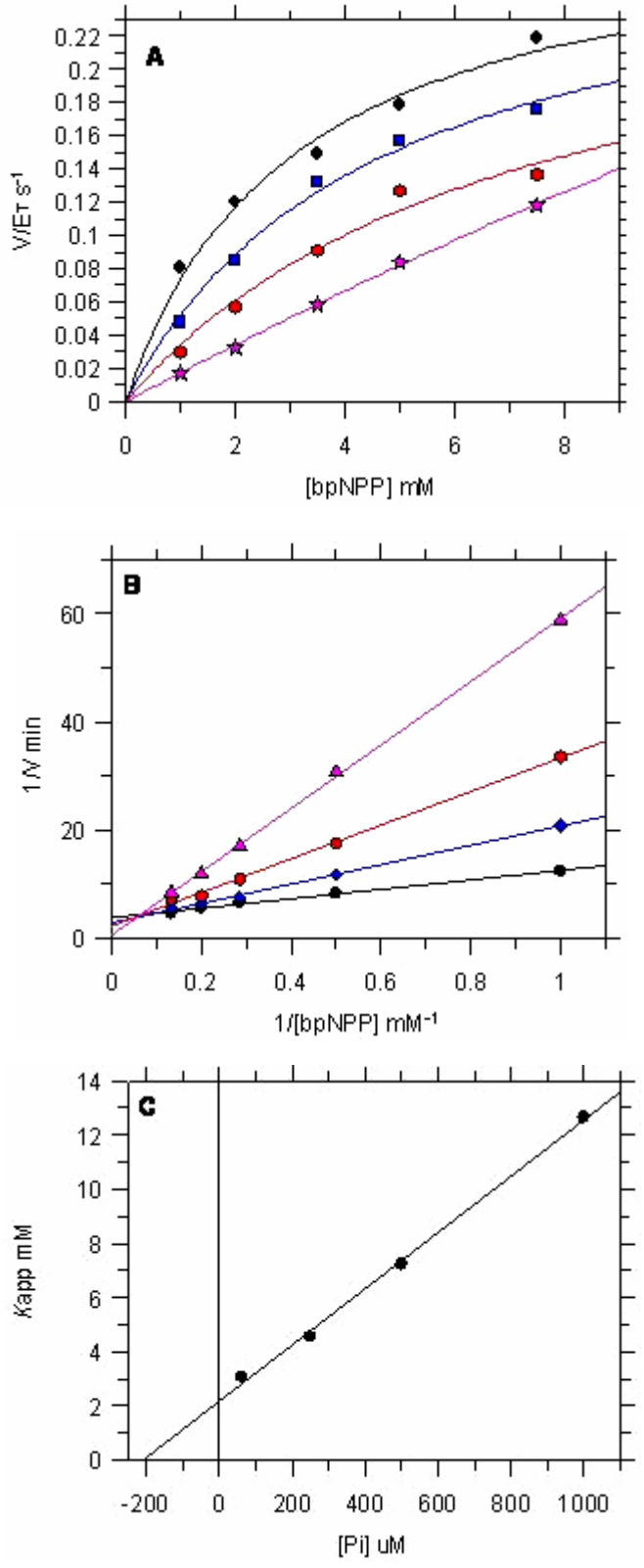

Figure 2-22. Michaelis-Menten plot (A), Lineweaver-Burk plot (B), and K_M^{app} vs [I] plot (C) of Pi inhibition of hydrolysis of bpNPP by phnP. The phosphate concentrations used were as the follows: ★ , 62.5 μM; ● , 250 μM; ♦ , 500 μM; ● ,1 mM.

2.3.11 Proposed mechanism for phnP

Based on the structural homology of phnP with tRNase Z enzymes and the kinetics studies of the active site mutants, the catalytic mechanism for cleavage of the phosphodiester bond of 2',3'-cyclic nucleotides by phnP, the best substrate identified thus far, can be proposed. The phosphodiester bond cleavage reaction would begin with deprotonation of a metal-bound water molecule by the D80 residue to create hydroxide ion to attack the phosphorous centre. This would displace the 2'–OH of ribose in an S_N2 fashion, proceeding through a phosphorane like transition state. For the final step, a proton must be donated to produce the 2'-OH on the ribose, but it is not clear which active site residue serves as a general acid catalyst, or whether another water molecule performs this role. Ultimately the phosphodiester bond is cleaved, leaving the phosphate at the 3' side (**Figure 2-23**). The binuclear metals contribute to the catalysis by lowering the pK_a of the attacking water to facilitate deprotonated by D80, as well as by polarizing the phosphoryl oxygen bond of the substrate and stabilizing the negative charge built up at the transition state during hydrolysis. Additionally, one or both of these metal ions could stabilize the negative charge on the leaving group as the reaction proceeds. It has been suggested that the more solvent-exposed metal ion (MnII), which is within 2.5 Å of the phosphoryl oxygen of a non-hydrolyzable inhibitor, polarizes the P=O bond for nucleophilic attack by the hydroxide ion (37). Kinetics studies of the H200A and D187A mutants suggest that the former residue participates in ground state binding of the phosphate

diester.

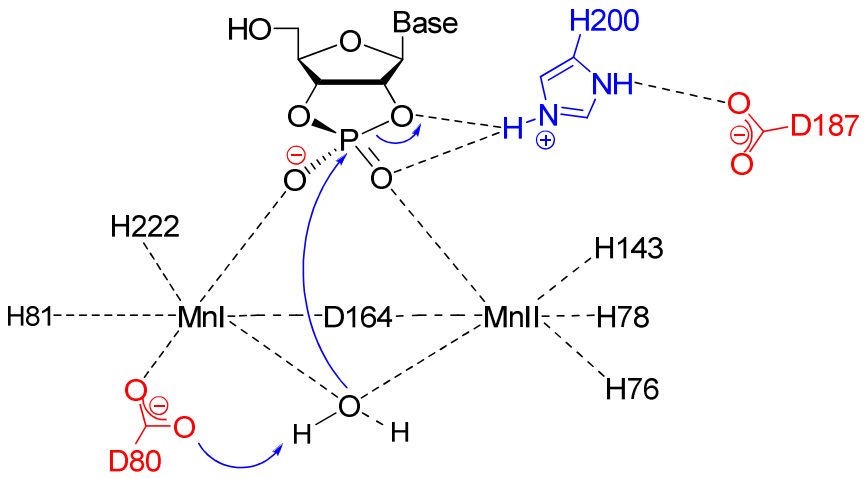

Figure 2-23. A potential mechanism scheme for hydrolyzing 2'3'-cyclic nucleotides by *E. coli* phnP. D80 acts as a general base and H200 is likely involved in substrate binding in the ground state. D187 forms a hydrogen bond to stabilize the protonated state of H200.

2.3.12 A potential physiological role for phnP

Although genetic studies indicate that phnP is not required for direct cleavage of a C-P bond, (1, 44), phnP is required for viable growth of *E. coli* on organophosphonates (44). This suggests a regulatory or accessory role for phnP in the C-P lyase pathway. Even though phnP was identified as a phosphodiesterase that can hydrolyze 2':3'-cyclic nucleotides, it is not certain that these are the true physiological substrates for phnP in relation to the C-P lyase pathway. However, 2':3'-cyclic nucleotides are known signaling molecules in the 'stringent response' pathway of bacteria (40,41). The stringent response

is one strategy that bacteria and other microorganisms have evolved to survive under stressful conditions such as nutrient deprivation. High levels of pppGpp and ppGpp (40-42) was discovered to accumulate in response to nutrient starvation by Gallant and Cashel (43). Both the synthesis and hydrolysis of (p)ppGpp are carried out by the RelA and SpoT proteins, respectively (**Figure 2-24**). Recently, the crystal structure of SpoT from *Streptococcus dysgalactiae* was reported with ppG2':3'p bound in the active site (40). This appeared to be a product of a cyclization reaction on ppGpp, where the 2'-OH attacked the neighbouring 3'-phosphoanhydride group, although it is not clear whether SpoT itself performed this reaction. This 2':3'-cyclic nucleotide appears to be a competitive inhibitor for the hydrolase active site of SpoT, which would prevent the degradation of the stringent response signal (p)ppGpp (40). Genetic studies have demonstrated P_i starvation activates the stringent response pathway and increases ppGpp levels in *E. coli*, which in turn activates the *pho* regulon, of which the *phn* operon (C-P lyase) is a member (44). Therefore, it is possible that ppG2':3'p (**Figure 2-24**) is a substrate for phnP. The fact that phnP can hydrolyze 2':3'-cyclic nucleotides to 3'-monophosphate products may be considered as a regulatory feedback that depends on the phosphorus source in the environment. Specifically, once the C-P lyase pathway is activated and organophosphonates are available at sufficient levels to satisfy cell growth, phnP may be used to degrade ppG2':3'p and relieve the inhibition of SpoT, which in turn would degrade ppGpp and turn off the stringent response.

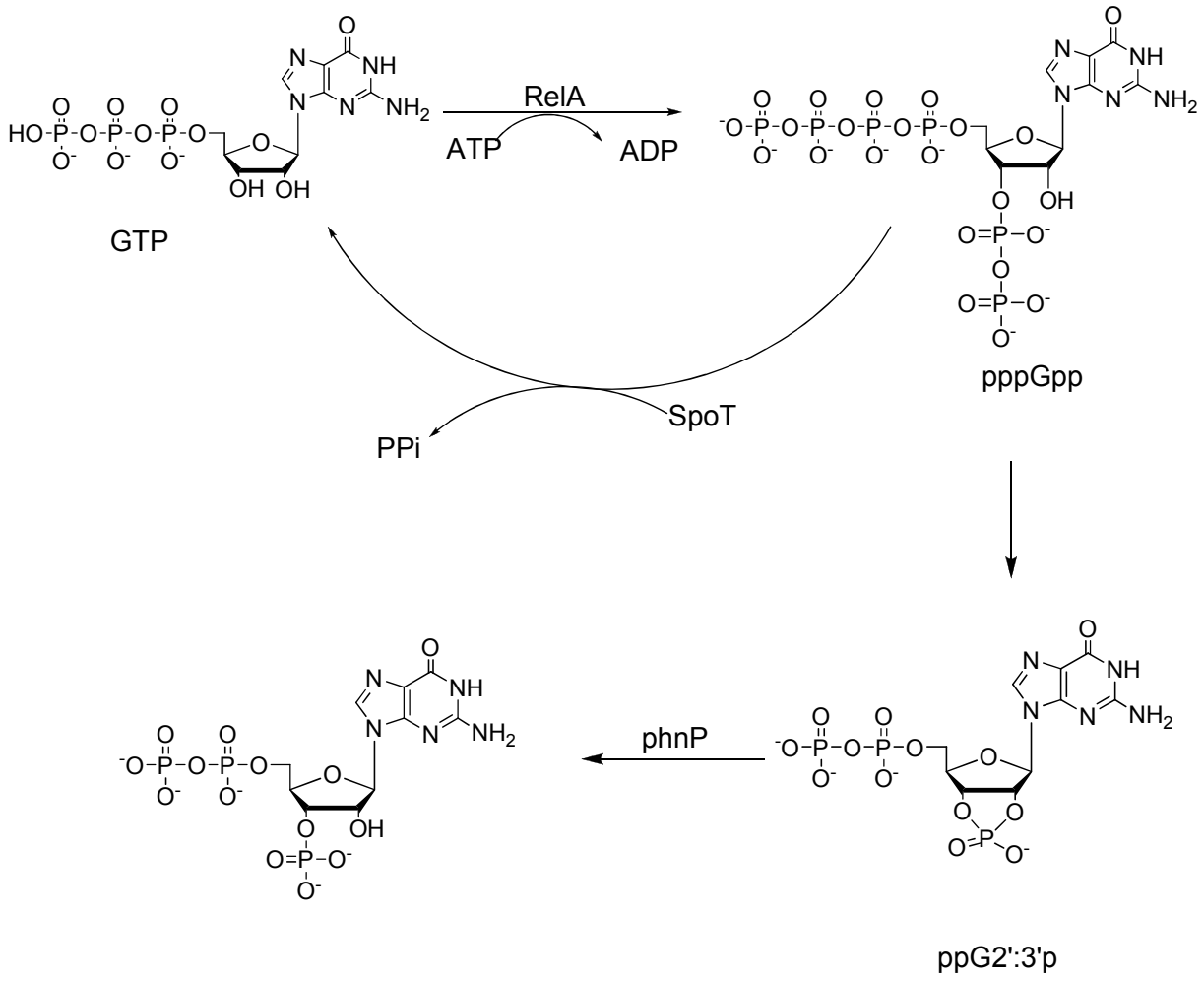

Figure 2-24. Potential physiological role that phnP may play in the bacterial stringent response pathway.

2.4 Conclusions

Sequence analysis assigned *E. coli* phnP to the metallo-β-lactamase superfamily (2), which utilize a binuclear metal binding site characterized in part by residues from the highly conserved sequence motif HXHXDH. With the use of general enzymatic screens and detailed biochemical and structural analysis, we demonstrated that phnP hydrolyzes the artificial phosphodiesterase substrate bpNPP and the potentially physiologically relevant substrate 2':3'-cAMP with greater specificity. The X-ray crystal structure of phnP at 1.4 Å resolution revealed a homodimer with two metal binding sites per monomer, one site occupied by two Mn^{2+} ions and the other occupied by a single Zn^{2+} ion. ICP-MS confirmed manganese and zinc as co-purifying with phnP, the latter metal apparently residing in a high affinity site. Alignment of phnP crystal structure with other homologues from the same family demonstrates that phnP has high structural homology to tRNase Z enzymes and a pyrroloquinoline quinone (pqq) biosynthesis enzyme pqqB. Notably, the tRNaseZ enzymes have virtually identical active site residues yet depend on zinc for catalysis.

Kinetic studies with all the alanine mutants toward bpNPP hydrolysis were carried out to elucidate the roles of all the highly conserved residues at the active site for the hydrolysis. It is observed that the affinity to manganese decreased with all the mutants compared to the wild type (apparent K_M values increased 24-563 times relative to wild type), and ICP-MS on several of the mutants further exhibited that essentially no manganese is present in the mutant

proteins, but the amount of zinc incorporated did not change significantly. This indicates that phnP selectively incorporates manganese at the active site for carrying out catalysis, whereas the single zinc atom plays a structural role, which was confirmed by the high resolution structure of the enzyme. Kinetic studies with all the mutants also demonstrated that substitution of all the residues coordinating two manganese ions with alanine did not change the K_M values, but decreased k_{cat} values to great extent (8-1430 times as relevant to wild type). Replacement of H200 with alanine did not change the k_{cat}, but the K_M value changed dramatically, indicating this residue is not involved in transition state stabilization, but rather in substrate binding.

In light of what is known about the mechanism of the catalysis of the diester bond cleavage from other binuclear zinc or iron enzymes with an established physiological function from the metallo-β-lactamase superfamily, it is likely that phnP catalyzes the phosphodiesterase bond cleavage of 2':3'-cyclic nucleotides in a similar way. The hydrolysis is initiated by the deprotonation of a water molecule by D80, producing hydroxide as a nucleophile to attack the phosphate. Two Mn^{2+} ions may function in concert to lower the pK_a of the attaching water, and polarize the P=O bond for nucleophilic attack by the hydroxide ion. As the hydrolysis proceeds, the two metal ions may also serve to neutralize the negative charge on the leaving group. A proton from a yet to be identified active site residue or a water molecule would be donated to the 2'-alkoxide on the ribose, yielding a cleaved phosphodiester bond and expulsion of

the phosphate at the 3’ position of the ribose. Of particular interest is the substrate specificity and regioselectivity of phnP. It is only known to catalyze the hydrolysis of 2’:3’-cyclic nucleotides, and the only product from the hydrolysis is 3’-monophosphate. It is likely that this regioselectivity is dictated by an in-line attack of water on the phosphodiester, displacing the 2’-OH (39). Further structural studies including co-crystallization of phnP complexed with 2’:3’-cyclic nucleotides may help elucidate the factors that determine the substrate specificity and regioselectivity, such as recognition of 2’:3’-cyclic nucleotides, but not 3’:5’-cyclic nucleotides, as well as regioselectivity.

The possible physiological function of phnP as a regulatory feedback to the level of phosphorus source still needs to be identified. Additional biochemical experiments such as *in vivo* studies with phnP knockout strains would help clarify the possibility that ppG2’:3’p is the *in vivo* substrate for phnP as part of the bacterial stringent response.

REFERENCES

1. Yakovleva GM, Kim SK, Wanner BL: **Phosphate-independent expression of the carbon-phosphorus lyase activity of *Escherichia coli***. *Appl. Microbiol. Biotechnol.* 1998, **49**:573-578.
2. Daiyasu H, Osaka K, Ishino Y, Toh H: **Expansion of the zinc metallo-hydrolase family of the beta -lactamase fold**. *FEBS Lett.* 2001, **503**:1-6.
3. Crowder MW, Spencer J, Vila AJ: **Metallo-beta -lactamases: Novel weaponry for antibiotic resistance in bacteria**. *Acc. Chem. Res.* 2006, **39**:721-728.
4. Schilling O, Wenzel N, Naylor M, Vogel A, Crowder M, Makaroff C, Meyer-Klaucke W: **Flexible Metal Binding of the Metallo-beta -lactamase Domain: Glyoxalase II Incorporates Iron, Manganese, and Zinc in vivo**. *Biochemistry* 2003, **42**:11777-11786.
5. Campos-Bermudez VA, Ribeiro Leite N, Krog R, Costa-Filho AJ, Soncini FC, Oliva G, Vila AJ: **Biochemical and Structural Characterization of Salmonella typhimurium Glyoxalase II: New Insights into Metal Ion Selectivity**. *Biochemistry* 2007, **46**:11069-11079.
6. Frazao C, Silva G, Gomes CM, Matias P, Coelho R, Sieker L, Macedo S, Liu MY, Oliveira S, Teixeira M, et al.: **Structure of a dioxygen reduction enzyme from *Desulfovibrio gigas***. *Nat Struct Bio.* 2000, **7**:1041-1045.
7. Kostelecky B, Pohl E, Vogel A, Schilling O, Meyer-Klaucke W: **The crystal structure of the zinc phosphodiesterase from *Escherichia coli* provides insight into function and cooperativity of tRNase Z-family proteins**. *J. Bacteriol.* 2006, **188**:1607-1614.
8. de la Sierra-Gallay IL, Pellegrini O, Condon C: **Structural basis for substrate binding, cleavage and allostery in the tRNA maturase RNase Z**. *Nature (London, U. K.)* 2005, **433**:657-661.
9. Vogel A, Schilling O, Meyer-Klaucke W: **Identification of metal binding residues for the binuclear zinc phosphodiesterase reveals identical coordination as glyoxalase II**. *Biochemistry* 2004, **43**:10379-10386.
10. Yakunin AF, Proudfoot M, Kuznetsova E, Savchekno A, Brown G, Arrowsmith CH, Edwards AM: **The HD domain of the *Escherichia coli* tRNA nucleotidyltransferase has 2',3'-cyclic phosphodiesterase, 2'-nucleotidase, and phosphatase activities.** *J. Biol. Chem.* 2004, **279**:54973.
11. Baikov AA, Evtushenko OA, Avaeva SM: **A malachite green procedure for orthophosphate determination and its use in alkaline**

phosphatase-based enzyme immunoassay. *Anal. Biochem.* 1988, **171**:266-270.

12. Vogel A, Schilling O, Niecke M, Bettmer J, Meyer-Klaucke W: **ElaC encodes a novel binuclear zinc phosphodiesterase**. *J. Biol. Chem.* 2002, **277**:29078-29085.
13. Gloster TM, Macdonald JM, Tarling CA, Stick RV, Withers SG, Davies GJ: **Structural, Thermodynamic, and Kinetic Analyses of Tetrahydrooxazine-derived Inhibitors Bound to beta -Glucosidases**. *J. Biol. Chem.* 2004, **279**:49236-49242.
14. Genschik P, Billy E, Swianiewicz M, Filipowicz W: **The human RNA 3'-terminal phosphate cyclase is a member of a new family of proteins conserved in Eucarya, Bacteria and Archaea**. *EMBO J.* 1997, **16**:2955-2967.
15. Spaeth B, Settele F, Schilling O, D'Angelo I, Vogel A, Feldmann I, Meyer-Klaucke W, Marchfelder A: **Metal Requirements and Phosphodiesterase Activity of tRNase Z Enzymes**. *Biochemistry* 2007, **46**:14742-14750.
16. Chen S, Yakunin AF, Kuznetsova E, Busso D, Pufan R, Proudfoot M, Kim R, Kim S-H: **Structural and Functional Characterization of a Novel Phosphodiesterase from *Methanococcus jannaschii***. *J. Biol. Chem.* 2004, **279**:31854-31862.
17. Aravind L: **An evolutionary classification of the metallo-beta -lactamase fold proteins**. *In Silico Biol.* 1999, **1**:69-91.
18. Tomatis PE, Rasia RM, Segovia L, Vila AJ: **Mimicking natural evolution in metallo-beta -lactamases through second-shell ligand mutations**. *Proc. Natl. Acad. Sci. U. S. A.* 2005, **102**:13761-13766.
19. Spaeth B, Canino G, Marchfelder A: **tRNase Z: the end is not in sight**. *Cell. Mol. Life Sci.* 2007, **64**:2404-2412.
20. Ishii R, Minagawa A, Takaku H, Takagi M, Nashimoto M, Yokoyama S: **Crystal Structure of the tRNA 3' Processing Endoribonuclease tRNase Z from *Thermotoga maritima***. *J. Biol. Chem* 2005, **280**:14138-14144.
21. Karkashon S, Hopkinson A, Levinger L: **tRNase Z Catalysis and Conserved Residues on the Carboxy Side of the His Cluster**. *Biochemistry* 2007, **46**:9380-9387.
22. Shin Dong H, Proudfoot M, Lim Hyo J, Choi I-K, Yokota H, Yakunin Alexander F, Kim R, Kim S-H: **Structural and enzymatic characterization of DR1281: A calcineurin-like phosphoesterase from Deinococcus radiodurans**. *Proteins* 2008, **70**:1000-1009.

23. Minagawa A, Takaku H, Takagi M, Nashimoto M: **A novel endonucleolytic mechanism to generate the CCA 3' termini of tRNA molecules in *Thermotoga maritima***. *J. Biol. Chem.* 2004, **279**:15688-15697.

24. Spaeth B, Kirchner S, Vogel A, Schubert S, Meinlschmidt P, Aymanns S, Nezzar J, Marchfelder A: **Analysis of the Functional Modules of the tRNA 3' Endonuclease (tRNase Z)**. *J. Biol. Chem.* 2005, **280**:35440-35447.

25. Minagawa A, Takaku H, Ishii R, Takagi M, Yokoyama S, Nashimoto M: **Identification by Mn2+ rescue of two residues essential for the proton transfer of tRNase Z catalysis**. *Nucleic Acids Res.* 2006, **34**:3811-3818.

26. Crowder MW, Wang Z, Franklin SL, Zovinka EP, Benkovic SJ: **Characterization of the Metal-Binding Sites of the beta -Lactamase from *Bacteroides fragilis***. *Biochemistry* 1996, **35**:12126-12132.

27. De Seny D, Prosperi-Meys C, Bebrone C, Rossolini GM, Page MI, Noel P, Frere J-M, Galleni M: **Mutational analysis of the two zinc-binding sites of the *Bacillus cereus* 569/H/9 metallo-beta -lactamase**. *Biochem. J.* 2002, **363**:687-696.

28. de la Sierra-Gallay IL, Mathy N, Pellegrini O, Condon C: **Structure of the ubiquitous 3' processing enzyme RNase Z bound to transfer RNA**. *Nat. Struct. Mol. Biol.* 2006, **13**:376-377.

29. Mandel CR, Kaneko S, Zhang H, Gebauer D, Vethantham V, Manley JL, Tong L: **Polyadenylation factor CPSF-73 is the pre-mRNA 3'-end-processing endonuclease**. *Nature (London, U. K.)* 2006, **444**:953-956.

30. Ryan K, Calvo O, Manley JL: **Evidence that polyadenylation factor CPSF-73 is the mRNA 3' processing endonuclease**. *RNA* 2004, **10**:565-573.

31. Davies DR, Hol WGJ: **The power of vanadate in crystallographic investigations of phosphoryl transfer enzymes**. *FEBS Lett.* 2004, **577**:315-321.

32. Stankiewicz PJ, Gresser MJ: **Inhibition of phosphatase and sulfatase by transition-state analogues**. *Biochemistry* 1988, **27**:206-212.

33. Stankiewicz PJ, Tracey AS, Crans DC: **Inhibition of phosphate-metabolizing enzymes by oxovanadium(V) complexes**. *Met Ions Biol Syst* 1995, **31**:287-324.

34. Gill SC, Von Hippel PH: **Calculation of protein extinction coefficients from amino acid sequence data**. *Anal. Biochem.* 1989, **182**:319-326.

35. Holm L, Park J. **DaliLite workbench for protein structure comparison**. *Bioinformatics* 2000, **16**, 566-567.

36. Schilling O, Spaeth B, Kostelecky B, Marchfelder A, Meyer-Klaucke W, Vogel A: **Exosite Modules Guide Substrate Recognition in the ZiPD/ElaC Protein Family**. *J. Biol. Chem.* 2005, **280**:17857-17862.

37. Benning MM, Shim H, Raushel FM, Holden HM: **High Resolution X-ray Structures of Different Metal-Substituted Forms of Phosphotriesterase from *Pseudomonas diminuta***. *Biochemistry* 2001, **40**:2712-2722.

38. Magnusson OT, Toyama H, Saeki M, Schwarzenbacher R, Klinman JP: **The Structure of a Biosynthetic Intermediate of Pyrroloquinoline Quinone (PQQ) and Elucidation of the Final Step of PQQ Biosynthesis**. *J. Am. Chem. Soc.* 2004, **126**:5342-5343.

39. Westheimer FH: **Pseudo-rotation in the hydrolysis of phosphate esters**. *Accounts Chem. Res.* 1968, **1**:70-78.

40. Hogg T, Mechold U, Malke H, Cashel M, Hilgenfeld R: **Conformational antagonism between opposing active sites in a bifunctional RelA/SpoT homolog modulates (p)ppGpp metabolism during the stringent response.** *Cell (Cambridge, MA, U. S.)* 2004, **117**:415.

41. Hou Z, Cashel M, Fromm HJ, Honzatko RB: **Effectors of the stringent response target the active site of *Escherichia coli* adenylosuccinate synthetase**. *J. Biol. Chem.* 1999, **274**:17505-17510.

42. Chatterji D, Ojha AK: **Revisiting the stringent response, ppGpp and starvation signaling**. *Curr. Opin. Microbiol.* 2001, **4**:160-165.

43. Cashel M, Gallant J: **Two compounds implicated in the function of the RC gene of *Escherichia coli***. *Nature* 1969, **221**:838-841.

44. Metcalf WW, Wanner BL: **Mutational analysis of an *Escherichia coli* fourteen-gene operon for phosphonate degradation, using TnphoA' elements**. *J. Bacteriol.* 1993, **175**:3430-3442.

45. Spira B, Silberstein N, Yagil E: **Guanosine 3',5'-bispyrophosphate (ppGpp) synthesis in cells of *Escherichia coli* starved for Pi**. *J. Bacteriol*. 1995, **177**, 4053-4058.

46. Larkin MA, Blackshields G, Brown NP, Chenna R, McGettigan PA, McWilliam H, Valentin F, Wallace IM, Wilm A, Lopez R, et al.: **Clustal W and Clustal X version 2.0**. *Bioinformatics* 2007, **23**:2947-2948.

Chapter 3

In vitro analyis of phnH, an essential enzyme directly involved in C-P bond cleavage in *E. coli*

3.1 Introduction

Carbon-phosphorus lyase (C-P lyase) is a multienzyme system found widely in Gram-negative bacteria that can directly cleave the C-P bond of a broad array of organophosphonates (1). C-P lyase is encoded by the *phn* operon, which in *E. coli* contains 14 genes (*phnCDEFGHIJKLMNOP*) that allows for the internalization and degradation of phosphonates (1). The highly conserved *phnGHIJKLM* set of genes (2) has been shown to be essential for C-P bond cleavage (3,4), but has yet to be characterized at the protein level.

Adams *et al.* (4) have cloned, expressed and purified *E. coli* phnH and determined the crystal structure to 1.70 Å resolution. The X-ray crystallographic structure of phnP exhibits weak structural similarities with pyridoxal 5'-phosphate dependent enzymes. The three dimensional structure of phnH protein may provide some insight into the specific function of this protein in the absence of its biochemical data.

Isothermal Titration Calorimetry (ITC) was used in this study as a tool to screen potential ligands for phnH. ITC is suitable for the calorimetric

characterization of non-covalent complex formation, particularly in biomolecular systems having K_d values (dissociation constant) in the nanomolar to micromolar range. In this technique, the two reaction partners are mixed by stepwise injections, and the resulting heat uptake or release is detected under conditions of constant temperature (Wiseman *et al.* 1989). **Figure 3-1** shows a schematic of an isothermal titration calorimeter (5). The core of the apparatus consists of a reference cell and a sample cell. The sample cell is filled with the protein solution, and a solution of the ligand is held in an injection syringe connected to the sample cell. The cells are enclosed in an adiabatic jacket to protect them from external temperature fluctuations. A small and precisely controlled heating current is applied to the cells to ensure a constant temperature. After injection of an aliquot of the ligand, the reaction taking place in the sample cell leads either to the release of heat or to the uptake of heat. The calorimeter responds immediately to counteract the heat change caused by the chemical reaction. Therefore, the changes in the calorimeter's heating power, integrated over time, yield the heat increment, released or taken up in the sample cell after the injection. The size of the heat increments decreases after each injection as progressive complex formation leads to decreasing concentration of the reactant B in the cell in its unbound form. The resulting titration curve yields the affinity constant for the interaction stoichiometry of binding, and the enthalpy of binding.

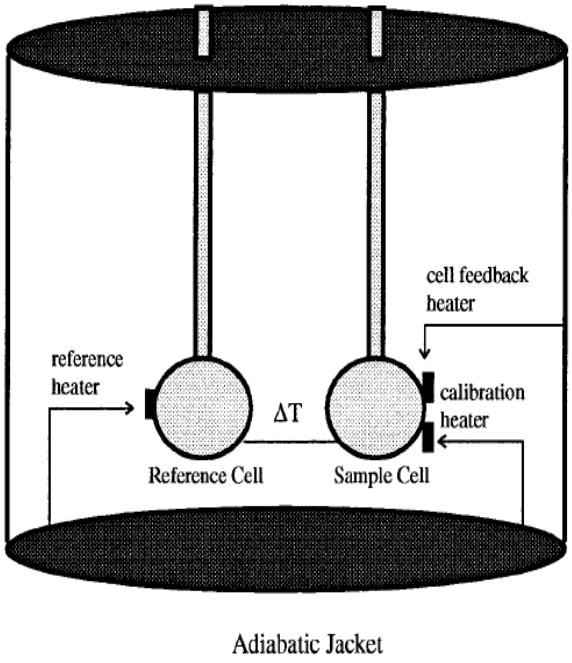

Figure 3-1. Schematic diagram of an ITC instrument. The figure was adopted from (5).

High-throughput analysis of phnH binding was also carried out by Dr. Alexander Yakunin and Prof. Aled Edwards at the Banting and Best research institute, University of Toronto. However, with all these efforts, no naturally occurring ligands or substrates were found to bind to phnH (including amino acids and nucleotides). Only one metal ion, calcium, was found to bind with phnH with the ITC technique.

3.2 Materials and Methods

3.2.1 Materials

All chemicals were purchased from Sigma Aldrich (Oakville, Ontario and US). Luria Bertani (Miller) agar and Luria Bertani (Miller) broth, HEPES, sodium

chloride and glucose are from Fisher Biosciences, Canada. Ampicillin was obtained from Roche Diagnostics Canada, IPTG was from Invitrogen, and protein standards used in SDS-PAGE were purchased from BioRad.

3.2.2 Expression and purification of recombinant phnH.

The conditions were described previously (4). Briefly, *E. coli* BL21 cells (Novagen) harboring pQI-phnH plasmid were grown in Luria-Bertani broth containing 100 µg/mL ampicillin and 1% glucose in an air shaker set to 37°C until an A_{600} of 0.6 was reached. Expression was then induced with 1 mM IPTG and the cells were left to grow for a further 4 hours at 30°C. The protein was purified with AKTA FPLC system (GE Healthcare Life Sciences, USA). Fractions containing pure phnH were pooled, concentrated with an Amicon ultrafiltration device to a final concentration of 20 mg/mL and dialyzed into 2 L of 50 mM HEPES, 150 mM NaCl, 1 mM of DTT, pH 7.5 overnight at 4°C before use.

3.2.3 Isothermal titration calorimetry (ITC) analysis

ITC experiments were performed using a VP calorimeter (MicroCal Inc., Northhampton, MA). PhnH was dialyzed overnight into 50 mM HEPES-150 mM NaCl (pH 7.5). Ligand samples were prepared in buffer saved from the dialysis of PhnH. All samples were passed through 0.45 µm filters and extensively degassed with stirring prior to use. Titration was performed by injecting 10 µl aliquots of 2.5 mM ligand into the ITC sample cell (1.5 mL) containing phnH (200 µM) equilibrated at 30°C. The following compounds were tested by ITC: methyl phosphonic acid, ethylphosphonic acid, 2-aminoethylphosphonic acid,

phenylphosphonic acid, α-D-ribofuranosyl-1-ethylphosphonic acid, ATP, ADP, AMP, GTP, 3':5'-cAMP, adenosine, acetyl-CoA, pyridoxal phosphate, pyridoxal, flavin adenine dinucleotide, flavin mononucleotide, NAD+, NADP+, thiamine diphosphate and *S*-adenosylmethionine. Metal ions such as Ca^{2+}, Mg^{2+}, Zn^{2+}, Ni^{2+}, Mn^{2+}, Co^{2+}, and Fe^{3+} (all in chloride forms) were tested as well. All compounds were purchased from Sigma-Aldrich (Oakville, Ontario); the exception was α-D-ribofuranosyl ethylphosphonic acid, which was synthesized as described previously (6).

3.2.4 High-throughput analysis of ligand binding to phnH

High-throughput ligand screening of phnH was analyzed by following temperature-dependent protein aggregation using static light scattering (StarGazer; Harbinger Biotech, Toronto, Canada and 4) as described (7). This technique is based on the concept that binding of small molecules to the target protein will affect protein thermal stability, which will result in a shift in the denaturation or aggregation temperature (7). 430 common metabolites, amino acids, metals, sugars, nucleotides, and antibiotics were screened in this way as potential ligands for phnH. Reactions were performed in 384-well plates (Nunc, VWR, Canada) in 50 µl aliquots containing 0.1 M HEPES buffer (pH 7.5), 0.15 M NaCl, 1 mM ligand, and 15 µg phnH. To prevent evaporation of water, the samples were covered with 50 µl of mineral oil, and the temperature range used was 27- 80°C.

3.3 Results and Discussion

3.3.1. Expression and purification of phnH

PhnH was expressed in a soluble form in LB media with 100 µg/mL ampicillin and 1% Glucose. Purification was achieved in one step with a Ni-NTA column to yield 170 mg/L of culture (**Figure 3-2**).

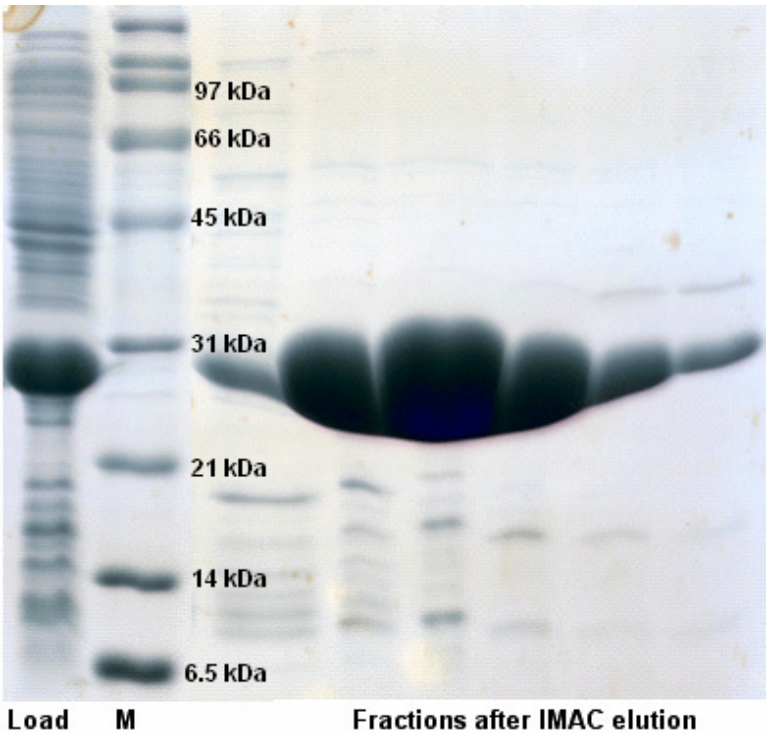

Figure 3-2. Purification of phnH by Ni-NTA chromatography. Shown is a 15% SDS-PAGE gel. M: BioRad broad range marker.

3.3.2 Ligand binding studies of phnH with phosphonates and cofactors

Isothermal titration calorimetry was also used to screen the ligands or potential substrate that can bind to phnH. Such cofactors as FAD, FMN, acetyl-CoA, thiamine diphosphate, PLP (pyridoxal 5-phosphate), NAD+, NADP+, and

S-adenosylmethionine failed to bind phnH. No binding was detected with organophosphonates such as methylphosphonic acid, phenylphosphonic acid, propylphosphonic acid, or α-D-ribofuranosyl ethylphosphonate, an intermediate produced by *E. coli* during alkylphosphonate metabolism (3) as well as ATP, ADP, AMP, and cAMP. Divalent metal ions such as Ni^{2+}, Co^{2+}, Mn^{2+}, Zn^{2+}, Mg^{2+} and Ca^{2+} were also probed for binding activity. PhnH failed to bind any of the metals except calcium. Integration of the binding heats for calcium demonstrated a dissociation constant (K_d) of 200 μM with the stoichiometry of 0.2 (**Figure 3-3).** The stoichiometry is uncertain due to the difficulty in fitting data derived from weak binding. A screen of potential substrates and cofactors were performed in the presence of calcium and magnesium as well. However, these metals failed to promote the interaction of any of these compounds with phnH. High throughput screening with 430 common metabolites, metals, cofactors, sugars, nucleotides, amino acids, and antibiotics also proved to be unsuccessful. The negative screening results mentioned above might be an indication that phnH, with no sequence homology to other putative homologues with known function, may be specific for an as yet unidentified substrate or ligand. Since genetic studies have demonstrated that *phnG-phnM* are required to cleave the C-P bond (10,11), it is also important to consider the possibility that phnH may only achieve its catalytic activity by interacting with another member, or several other members of the *phn* operon by forming an active complex, which makes it difficult to search and identify the physiological substrate for phnH.

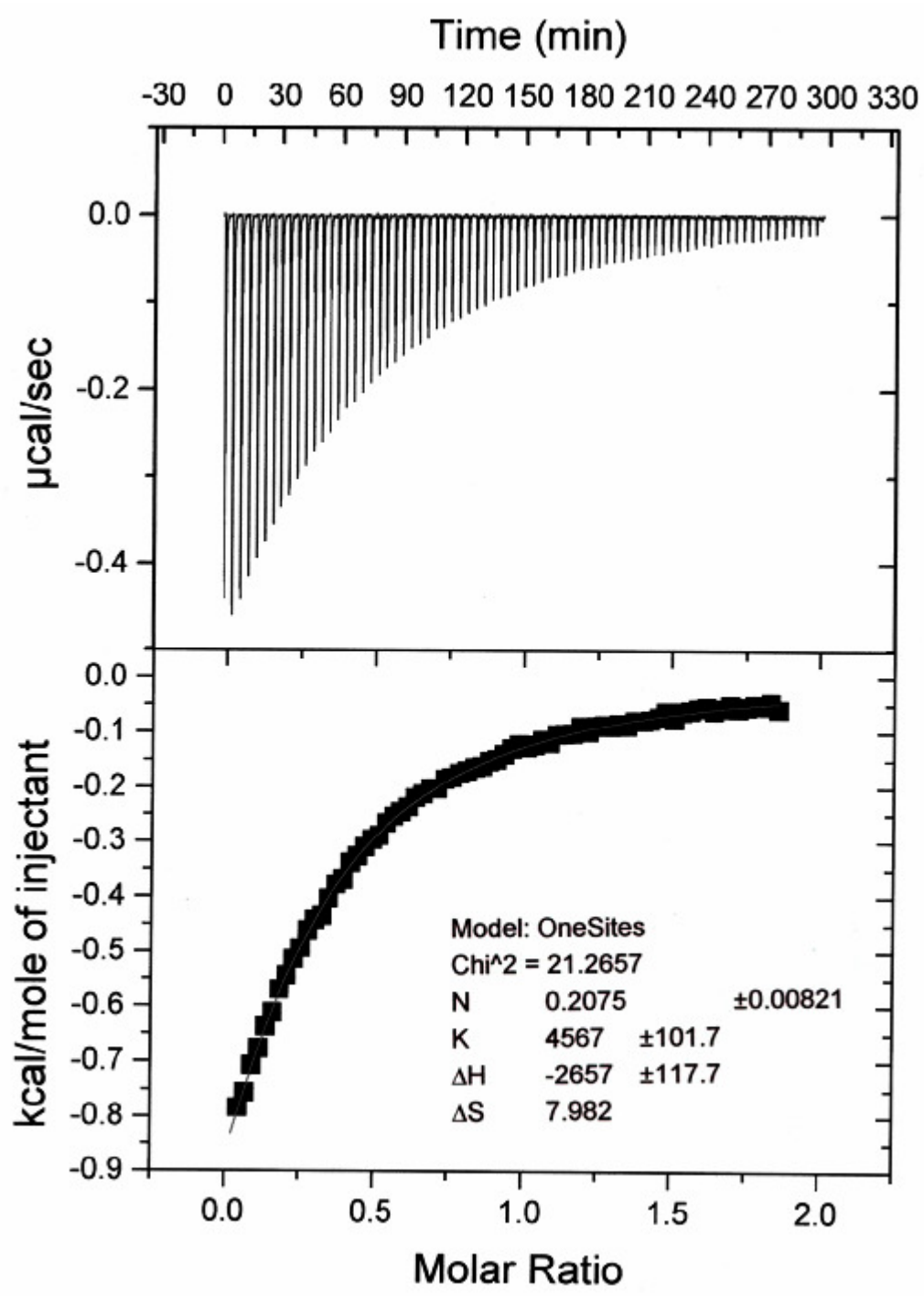

Figure 3-3. ITC curves of calcium binding to phnH. Data was fit to a one site model and yielded the following thermodynamics parameters: K_a = 4600 M^{-1} ± 100 M^{-1} (or K_d = 220 μM) Δ*H*= -2.7 kcal/mol ± 0.1 kcal /mol, Δ*S* = 8.0 cal/mol. Upper panel: raw data for sequential titrations of calcium solution into the protein solution. Lower panel: intergrated heats as a function of the Ca^{2+}/protein ratio.

REFERENCES

1. Chen CM, Ye QZ, Zhu Z, Wanner BL, Walsh CT: **Molecular biology of carbon-phosphorus bond cleavage. Cloning and sequencing of the phn (psiD) genes involved in alkylphosphonate uptake and C-P lyase activity in *Escherichia coli* B**. *J. Biol. Chem.* 1990, **265**:4461-4471.
2. Huang J, Su Z, Xu Y: **The evolution of microbial phosphonate degradative pathways**. *J. Mol. Evol.* 2005, **61**:682-690.
3. Yakovleva GM, Kim SK, Wanner BL: **Phosphate-independent expression of the carbon-phosphorus lyase activity of *Escherichia coli***. *Appl. Microbiol. Biotechnol.* 1998, **49**:573-578.
4. Adams MA, Luo Y, Hove-Jensen B, He S-M, van Staalduinen LM, Zechel DL, Jia Z: **Crystal structure of PhnH: an essential component of carbon-phosphorus lyase in *Escherichia coli***. *J. Bacteriol.* 2008, **190**:1072-1083.
5. Pierce MM, Raman CS, Nall BT: **Isothermal titration calorimetry of protein-protein interactions**. *Methods* 1999, **19**:213-221.
6. Luo Y, Zechel DL: **A concise synthesis of alpha -D-ribofuranosyl alkylphosphonates, Putative substrate intermediates for the carbon-phosphorous lyase system**. *Can. J. Chem.* 2006, **84**:743-747.
7. Senisterra GA, Markin E, Yamazaki K, Hui R, Vedadi M, Awrey DE: **Screening for ligands using a generic and high-throughput light-scattering-based assay**. *J. Biomol. Screening* 2006, **11**:940-948.
8. Metcalf WW, Wanner BL: **Mutational analysis of an Escherichia coli fourteen-gene operon for phosphonate degradation, using TnphoA' elements**. *J. Bacteriol.* 1993, **175**:3430-3442.
9. Metcalf WW, Wanner BL: **Involvement of the Escherichia coli phn (psiD) gene cluster in assimilation of phosphorus in the form of phosphonates, phosphite, inorganic phosphate esters, and inorganic phosphate**. *J. Bacteriol.* 1991, **173**:587-600.
10. Dyhrman ST, Chappell PD, Haley ST, Moffett JW, Orchard ED, Waterbury JB, Webb EA: **Phosphonate utilization by the globally important marine diazotroph *Trichodesmium***. *Nature (London, U. K.)* 2006, **439**:68-71.
11. Yakovleva GM, Kim SK, Wanner BL: **Phosphate-independent expression of the carbon-phosphorus lyase activity of *Escherichia coli***. *Appl. Microbiol. Biotechnol.* 1998, **49**:573-578.

Chapter 4

A fluorescent probe of C-P lyase activity *in vivo*

4.1 Introduction

Genetic studies on C-P lyase activity towards organophosphonates has demonstrated the requirement of the *phn* operon encoded 14 genes (*phnCDEFGHIJKLMNOP*) in *E. coli* (5-12). Unfortunately, biochemical characterization of the C-P lyase pathway has been proven to be difficult. C-P lyase activity toward organophosphonate degradation is lost upon cell lysis, suggesting that the active system is membrane associated (13). The degradation products of *E. coli* growth on methylphosphonate are methane and P_i (see **Figure 1-4A and ref 18**). Wanner (14) and Hove-Jensen (15) have demonstrated C-P lyase activity by monitoring methane production from degradation of methylphosphonate by *E. coli* wild type and mutant strains with gas chromatography, through which the *phnGHIJKLM* set of genes was shown to be necessary for cleavage of the C-P bond. Murata *et al.* (16) claimed to have observed *in vivo* C-P lyase activity by monitoring the inorganic phosphate release from the degradation of phosphanates by *Enterobacter aerogenes* IFO 12010 in a cell free system. However, this study failed to distinguish if there is formation of phosphate from other metabolic reactions. More recently Kononova *et al*. claimed to have elicited C-P lyase activity in a cell-free system when ATP and NADH was added to the cell lysate (19).

Motivated by the difficulty in characterizing the C-P lyase individually or in a complex, we came up with a hypothesis that a fluorescently labeled phosphonate substrate could be degraded *in vivo* as the only phosphorus source by *E. coli* into fluorescently labelled intermediates, which could be easily detected and analyzed by TLC and HPLC. With this assumption, an amino alkyl phosphonate with a dansyl fluorophore was synthesized (FPn, **4** in **Figure 4-1**) after which it was fed to *E. coli* cultured in phosphate free media. Thin layer chromatography and mass spectrometry were used to detect the fluorescent alkane product in collaboration with Bjarne Hove-Jensen (University of Copenhagen, Denmark). *E. coli phn* mutant strains were also tested in the same way. Disappearance of spots or presence of new spots is an indication of intermediates or products produced by the degradation of FPn. With this useful chemical probe, the pathways for degrading the organophosphonates could be elucidated, and more promisingly, this may provide clues for potential substrates for individual C-P lyase enzymes.

4.2 Experimental procedures and Methods

4.2.1 Materials

All chemicals and MOPS minimal media components were purchased from Sigma Aldrich. Dry solvents such as THF, CH_2Cl_2, acetonitrile were produced on a Pure Solv solvent purification system (Innovative Technologies

Inc., Newburgport, MA). TLC silica gel plates (Merck Kieselgel 60 F_{254}) were obtained from EMD Chemicals Inc. The *E. coli phn*$^+$ strain (HO1429) and *phnH* knockout strain (HO2534) were obtained from Dr. Bjarne Hove-Jensen, University of Copenhagen, Denmark. All NMR spectra were acquired on Bruker AVANCE 300 and 400 instruments. EI-MS was performed with Waters ZQ Single Quad MS Instrument by Dr. Yimin She and Jessie Sui of the Queen's Department of Chemistry.

4.2.2 Synthesis of dansyl amino alkyl phosphonate (FPn)

Diethyl (3-aminopropyl) phosphonate (2). Reduction of diethyl (2-cyanoethyl) phosphonate (**1**, **Figure 4-1**) using $NaBH_4$ and $CoCl_2$ was performed according to Osby *et al.* (1). A solution of $CoCl_2 \bullet 6H_2O$ (0.124 g, 0.52 mmol) and diethyl (2-cyanoethyl)-phosphononate (1 g, 5.23 mmol) in THF (40 mL) and water (20 mL) was stirred vigorously and cooled intermittently with an ice-water bath while $NaBH_4$ (0.396 g, 10.46 mmol) was added in portions over 8 minutes. After 3 hours, TLC analysis indicated a trace amount of starting material, so additional $NaBH_4$ (0.1 g) was added. The reaction proceeded for another two hours, 28% NH_4OH solution was added, and the reaction was filtered. THF was removed from the filtrate under vacuum and the remaining aqueous residue was extracted with 4 x 40 mL of CH_2Cl_2. The combined CH_2Cl_2 layers were dried with sodium sulfate and concentrated to afford crude diethyl (3-aminopropyl) phosphonate (0.4 g, 2.05 mmol, 40%) (**2, Figure 4-1**).

[3-[[[5-(dimethylamino)-1-naphthalenyl]sulfonyl]aminopropyl] diethylphosphonate (3).

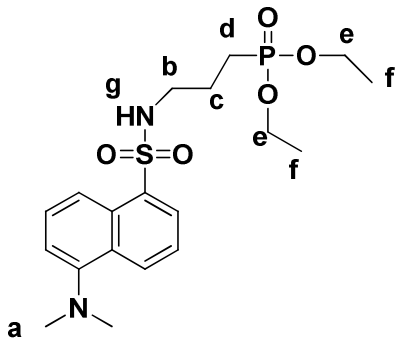

To the solution of the crude product 2 in dry CH_2Cl_2 was added dansyl chloride (0.663 g, 2.46 mmol) and triethylamine (0.415 g, 4.1 mmol) (2), and the reaction mixture was stirred at room temperature for 32 hours under nitrogen. After workup and removal of the solvent, the crude reaction product was purified by chromatography on silica gel column eluted with MeOH / CH_2Cl_2 (3 : 97). Evaporation of the solvent afforded the protected dansyl phosphate (**Figure 4-1**) in 53% yield. ^{1}H-NMR (Figure 4-2, 300 MHz, $CDCl_3$) δ 8.56 (d, *J*= 8.4 Hz, 1H, arom. H), 8.34 (d, *J*= 8.7 Hz, 1H, arom. H), 8.24 (dd, *J*=1.2 Hz, *J*=7.5 Hz, 1H, arom. H), 7.50-7.59 (m, 2H, arom. H's), 7.20 (d, *J*= 7.5 Hz, 1H, arom. H), 5.74 (br, s, 1H, NH^{g}), 4.05 (m, 4H, CH_2^{e}), 2.99 (m, 2H, CH_2^{b}), 2.91 (s, 6H, CH_3^{a}), 1.71 (m, 4H, $CH_2^{c,d}$), 1.29 (t, *J*= 3.6 Hz, 6H, CH_3^{f}); ^{31}P-NMR (400 MHz, $CDCl_3$), δ 31.65. LR-MS (EI): found *m/z* $[M]^{\bullet+}$ 428.1, calcd *m/z* 428.1.

[3-[[[5-(dimethylamino)-1-naphthalenyl]sulfonyl]aminopropyl] phosphonic acid (4).

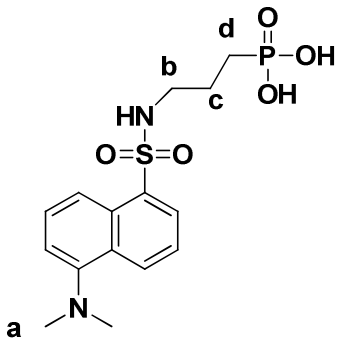

To the ice-cooled purified 3 (0.45 g, 1.05 mmol) reaction in dry acetonitrile, trimethylsilyl bromide (0.894 g, 5.84 mmol) was added in drops and allowed to react at room temperature for 24 hours. The solvent was removed under vacuum and 20 mL of methanol / water (9:1) was added to the remaining residue. The mixture was stirred at room temperature for 2 hours (2). The final product (**4, Figure 4-1**) was separated and purified with BioRad AG-1X8 ion exchange column according to (3). The column was eluted with gradient of 1 M to 4 M of formic acid and all the fractions containing the product (monitored by silica gel TLC, 12:3:5 of *n*-butanol: acetic acid: water) were pooled, followed by evaporation of the solvent yielding the pure product (300 mg, yield 77%, total overall yield 15.4%). The final product was neutralized with NaOH to yield the fluorescent phosphonate sodium salt (**5**, **Figure 4-1**). ^{1}H-NMR (Figure 4-3, 500 MHz, D_2O) δ 8.65 (d, *J*= 8.5 Hz, 1H, arom. H), 8.35 (d, *J*= 8.5 Hz, 1H, arom. H), 8.24 (d, *J*= 7.5 Hz, 1H, arom. H), 8.01 (d, *J*= 8.0, 1H, arom. H), 7.80 (m, 2H, arom. H's), 3.44 (s, 6H, CH_3^{a}), 2.91 (m, 2H, CH_2^{b}), 1.38 (m, 2H, CH_2^{c}), 1.26 (m,

2H, CH_2[d]); ^{13}C-NMR (100 MHz, D_2O) δ 138.4, 135.3, 130.5, 128.6, 128.1, 127.0, 126.4, 125.6, 125.6, 119.5, 46.8, 24.3, 23.0, 22.5; ^{31}P-NMR (500 MHz, D_2O), δ 30.13; LR-MS (ESI): found *m/z* ([M-H]$^-$) 371.2,([2M-H]$^-$) 743.1, calcd *m/z* 371.1

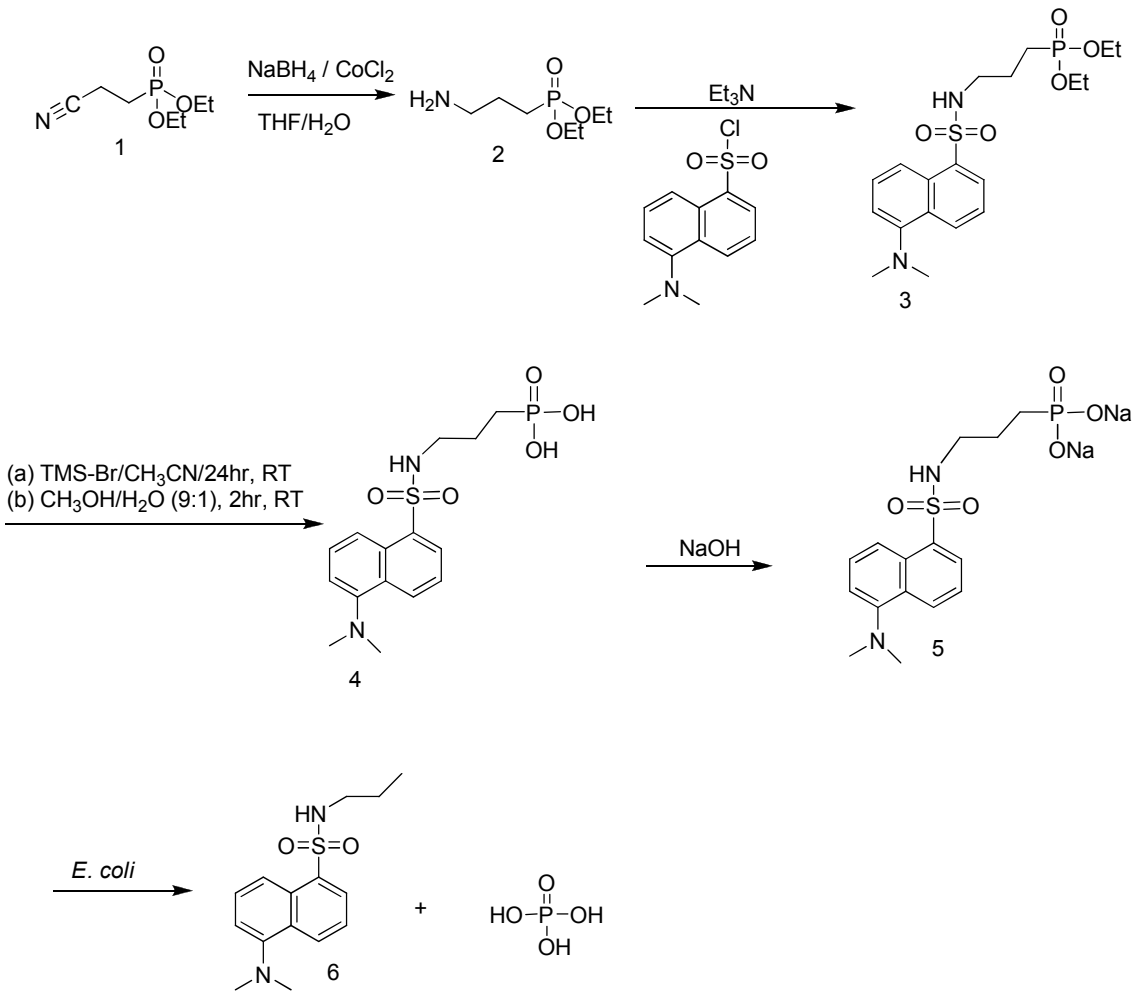

Figure 4-1. Synthetic scheme of FPn **5** and anticipated fluorescent alkane **6** and phosphate products.

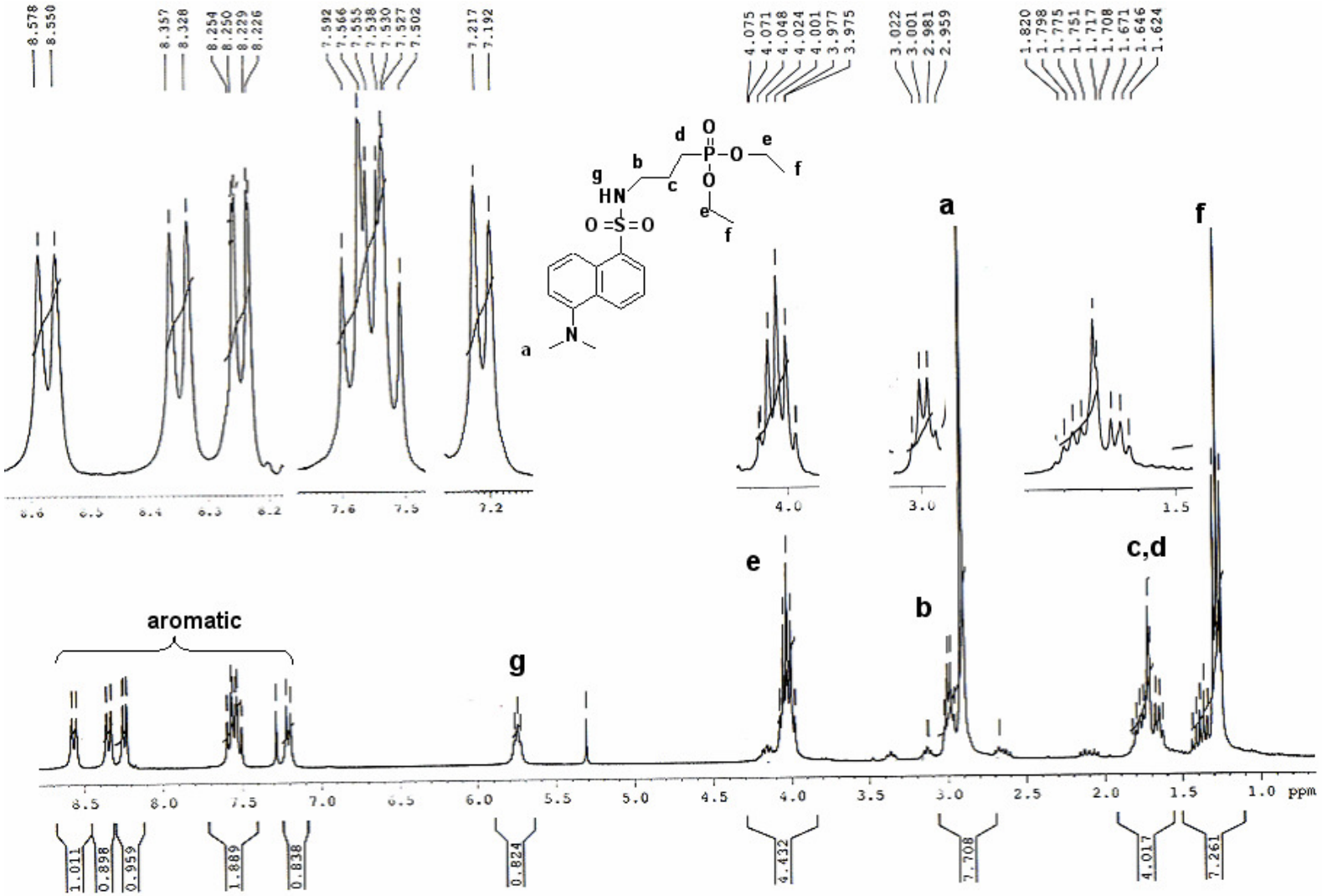

Figure 4-2. ^{1}H-NMR spectrum (300 MHz, $CDCl_3$) of dansylpropylamide diethyl phosphate **3**.

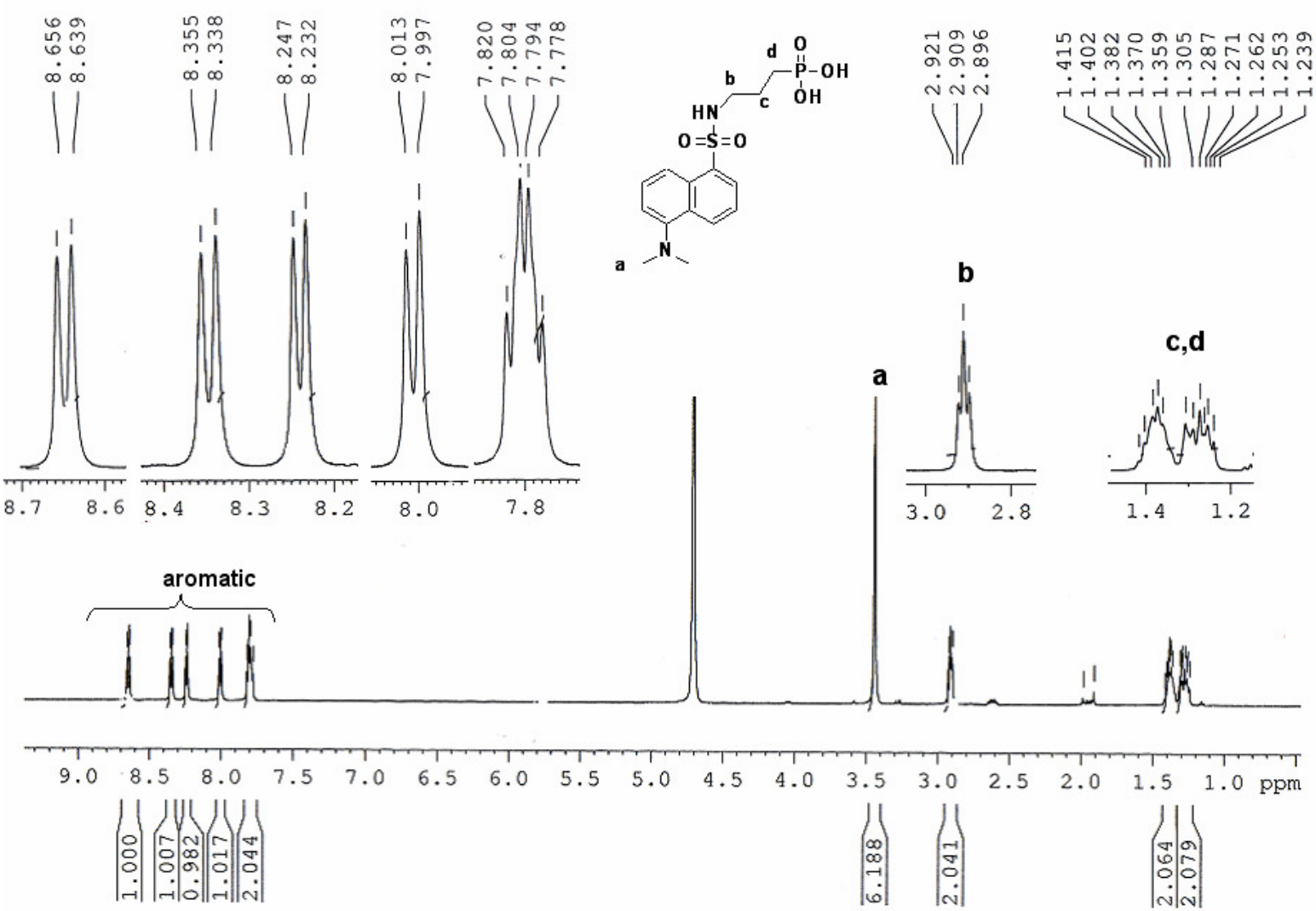

Figure 4-3. ^{1}H-NMR spectrum (500 MHz, D_2O) of dansylpropylamide phosphonic acid **4**.

4.2.3 Synthesis of dansylpropylamide as a standard

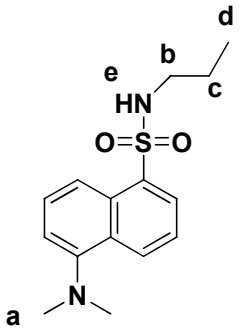

The pure reference dansyl propylamide product was synthesized using a procedure adopted from Summers (17). 0.2 mmol (0.054g) of dansyl chloride in 20 mL of dry acetonitrile was mixed with 2.43 mmol (0.144g) of propylamine and stirred at room temperature. After 1hr, TLC analysis demonstrated that no starting material (dansyl chloride) was left. Rotatory evaporation was employed to remove the solvent. The reaction mixture was dissolved in chloroform (20 mL) washed with water 3 times (20 mL each). The chloroform layer was filtered through 10 grams of silica gel, and the filtrate was concentrated under high vacuum, yielding the product (50 mg, 86% yield). The data is consistent with the reported values (17,20) as follows: ^{1}H-NMR (Figure 4-4, $CDCl_3$, 500 MHz) δ 8.63 (d, *J* = 7.5 Hz, 1H, arom. H), 8.37 (d, *J* = 8.4 Hz, 1H, arom. H), 8.27 (d, *J* = 7.2 Hz, 1H, arom. H), 7.57 (m, 2H, arom. H's), 7.26 (d, *J* = 7.2 Hz, 1H, arom. H), 4.84 (brs, 1H, NH^{e}), 2.96 (s, 6H, CH_3^{a}), 2.88 (m, 2H, CH_2^{b}), 1.43 (m, 2H, CH_2^{c}), 0.79 (t, *J* = 7.5 Hz, 3H, CH_3^{d}).

LR-MS (EI): found *m/z* $[M]^{\bullet+}$ 292.1, (M^{+}-$C_3H_8NSO_2$) 171.0, calcd *m/z*, 292.1.

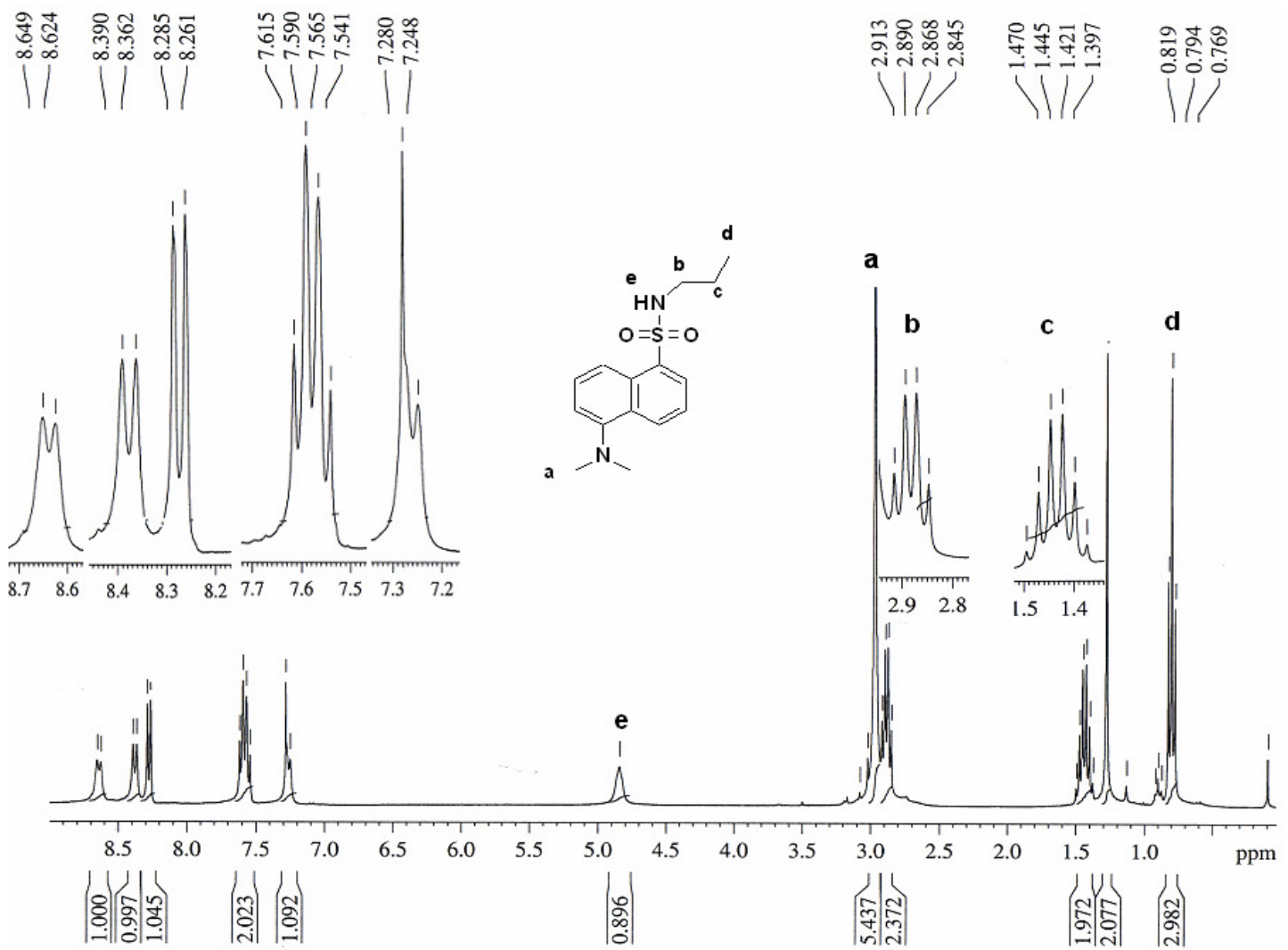

Figure 4-4. ^{1}H-NMR spectrum (500 MHz, $CDCl_3$) of dansylpropylamide.

4.2.4 Bacterial strain and growth conditions

FPn as the sole phosphorus source was first tested with an *E. coli phn*$^+$ strain (HO1429) that constitutively expresses the *phn* operon. The strain was grown on MOPS minimal media prepared according to Samina *et al.* (4). The minimal medium contained MOPS (40 mM), glucose (11.1 mM), NH_4Cl (9.5 mM), Tricine (4.4 mM), thiamine hydrochloride (30 μM), $FeSO_4 \cdot 7H_2O$ (10 μM), $CaCl_2$ (0.5 μM), $MnCl_2$ (0.8 nM), $CoCl_2$ (0.3 nM), $CuSO_4$ (0.16 nM), $ZnSO_4$ (0.1 nM), $(NH_4)_6Mn_7O_{24}$ (30 pM), and H_3BO_4 (4 pM). Electrophoresis grade agarose (1.5%, wt/vol, Sigma Aldrich) was included to produce solid media plates because it is especially low in phosphate compared to media grade agars. All the glassware used was rinsed with nitric acid, followed by multiple washes with deionized water. The plate streaked with the *E. coli* strain HO1429 was incubated at 37ºC for 2-3 days until visible colonies could be seen. Control plates without FPn (0.5 mM) or with methyl phosphonic acid (0.5 mM) as the only phosphorus source were grown in the same way. To test the product of the FPn processed *in vivo,* cells were grown in liquid culture containing MOPS minimal media. Strains were cultivated in Luria-Bertani broth (5 mL) under aerobic conditions at 37 ºC overnight to saturation. The next morning, the culture was centrifuged at 3000 g to harvest the cells. The cell pellet was then washed with MOPS minimal media 3 times to remove the majority of inorganic phosphate, after which it was resuspended in 5 mL of MOPS minimal media. Two mL of the resuspended culture was added to 48 mL of minimal media supplemented with 0.5 mM of FPn

as the only phosphorus source, which was then cultivated at 37 ºC until the A_{600} of the culture reached approximately 1. The culture was then extracted with CH_2Cl_2 and the organic layer concentrated on a Rotovap to obtain the final crude products. Silica gel TLC and EI-MS spectroscopy were then used to analyze the organic extract. The TLC developing system used was 4% MeOH: 96%CH_2Cl_2.

FPn was also incubated with the entire collection of *phn* knock-out strains at 37 ºC overnight (this work was done by Dr. Bjarne Hove-Jensen, University of Denmark). Cells were removed by centrifugation and aliquots of the supernatants were applied to silica gel TLC plates which were run in two solvent systems: MeOH / CH_2Cl_2 and the more polar *t*-butanol / acetic acid / H_2O. After chromatography, positions of various fluorescent spots as illuminated by UV light were drawn with a soft pencil directly on the chromatogram. Then spots were transferred to a piece of transparent paper, which was subsequently scanned (**Figure 4-8**).

4.3 Results and Discussion

4.3.1 Synthesis of FPn and *in vivo* assay with *phn*$^+$(HO1429)

Fluorescent aminoalkyl phosphonic acid (FPn, **4**, **Figure 4-1**) was successfully synthesized with a total yield of 15%. Cells from the *E. coli phn*$^+$ strain HO1429 successfully grew on the solid minimal media plates supplied with FPn as the sole phosphorus source after 2 days of incubation at 37ºC (**Figure 4-5B**). Similar growth was observed on plates supplied with methyl phosphonic

acid (**Figure 4-5A**), whereas no colonies were present on the plates without any phosphorus source (**Figure 4-5C**). This demonstrates that FPn can be degraded by the *E. coli* C-P lyase to release P_i, which is an essential element for sustaining cells growth.

An *in vivo* test with FPn as the only source of phosphorus was also carried out in liquid culture. *E. coli phn*$^+$ cells were grown in MOPS minimal medium with or without FPn (control). In the absence of FPn, *phn*$^+$ strain cells could not grow, suggesting that FPn was utilized as a source of phosphate. To detect the expected fluorescent labeled alkane product (**6**, **Figure 4-1**), the cell culture was extracted with dichloromethane, followed by TLC analysis using the synthesized product as the standard (R_f = 0.44) (**Figure 4-6**). The product was confirmed by EI-MS with a molecular ion observed *m/z* at 292.12 (expected *m/z* 292.12) and a fragment ion at 171.11 (expect *m/z* = 171.10 for the aromatic fragment) (**Figure 4-7**). This result clearly indicates that cells containing C-P lyase can catalyze the hydrolysis of a direct C-P bond from the fluorescent labeled substrate to produce the predicted fluorescently labeled alkyl product, further supporting that FPn can be utilized as a chemical probe of C-P lyase activity *in vivo*.

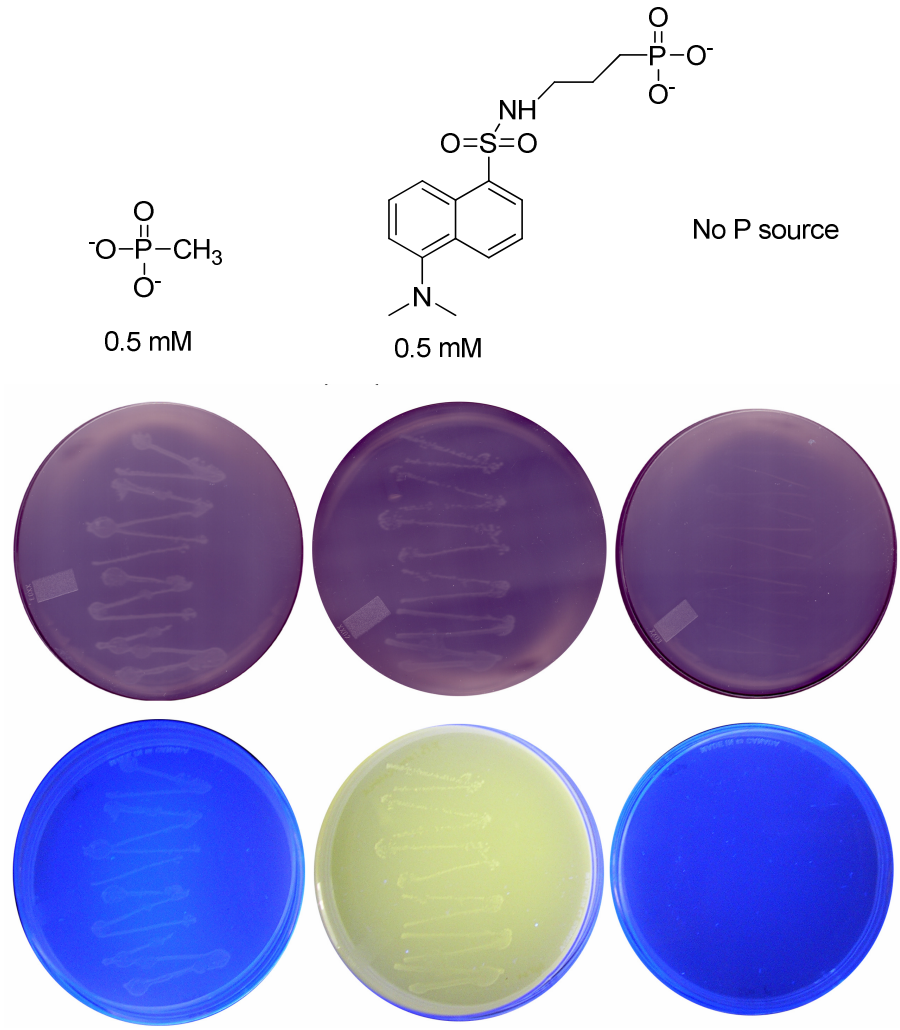

Figure 4-5. *In vivo* test of MePn (methylphosphonic acid, A), FPn (fluorescent phosphonate, B) as the only source of phosphorus for the *E. coli phn+* strain HO1429 growth on MOPS minimal media plates. C is the control plate without any phosphorus source. The top three plates were visualized under ambient light and the lower three plates pictures were taken under UV light (366 nm).

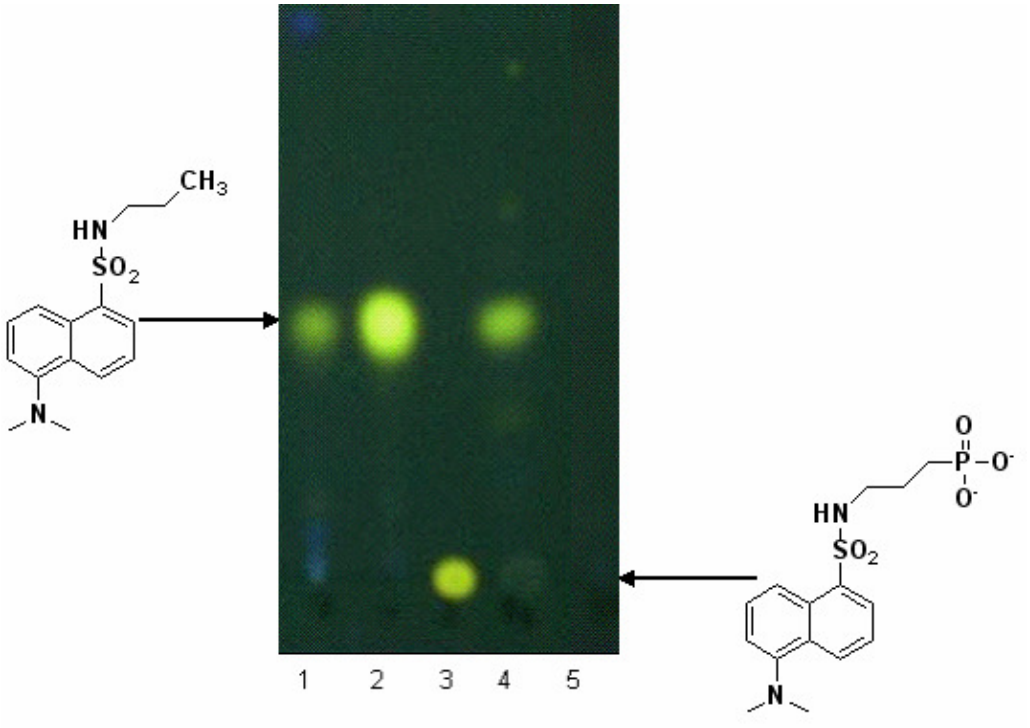

Figure 4-6. TLC analysis demonstrating that the *E. coli phn*+ strain HO1429 can utilize FPn as the sole source of phosphorus. Solvent system used was 2% MeOH: 98% CH_2Cl_2. TLC plate illuminated under UV light (366 nm). Lane 1, HO1429 (*phn*$^+$) CH_2Cl_2 extract (Rf 0.44); Lane 2, synthesized product standard (Rf 0.44); Lane 3, FPn; Lane 4, purified product from organic extraction of culture after preparative TLC (Rf 0.44); Lane 5, minimal media without FPn.

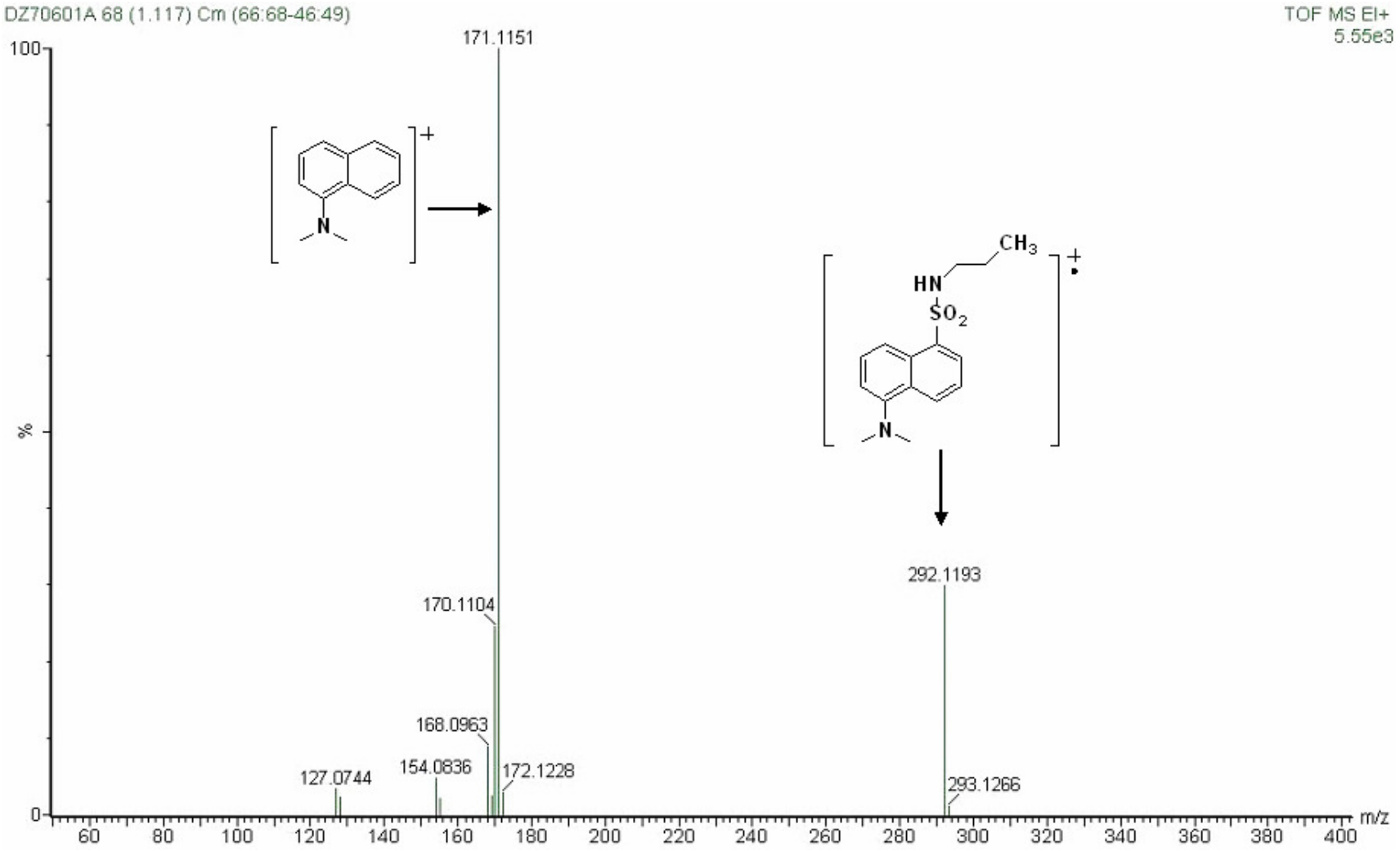

Figure 4-7. Electron impact-MS showing the presence of the product degraded from FPn by *E. coli* with the molecular ion at *m/z* 292.1.

4.3.2 *In vivo* test of FPn with *E. coli phn* mutants (In collaboration with Dr. Bjarne Hove-Jensen, University of Denmark)

FPn was tested *in vivo* with *E. coli phn*$^+$ wild type and a series of mutants where each *phn* gene had been deleted (**Figure 4-8**). It was observed that the wild type, the *phnP* and the *phnF* mutant strains produced similar type of pattern in that FPn appeared to be converted to two other spots (**Figure 4-8A** and **4-8B**), consistent with the result by measuring the methane production from degradation of MePn (15). This pattern indicated that phnP and phnF genes are not required by *E. coli* to directly cleave the C-P bond. More importantly, 3 other fluorescent products were observed (**A, B, and C, Figure 4-8B**), suggesting the presence of metabolic intermediates (or side products) and, by implication, a role for these genes in producing them. Further studies need to be done to identify those compounds by MS, HPLC, and NMR analysis.

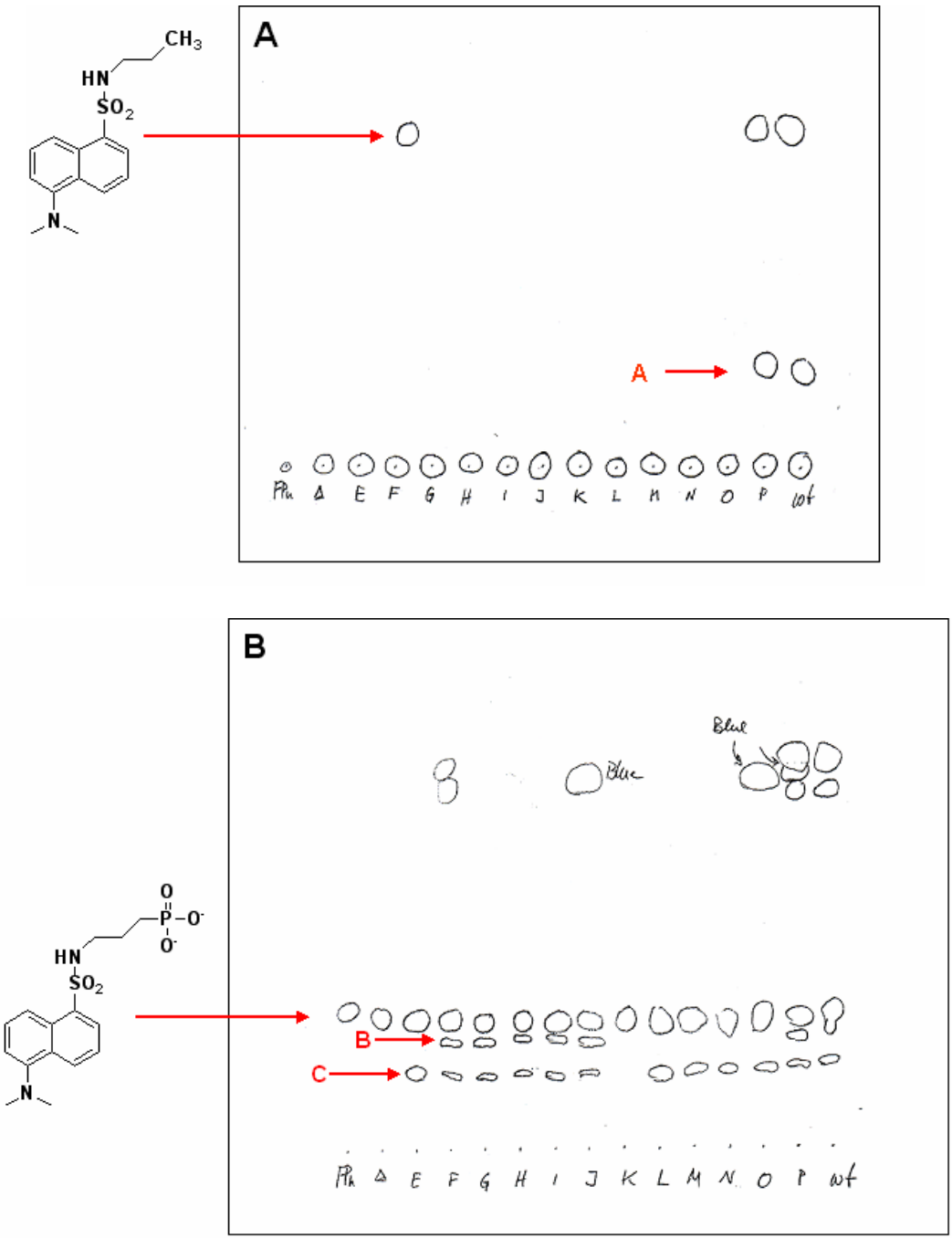

Figure 4-8. *In vivo* test of FPn as a sole source of phosphorus with *E. coli phn*$^+$ and various mutants. FPn indicates the compound directly from the FPn starting material, the triangle indicates deletion of the entire *phn* operon and the letters indicate the defective phn gene of the respective strains. (**A**) Cell free extracts applied to a TLC plate and resolved in MeOH/CH_2Cl_2. (**B**) Cell free extracts applied to a TLC plate and resolved in *t*-butanol / acetic acid / H_2O .

4.4 Conclusion

FPn was successfully synthesized and tested as a probe of C-P lyase activity *in vivo*. *E. coli* was shown to use FPn as the sole phosphorus source for maintaining growth. TLC analysis and mass spectrometry confirmed the presence of the expected product after cleavage of the C-P bond of FPn. In addition, improvements were achieved through *in vivo* experiments with *phn* mutant strains. Some potential intermediates were observed. These intermediates, once characterized structurally, may provide useful information for identifying physiological substrates for the individual C-P lyase enzymes, or complexes thereof. This information will be critical to elucidate the catalytic mechanism of the C-P lyase system.

REFERENCES

1. Osby JO: **Studies on the mechanism of transition metal-assisted sodium borohydride and lithium aluminum hydride reductions**. *J. Am. Chem. Soc.*1986, **108**: 67-72.
2. Kumar S, Zhou B, Liang F, Yang H, Wang W-Q, Zhang Z-Y: **Global Analysis of Protein Tyrosine Phosphatase Activity with Ultra-Sensitive Fluorescent Probes**. *J. Proteome Res.* 2006, **5**:1898-1905.
3. Frost JW, Loo S, Cordeiro ML, Li D: **Radical-based dephosphorylation and organophosphonate biodegradation**. *J. Am. Chem. Soc.* 1987, **109**:2166-2171.
4. Iqbal S, Parker G, Davidson H, Moslehi-Rahmani E, Robson RL: **Reversible phase variation in the phnE gene, which is required for phosphonate metabolism in *Escherichia coli K-12***. *J. Bacteriol.* 2004, **186**:6118-6123.
5. Chen CM, Ye QZ, Zhu Z, Wanner BL, Walsh CT: **Molecular biology of carbon-phosphorus bond cleavage. Cloning and sequencing of the phn (psiD) genes involved in alkylphosphonate uptake and C-P lyase activity in *Escherichia coli* B**. *J. Biol. Chem.* 1990, **265**:4461-4471.
6. Metcalf WW, Wanner BL: **Mutational analysis of an *Escherichia coli* fourteen-gene operon for phosphonate degradation, using TnphoA' elements**. *J. Bacteriol.* 1993, **175**:3430-3442.
7. Morais MC, Zhang G, Zhang W, Olsen DB, Dunaway-Mariano D, Allen KN: **X-ray Crystallographic and Site-directed Mutagenesis Analysis of the Mechanism of Schiff-base Formation in Phosphonoacetaldehyde Hydrolase Catalysis**. *J. Biol. Chem.* 2004, **279**:9353-9361.
8. Murai T, Tomizawa C: **Chemical transformation of S-benzyl O-ethyl phenylphosphonothiolate (Inezin) by ultraviolet light**. *J. Environ. Sci. Health* 1976, **B11**:185-197.
9. Seto H, Kuzuyama T: **Bioactive natural products with carbon-phosphorus bonds and their biosynthesis**. *Nat. Prod. Rep.* 1999, **16**:589-596.
10. Shames SL, Wackett LP, LaBarge MS, Kuczkowski RL, Walsh CT: **Fragmentative and stereochemical isomerization probes for homolytic carbon to phosphorus bond scission catalyzed by bacterial carbon-phosphorus lyase**. *Bioorg. Chem.* 1987, **15**:366-373.
11. Ternan NG, Grath JW, Mullan G, Quinn JP: **Organophosphonates: occurrence, synthesis and biodegradation by microorganisms**. *World J. Microbiol. Biotechnol.* 1998, **14**:635-647.
12. Wackett LP, Shames SL, Venditti CP, Walsh CT: **Bacterial carbon-phosphorus lyase: products, rates, and regulation of phosphonic and phosphinic acid metabolism**. *J. Bacteriol.* 1987, **169**:710-717.

13. Ternan NG, Grath JW, Mullan G, Quinn JP: **Organophosphonates: occurrence, synthesis and biodegradation by microorganisms**. *World J. Microbiol. Biotechnol.* 1998*,* **14**: 635-647.
14. Yakovleva GM, Kim SK, Wanner BL: **Phosphate-independent expression of the carbon-phosphorus lyase activity of *Escherichia coli***. *Appl. Microbiol. Biotechnol.* 1998, **49**:573-578.
15. Adams MA, Luo Y, Hove-Jensen B, He S-M, van Staalduinen LM, Zechel DL, Jia Z: **Crystal structure of PhnH: an essential component of carbon-phosphorus lyase in *Escherichia coli***. *J. Bacteriol.* 2008, **190**:1072-1083.
16. Murata K, Higaki N, Kimura A: **Detection of carbon-phosphorus lyase activity in cell free extracts of Enterobacter aerogenes**. *Biochem. Biophys. Res. Commun.* 1988, **157**:190-195.
17. Summers WA, Lee JY, Burr JG: **Synthesis of fluorescent labeled derivatives of aminopropylpyrimidines**. *J. Org. Chem.* 1975, **40**:1559-1561.
18. Cordeiro ML, Pompliano DL, Frost JW: **Degradation and detoxification of organophosphonates. Cleavage of the carbon-phosphorus bond**. *J. Am. Chem. Soc.* 1986, **108**:332-334.
19. Kononova SV, Trutko SM, Laurinavichus KS: **Detection of C-P-lyase activity in a cell-free extract of *Escherichia coli***. *Appl. Biochem. Microbiol.* 2007, **43**:394-398.